The University Of Sheffield.

The effect of inkjet printed polymer on the mechanical properties of carbon fibre reinforced plastic

by

Yi Zhang

Supervisor: Dr Patrick J. Smith

A thesis submitted to

The Department of Mechanical Engineering

for the degree of Doctor of Philosophy

July 2015

Acknowledgements

I would like to express my gratitude to my supervisor Dr. Patrick J. Smith for all his kind help, encouragement and dedicated guidance, without which, this project would not have been possible. He gave me flexibility to follow my research interests, but at the same time, he kept me going in the right direction. His patience with proof reading my thesis is highly appreciated.

I am also grateful to Professor Alma Hodzic for her invaluable advices and fruitful discussions. I would like to thank her for supporting financially my project (Air Force Office of Scientific Research, under grant number FA8655-11-1-3072), and my attendance at the 19th International Conference on Composite materials in Montreal.

I acknowledge with gratitude the generous financial support of the US Army Forward Element, under grant number W911NF-14-1-0581 for supporting me to pursue my PhD in the final year.

I would like to thank Dr. Jonathan Stringer for his kind help and valuable advices through my PhD studies, and I am also grateful to Dr. Simon A. Hayes, Dr. Joel Foreman, Dr. Xiubo Zhao and Dr. Austin D. Lafferty for providing me valuable advices and technical information. Special thanks to Dr. Difei Zhou for helping me out on computational topics. I wish to thank my friends Christopher, Patrick, Alon, Pete, Elliot and Andrew for their help. Staff, students and fellows at CSIC have helped make my time at CSIC really enjoyable. Thanks to my friends here in Sheffield for enjoyable moments we have shared during the three years.

I am extremely thankful for my parents for their constant understanding, support and help. And I would like to thank my husband and my daughter for their love and the happy life we share together.

Abstract

A new toughening method is presented in this thesis that uses inkjet printing to deposit toughening materials between carbon fibre reinforced plastic (CFRP) laminate plies prior to the curing cycle. Inkjet printing has the ability of precisely depositing material onto targeted positions, thus a controlled amount of toughening materials can be used to print dimension controllable patterns. Poly(methyl methacrylate) (PMMA) and polyethylene glycol (PEG) were dissolved in suitable solvents respectively to form printable solutions for inkjet printing. Different patterns and substrates were employed to investigate the repeatability of using inkjet printing to deposit polymer solutions. Microscopy showed that the designed patterns can be repeatedly printed onto substrates with controllable dimensions. A range of 0.025 – 0.2 vol.% of toughening material was used to prepare CFRP laminates for mechanical tests.

Mechanical properties of the inkjet printed CFRP laminates were tested by means of double cantilever beam and short beam shear tests to determine mode I interlaminar facture toughness (G_{Ic}) and apparent interlaminar shear strength (ILSS) respectively. The G_{Ic} of polymer printed laminates increased as the overall amount of polymer deposits increased before reaching to an optimum. A maximum 40% increase in G_{Ic} was observed in a system with printed 10 wt.% PMMA deposits that were hexagonally patterned. Different patterns and pattern densities were investigated, among which the hexagon with a higher pattern density performed the best in terms of material usage efficiency. Although laminates with a printed PMMA film possessed the highest G_{Ic} compared to the other printed groups that used discrete dots, the crack propagation was unstable. Additionally, the improvement in G_{Ic} did not result in a reduction of the ILSS for the polymer printed laminates, except for the film printed group. The damage tolerance of PMMA printed laminates was also enhanced based on the images obtained from X-ray tomography and scanning electron microscopy (SEM).

The proposed toughening mechanism is as follows: the polymer deposits remain strategically dispersed along predicted crack pathways with controllable size. Once microcracks occur between composite plies, the arrayed toughening materials can address crack propagation by plastic deformation and/or deflection of crack pathways due to debonding between toughening material and surrounded epoxy resin. The plasticization of localised epoxy region is also believed to be a contribution to the observed mechanical improvement.

Contents

Contents

Contents

List of figures and tables

Figures

Tables

Nomenclature

Latin symbols

G_{Ic}	Mode I interlaminar fracture toughness (critical energy release rate)
G_{IIc}	Mode II interlaminar fracture toughness (critical energy release rate)
dx	Droplet spacing in x axis
dy	Droplet spacing in y axis
T_g	Glass transition temperature
prepreg	Pre-impregnated
Oh	Ohnesorge number
Z	Reciprocal of Ohnesorge number
d	Diameter of printhead orifice
$S_{printed}$	Area of the repeating unit cell with the pattern
S_{unit}	Area of the repeating unit cell
$V_{printed}$	Volume of printed droplet
V_{sample}	Volume of test sample
V_0	Volume of jetted droplet
D_0	Diameter of jetted droplet
f	Volume fraction of polymer in solution
t	Thickness
P	Load of double cantilever beam test
a	Delamination length
C_0	Initial compliance
F	Large-displacement correction
N	Block correction
l_1	Distance from centre of the loading pin to the mid-pane of the specimen
l_2	Distance from the loading-pin centre to its edge
b	Width of short beam shear sample
h	Thickness of short beam shear sample
F_M	Maximum load of short beam shear test

Greek symbols

η	Viscosity
ρ	Density
σ	Surface tension
ξ	Surface coverage of polymer deposits
δ	Load line extension
Δ	Calibration parameter for mode I interlaminar fracture toughness calculation
τ	Apparent interlaminar shear stress
τ_M	Apparent interlaminar shear strength

Acronyms

CFRP	Carbon fibre reinforced plastic
3D	Three dimensional
ATL	Automated tape laying
AFP	Automated fibre placement
RFI	Resin film infusion
CIJ	Continuous inkjet printing
DOD	Drop-on-demand inkjet printing
PMMA	Poly(methyl methacrylate)
PEG	Polyethylene glycol
ILSS	Interlaminar shear strength
NL	Non-linear
PROP	Propagation
SEM	Scanning electron microscope

Chapter 1

Introduction and Literature review

This chapter firstly introduces fibre reinforced composites, including commonly used fibre and matrix types, their typical mechanical and physical properties, advantages and disadvantages of using fibre reinforced composites with a focus on carbon fibre reinforced composites. Several advanced and multifunctional applications of these fibre reinforced composites are introduced. Secondly, composite laminate toughening methods which have been explored are briefly introduced, their successes and drawbacks are discussed in practical applications. The chapter thirdly introduces the inkjet printing technique, offering an explanation of why more researchers are interested in this novel method and its applications to date. Lastly, the scope and objectives of this thesis are introduced.

1.1 General introduction of composites

Composites generally consist of two or more different materials which offer respective properties to suit the performance requirements of the end applications. A variety of natural materials are composites such as wood and bone. Researchers were inspired by these natural composites to integrate two or more materials to form a new material. By combining these two or more components, the resultant material, which has properties from all constituents, performs better than using either one of the components alone. In most cases, a strong and stiff component which acts as the reinforcement is embedded in a softer material called matrix to form a composite material [1].

Generally, composites are divided into three categories: polymer matrix composites (PMCs), metal matrix composites (MMCs) and ceramic matrix composites (CMCs). The properties of potential components are key factors to the success of final formulated composites. Typically, modulus, strength, thermal properties and density are the most important properties which are particularly interesting to researchers. PMCs have been extensively investigated during the past a few decades due to their outstanding properties and relatively

easy fabrication processes. Both thermosets and thermoplastics are used as matrices respectively, and are commonly reinforced with strong and stiff fibres such as glass and carbon. In this thesis, fibre reinforced PMCs are the main focus which will be discussed in detail.

1.2 Fibre reinforced composites

1.2.1 Fibres

Fibre reinforced composites are increasingly used in applications where weight is a crucial issue. This material mainly consists of fibres with high modulus and strength and a matrix which has the capability to hold fibres together and protect them from damage during service. Normally, fibre is the load carrying part due to its outstanding mechanical properties such as high stiffness and high strength [2, 3]. Thus, fibres have the dominant influence on the mechanical performance of the final composites. The most common fibre types used in commercial products are glass, carbon, and aramid fibres, either in continuous or dis-continuous form when combined with the matrix [4]. Glass fibre has been widely used as reinforcements in industry for decades due to the combination of its low price and good mechanical and physical properties such as high tensile strength and chemical resistance [5]. Therefore, this material is extensively used to produce consumer products. To date, glass fibre reinforced composite is the dominant material in terms of industrial volumetric consumption. However, its relatively low fatigue resistance and low tensile modulus limit its application to areas where higher mechanical requirements are needed [6, 7]. Aramid fibres such as Kevlar which generally have high specific strength (which is a material's strength divided by its density) and high specific (Young's) modulus (the material's modulus divided by its density), high damage tolerance and chemical resistance owing to their highly crystalline molecular structure [8]. However, relatively low compressive strength and high cost are major drawbacks of using aramid fibres [9]. Natural fibres have recently received increasing attentions from researchers on account of their environmental friendliness and recyclability, however, the compatibility of natural fibres with matrices and moisture resistance of their composites need to be improved before natural fibre reinforced composites can be used further in structural applications [6, 10-14].

Carbon fibre has a highly crystalline structure. Usually, the diameter of carbon fibre ranges from 5 – 8 μm, it contains amorphous and crystalline carbon [15]. Carbon atoms in crystalline form are arranged in hexagonal lattices, where the hexagons of carbon atoms connected by covalent bonds. These carbon hexagons are parallel to each other to form layer/plane-structure known as graphitic carbon [9]. The formed plane is called basal plane. The covalent bonds between carbon atoms are very strong (~ 525 kJ/mol) [15] and the basal planes are arranged parallel to the fibre axis, which results in carbon fibre's high tensile modulus along the fibre axis. As the density of carbon fibre is quite low (~ 2 g/cm^3), carbon fibre has superior specific modulus and strength compared to other commercial fibres and metallic materials. The bonds between carbon atoms' planes are van der Waal bonds which are much weaker (< 10 kJ/mol) than the covalent bonds [1, 16]. This large difference makes carbon fibre highly anisotropic, or directionally dependent. In the transverse direction, the alignment of graphite crystals is more complicated. They could be in circumferential, radial, random form or a combination as shown in Figure 1.1. Physical and mechanical properties of the carbon fibres depend on the type of arrangement of the graphite crystals.

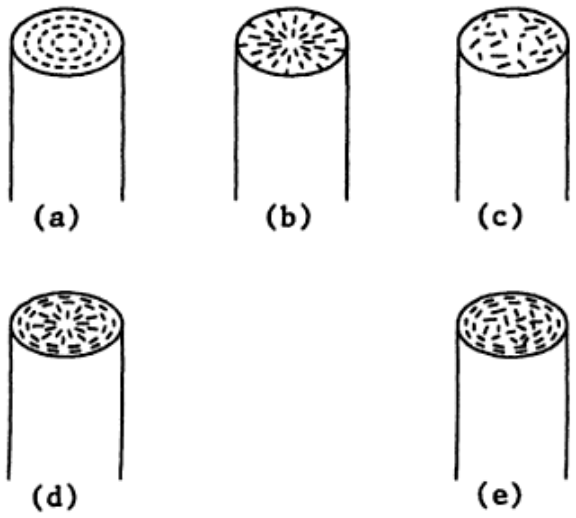

Figure 1.1 Arrangement of graphite crystals in a direction transverse to the fibre axis: (a) circumferential; (b) radial; (c) random; (d) radial-circumferential; e) random-circumferential [9].

Using carbon fibres as reinforcement also has other advantages such as low coefficient of thermal expansion, which provides good geometrical stability of structures during service, and high fatigue strength which extends the lifetime of products. However, there are disadvantages of using carbon fibres. First, carbon fibre has a low strain-to-failure value and low impact resistance. Second, the cost of producing carbon fibre is high, which narrows its applications to high value areas. Finally, although carbon fibre reinforced composites are used commercially in the aerospace industry, the processing technique of carbon fibre still needs to be improved further [17]. Currently, there are two main commercial ways of manufacturing carbon fibres as shown in Figure 1.2.

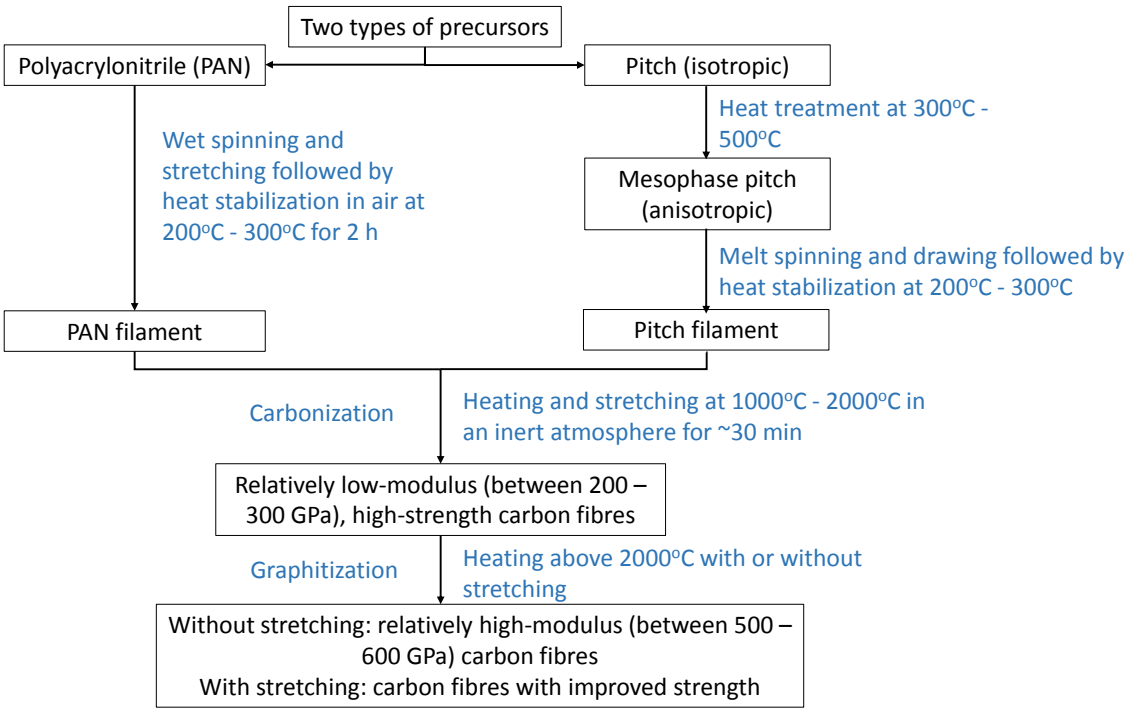

Figure 1.2 Manufacturing methods in production of carbon fibres [9].

As can be seen in Figure 1.2, every manufacturing step in carbon fibre production needs relatively high temperatures. As a result, the manufacturing of carbon fibres requires a large amount of energy, which increases the cost for commercial applications. Table 1.1 shows typical mechanical properties of a few selected fibres commonly used in fibre reinforced composites. It can be seen that carbon fibres are much stronger in terms of the specific modulus and strength.

Table 1.1 The typical properties of several commercial fibres [9, 14, 18, 19].

Fibre		Density (g/cm^3)	Tensile strength (GPa)	Tensile modulus (GPa)	Strain to failure %	Specific strength ($kN \cdot m/kg$)	Specific modulus (10^6 m^2/s^2)
Glass	E-glass	2.6	3.5	73.5	4.8	1337	28.5
	S-glass	2.5	4.9	86.8	5.7	1988	35.3
Carbon (PAN-based)	High modulus	1.8-2.2	1.9-3.7	350-550	0.4-0.7	1056-1721	194.4-255.8
	Intermediate modulus	1.8-2.0	3.1-4.4	230-300	1.3-1.6	1722-2200	127.7-150.0
	High strength	1.8-2.0	4.3-7.1	240-300	1.7-2.4	2389-3550	133.3-150.0
Aramid	Kevlar 49 High modulus	1.5	3.6-4.1	131	2.8	2483-2828	90.3
	Kevlar 29 High toughness	1.4	3.6	83	4.0	2500	57.6
	Kevlar 149 Ultrahigh modulus	1.5	3.4	179	2.0	2313	121.8
Natural	Silk	1.2-1.3	0.5-1.0	5-13	20-25 (wet)	400-737	4.0-9.8
	Hemp	1.5	0.6-1.0	8.6-9.5	2.3	372-669	5.8-6.5

The adhesion between fibres and matrix is of great importance to the final mechanical properties of fibre reinforced composites. When fibre reinforced composites are subjected to an applied load, the load is transferred to the fibres from the matrix, which requires that the interface between fibre and matrix should be sufficiently strong. The surfaces of fibres usually receive various treatments, such as coating with silane coupling agents, in order to have a good bond with the matrix, which enables the superior properties of the fibres to be imparted to the final composite system [20, 21]. A strong interface makes the composite stiff, because the high stiffness of fibres such as carbon and Kevlar fibres is imparted into the composite. As well as the stiffness of composite being affected by the interface between fibre and matrix, there are other properties such as strength, creep resistance, fatigue and resistance that also largely depend on the interface between fibre and matrix [22].

1.2.2 Composite matrices

Although the fibres are the dominant constituent in providing necessary mechanical properties such as tensile strength and modulus, the mechanical and physical properties of the matrix are also important to the proper performance of the fibre reinforced composites as shown in Table 1.2. A suitable matrix selection, to some extent, is vital to the performance of composite in terms of out-of-plane (interlaminar) shear and in-plane (intralaminar) shear properties and compressive strength [9]. For polymeric based composites, the properties such as viscosity, curing time and temperature also have influences on the processing of fibre reinforced PMCs. Therefore, a comprehensive consideration of matrix selection when designing a composite is critical to the success of the finished product [17].

Table 1.2 Functions of fibre and matrix in composite materials [17].

Fibres	Matrix
• Provide stiffness, strength, resistance to fatigue and other mechanical properties • Give unique properties such as the low coefficient of thermal expansion and conductivity	• Protect fibres from environmental damage • Provide shape to composites • Transfers loads to fibres and contributes to mechanical properties such as stiffness and strength

There are different types of matrices such as metals, ceramics and polymers that can be combined with various fibres. The most common matrix used in commercial fibre reinforced composites is polymer. Polymer is commonly light and has some desirable properties such as electrical insulation and chemical resistance. Moreover, the processing of polymer matrix composites commonly does not need high temperature and pressure compared to metal and ceramic based composites, which eases the problems associated with the degradation of the fibres during processing, and reduces the cost of manufacturing polymer matrix composites. There are two main types of polymer, which are thermosetting polymers (e.g. epoxy, phenolic resin) and thermoplastic polymers (e.g. polyether ether ketone (PEEK), polypropylene, poly(methyl methacrylate) (PMMA)). These polymers are often combined with fibres due to their good mechanical properties, low density and relative ease of processing.

Typically, thermosetting polymers are mainly used as the matrix in continuous fibre reinforced composites, because they have low viscosities when in liquid form before cure, thus, it is relatively easy to evenly distribute the resin between continuous fibres. Whereas, thermoplastic polymers are likely to be used as the matrix in discontinuous fibre reinforced composites. This is because of the difficulty of combining continuous fibre with high viscous thermoplastics. Matrices like metals and ceramics are mainly used in high temperature applications due to their high melting points. Table 1.3 shows a few selected matrices and their common applications.

The main disadvantages of using polymers as the matrix in composites are their low working temperatures, sensitivity to radiation and moisture and high coefficients of thermal expansion.

However, these drawbacks can be optimised by varying formulations of polymerisation, curing agents and reinforcements.

Table 1.3 Some matrices and their common applications [9, 17].

Matrix		**Common applications**
Thermoplastic polymers	PEEK, polyamide-imide (PAI), polyphenylene sulphide (PPS)	High temperature applications (combined with continuous fibre)
	Nylons, polycarbonate (PC)	Automotive and sports goods applications (Normally combined with discontinuous fibres)
Thermoset polymers	Epoxies	Aerospace and aircraft applications
	Thermoset polyesters	Automotive, marine, chemical and electrical applications
	Polyimides, polybenzimidazoles (PBI)	High temperature aerospace applications
Metallic materials	Aluminium and its alloys, titanium alloys, stainless steel	High temperature applications
Ceramics	Aluminium oxide (Al_2O_3), silicon carbide (SiC), silicon nitride (Si_3N_4)	High temperature applications

1.2.2.1 Thermosetting polymers

Thermosetting polymers have cross-linked chains bonded by irreversible chemical bonds forming highly cross-linked three dimensional (3D) network structure. As a result, fibre reinforced composites using thermosetting polymers as matrices possess high modulus and strength compared to using thermoplastic polymers as matrices. The cross-linked chains in thermosetting polymers are inflexible, therefore, thermosetting polymers usually exhibit higher glass transition temperatures (T_g: reversible transition from a hard state to a rubber-like state). This means thermoset polymers can be used under higher temperature circumstances compared to polymers with lower T_g. On the other hand, because the cross-linked 3D network structure limits the flexibility of their polymer chains, the thermosetting

polymers are brittle and have relatively poor fracture toughness [23], neither can they be re-shaped nor melted by heat. There are several thermosetting polymers that are commonly used as matrix materials, such as epoxy, thermoset polyester and vinyl ester. Table 1.4 shows typical properties of several commonly used thermosetting polymers.

Table 1.4 Typical properties of several commonly used thermosetting polymers (RT) [17, 23].

	Epoxy	Thermoset polyester	Vinyl ester
Density (g/cm^3)	1.2-1.3	1.1-1.4	1.1-1.3
Tensile strength (MPa)	55-130	35-104	73-81
Tensile modulus (GPa)	2.7-4.1	2.1-3.5	3.0-3.5
Cure shrinkage (%)	1-5	5-12	5-10

Epoxy is a popular matrix used in fibre reinforced composites and in various structural parts on account of its good mechanical properties and good adhesive properties. The good mechanical properties ensure the final composite structures have stable shape during service. The good adhesive properties ensure there is excellent adhesion between epoxy and fibre, which is critical to fracture toughness and interlaminar strength of the final composites. In addition to that, epoxy has low shrinkage during curing, which is important to reduce stress between the matrix and the fibre in finished parts. These distinct properties enable epoxy to be used as the principle matrix resin in most high performance composites (mainly combined with carbon fibres).

The cured epoxy starts with low molecular weight compounds, commonly, diglycidyl ether of bisphenol A (DGEBA) is a popular starting material which has an epoxide group at both ends of a DGEBA molecule as shown in Figure 1.3.

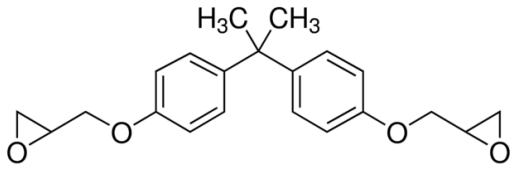

Figure 1.3 A molecule of DGEBA epoxy.

Polymerisation of epoxy usually consists of three stages which are called the A, B and C stages. In the A stage, thermosetting polymers are still in a low viscosity state, hence, combination by infiltration is easy in this stage. In the B stage, cross-linking has formed to a large extent throughout the resin, as a result, the viscosity of the resin is increased to a very high level. If the resin is kept in a low temperature environment, the resin would stay in the B stage for a period of time depending on the nature of resins [9, 17]. When the external curing conditions are provided (e.g. elevated temperature), the curing process continues until fully cured, which is the C stage of thermoset polymer's polymerisation. In order to form a cross-linked 3D network, a cross-linking agent (curing agent) is needed [17, 24]. Diethylene triamine (DETA) is a typical curing agent which has been widely used in epoxy curing. As shown in Figure 1.4, a cross-linked 3D network forms which turns the low viscosity liquid resin into a solid insoluble polymer after curing.

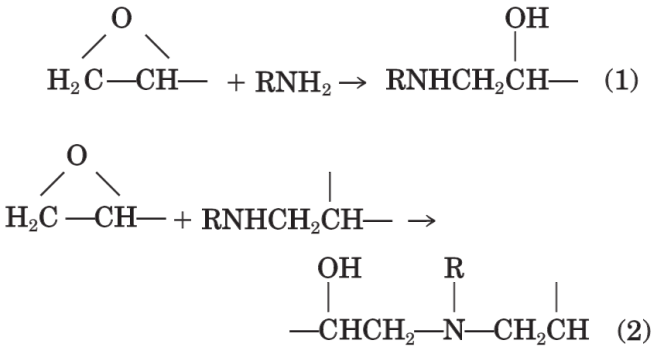

Figure 1.4 Schematic polymerisation between DGEBA and DETA to form a cross-linking 3D network [25].

1.2.2.2 Thermoplastic polymers

Unlike thermosetting polymers that form a rigid covalently bonded 3D network, the thermoplastic polymers' (e.g. PEEK, PPS) chains remain free after processing. Typically, the processing of thermoplastics is carried out in their molten state, when temperature cools down below their melting point or T_g, the moulded thermoplastics gain their final shapes or structures. Since the chains inside thermoplastics are still in free-state, they can rearrange their positions when under pressure or elevated temperature, ultimately the thermoplastics

can be re-shaped or re-melted to form a new structure. Figure 1.5 schematically shows the molecular chains of thermosetting and thermoplastic polymers.

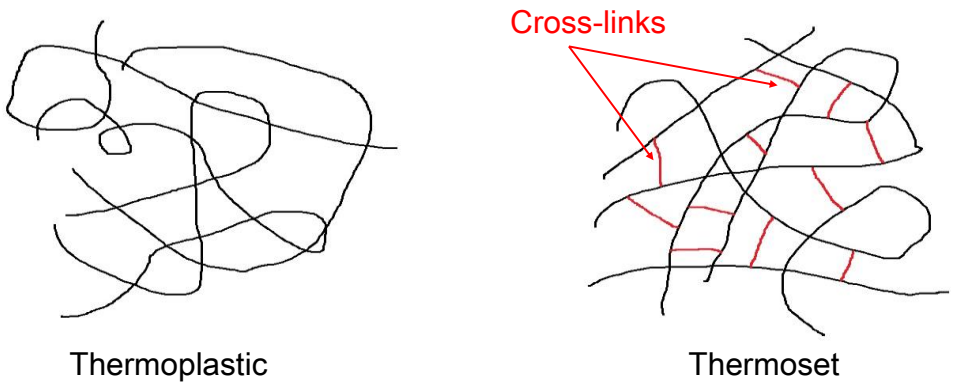

Figure 1.5 Thermoplastic and thermosetting polymer chains.

High impact strength and high fracture resistance are the most important advantages of using thermoplastics as matrix over thermosetting polymers [26, 27]. The high strain-to-failure of thermoplastic polymers enables the matrix to have better resistance to micro-cracking which is the initial form of delamination. However, the processing of thermoplastics with fibres is more difficult due to their high viscosities. Also, their low creep resistance and low thermal stability due to lack of cross-links prevent their application to areas where high dimension stability of structures is required.

1.2.2.3 Selection of thermosetting or thermoplastic polymers

As mentioned before, an appropriate selection of matrix when designing a composite is critical to the final fibre reinforced composites. High tensile modulus, tensile strength and high fracture toughness are favoured when designing high performance fibre reinforced composites.

Since polymers have their own particular properties such as T_g, these properties need to be considered as well when designing a composite. For example, the T_g of a polymer should be higher than the service temperature to ensure the dimensional stability of the composite structure. Usually, thermosetting polymers have better dimensional stability than that of

thermoplastic polymers due to their covalently bonded cross-linked 3D network chains. This means that elevated temperature causes minimal deformation of thermosetting polymer based composite structures. Thermoplastic polymers have lower creep resistance and thermal stability due to the mobility of the polymer chains under elevated stress or temperature. Table 1.5 compares the advantages and disadvantages of using thermosetting and thermoplastic polymers as matrices in fibre reinforced composites.

Table 1.5 Comparison of using thermosetting and thermoplastic polymer as matrix.

Polymer	Advantages	Disadvantages
Thermoset	• Ease of co-working with fibres • Good dimensional and thermal stability	• Limited storage life • Low strain to failure ratio • Long fabrication time
Thermoplastic	• High strain to failure ratio • High impact and fracture resistance • Unlimited storage life • Can be re-processing	• High viscosity for incorporation with fibres • Low dimensional and thermal stability

Taking the aforementioned advantages of carbon fibre and polymer matrices, CFRPs have been extensively studied and their mechanical properties have been improved. For example, carbon fibre reinforced thermoset epoxies generally offer superior specific modulus and specific strength, low coefficient of thermal expansion, high corrosion resistance over other fibre reinforced composites. CFRPs are increasingly applied to structural applications such as aircraft primary/secondary structures, vehicles components and sports equipment to save their weight.

1.2.3 Prepregs and laminates

Fibres are pre-impregnated in the matrix with predetermined direction and volume fraction to form a ready-to-use thin sheet called prepreg [17]. Epoxy is the most popular thermosetting polymer used as prepreg matrix. In order to reduce the risk of manipulating liquid resin (A

stage), a pre-cure process which is heat and solvent controlled is provided to partially cross link liquid resin to form B staged prepreg. By doing this, harmful chemicals are less likely to be an environmental and health hazard, and the formed prepreg is easier to manipulate for the subsequent processing. Since the curing reaction in the resin is triggered, B staged prepreg needs to be stored at a low temperature (~ −20°C) to slow down the curing reaction. As a result, the storage time of prepreg before moulding is finite (e.g. the out of freezer life of epoxy prepregs is 6 – 8 days at 23°C typically depending on the matrix, but at −18°C, the storage time of epoxy prepregs can be prolonged up to 12 months form the date of manufacture) [9, 28].

Prepregs are usually available in forms of unidirectional tape (Figure 1.6 (a)) or woven fabrics (Figure 1.6 (b)). A single sheet of prepreg is also called a lamina. Laminates are constructed by stacking individual laminae following a sequence which balances properties with a designed thickness. When using unidirectional prepregs/laminae to make laminates, the stacking sequence of laminae plays an important role in the final performance of laminates. Commonly, according to the different stacking sequence, laminates can be divided into three different groups as follows: 1) Unidirectional laminate, consists of parallel fibre angle in the same direction for all laminae (e.g. in unidirectional 0° laminate, all fibres are parallel to tensile loading direction) as shown in Figure 1.7(a); 2) Angle-ply laminate, directions of fibres alternate in each lamina as shown in Figure 1.7(b) (e.g. $/\theta/-\theta/-\theta/\theta/$, $-\theta \neq 0°$ or $90°$); 3) Symmetric laminate, the fibre directions are symmetrically orientated about the centreline of a laminate as shown in Figure 1.7(c) [9]. Since the strong fibres are the constituent of the composite that takes the applied load, the tensile strength and modulus are dependent on the orientation of fibres in laminas. Unidirectional laminate ($\theta = 0°$) has the maximum tensile strength and tensile modulus. But in the transverse direction, mechanical properties are weak. In order to overcome this drawback, mechanical properties are balanced in all directions by angling fibre orientation in each lamina, which results in multidirectional laminates.

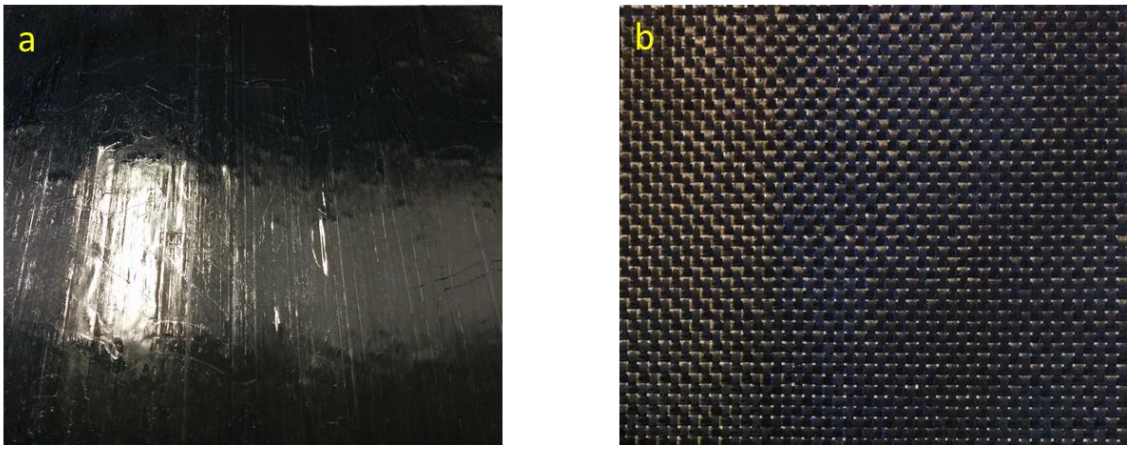

Figure 1.6 Unidirectional and woven prepreg.

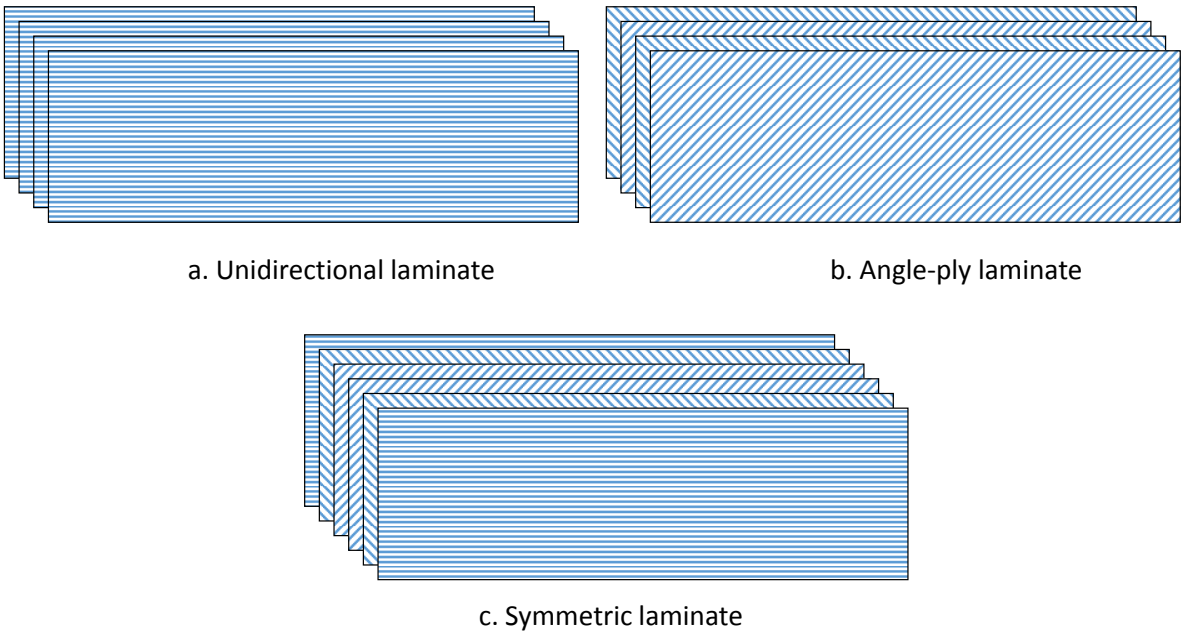

Figure 1.7 Different stacking sequences of laminates using unidirectional tape.

One major problem of multi-layered laminates is their low interlaminar properties, they are typically susceptible to early failure by delamination, in which cracks originate at the interface between plies due to high interlaminar tensile and shear stress cause separation of laminate plies.

Woven laminates provide properties that are more balanced in horizontal and transverse directions in every ply than unidirectional laminates. Using the multi-layered method to lay up unidirectional prepreg can produce laminates with balanced mechanical properties, but the fabrication time is much longer than that of using woven fabric prepregs. However, there are drawbacks of using woven prepreg to fabricate composites. The tensile modulus and strength of composites fabricated using woven prepreg are normally lower than that of multi-layered laminates using unidirectional prepreg tape [9]. The relatively large stress formed between the fibres and the matrix under loading is the main cause of the low tensile modulus and strength.

1.2.4 Toughening

Although fibre reinforced composite laminates are increasingly used to replace metallic materials wherever is possible, their own drawbacks limits their appeal. For example, carbon fibre reinforced composites are widely used in aircraft manufacture on account of their superior mechanical properties and light weight. However, their low impact resistance and susceptibility to delamination is of great concern for load carrying applications. This is because of the brittleness of the epoxy matrix and the lack of reinforcement in the through thickness direction [29]. Delamination is considered as the most critical and common failure mode of this material, it develops from microcracks which can be generated from manufacturing defects or in-service damages [30-32]. Unfortunately, these microcracks, which are difficult to detect at their early stage (known as barely visible impact damage, BVID), can result in catastrophic failure, thus it is of great importance to improve the damage tolerance of fibre reinforced composite laminates [32].

Thermosetting epoxy based laminates have poor low-energy impact resistance due to the brittle nature of the matrix. Although the highly cross-linked matrix of epoxy provides good mechanical properties and high chemical resistance, it causes the brittleness of epoxy due to limited movement of epoxy molecular chains. Toughened epoxy is modified by adding tougher material(s) to enhance its toughness, it has a better fracture resistance compared to the unmodified. However, it is not usually as good as thermoplastics based laminates [4], because thermoplastics are typically less brittle. For example, using 5 – 10 J impact energy

can cause considerable cracking in carbon fibre reinforced epoxy laminates [15]. The interlaminar fracture toughness is one of the parameters used to evaluate the capability of composite laminates to resist delamination growth. There are two main modes of interlaminar fracture toughness which are commonly used based on different applied load directions. Mode I interlaminar fracture toughness, G_{Ic}, has a load perpendicular to the test beam; Mode II interlaminar fracture toughness, G_{IIc}, has a shear load parallel to the test beam. A mixed mode of mode I and mode II is also used to evaluate the resistance to delamination of laminated composites.

1.2.4.1 Matrix toughening

Currently, there are several extensively explored methods which are used to improve the interlaminar fracture toughness of fibre reinforced composite laminates. Matrix toughening commonly uses tough materials (e.g. elastomers/rubbers, thermoplastic particles) or inorganic nanoparticles (e.g. alumina, silica) as fillers to mix with the matrix in order to increase the fracture toughness of the matrix. The matrix toughening mechanisms such as plastic deformation of fillers and reducing cross-linking density to make matrix less brittle have been comprehensively explored [33-39]. As discussed in Section 1.1.2, the matrix of fibre reinforced composites plays a critical role in the interlaminar and intralaminar properties of laminates, and interlaminar failure is a result of the fracture of the matrix or/and the interface between fibres and matrices [40]. Therefore, toughening matrix is one of the effective methods which can be used to improve the interlaminar fracture toughness of fibre reinforced laminated composites.

The toughening of thermoset epoxies by adding elastomers/rubbers has been in existence for over 40 years. Scott and Phillips [41] reported the fracture toughness (G_{Ic}) of an epoxy resin can be improved by ten times by adding 9 wt.% butadiene-acrylonitrile co-polymers (CTBN). Chikhi et al. [42] used the liquid amine-terminated butadiene acrylonitrile (ATBN) copolymers containing 16 wt.% acrylonitrile as an epoxy toughening agent. The addition of ATBN (11 wt.%) led to a 3-fold increase in impact strength compared to the unmodified resin. The fracture toughness was also increased by approximately 50%. In terms of the shear properties, the tensile shear strength increased from 9.14 MPa to 15.96 MPa by adding 5 wt.%

of ATBN. The improvement can be attributed to the influence of various material parameters such as cross-linking density of epoxy and size of rubber particles [37, 43]. The fracture behaviour of rubber toughened epoxy may involve the following most discussed mechanisms: 1) stretching and tearing of rubber particles; 2) localised crazing around rubber particles; 3) plastic zone effect by plasticisation of the resin; and 4) localised cavitation in the vicinity of crack tip [38].

However, the addition of soft elastomer/rubber particles decreases the modulus of modified epoxy. For example, the tensile modulus of ATBN added epoxy decreased from 1.85 GPa to about 1.34 GPa with increasing ATBN content in Chikhi's work [42]. Other than that, it has been reported that the toughening effectiveness of elastomer/rubber addition was diminished in the epoxy system which has a high cross-linking density [44, 45]. Therefore, it is undesirable for advanced high performance fibre reinforced composites which usually use a highly cross-linked epoxy as composite matrix.

In order to avoid the compromises of rubber toughening, inorganic nanoparticles or rigid thermoplastic particles are embedded into epoxies instead of elastomers/rubbers. Hsieh et al. [46] used silica nanoparticles as modifier to toughen epoxy polymers. The presence of silica nanoparticles (volume fraction of added silica nanoparticles: 13.3 vol.%) improved the fracture toughness of modified epoxy up to 280% compared to unmodified. Also, the addition of silica nanoparticles increased the modulus of modified epoxy due to the high modulus of silica. A maximum 30% increase in modulus of silica added epoxy was achieved. However, this toughening was only applied to the neat epoxy. Whether this observed toughening effectiveness can be transferred to fibre reinforced composites needs further investigation. Tang et al. [47] added silica nanoparticles into the matrix of carbon fibre reinforced epoxy composite with the aim of toughening. The results showed that the tensile properties and the plane strain fracture toughness of nanosilica-modified epoxies were improved by the addition of certain nanosilica (10 and 20 wt.%), and the transverse tension properties and the G_{Ic} of modified laminates were also improved. However, the interlaminar shear strength (ILSS) and the G_{IIc} decreased as the nanosilica concentration increased, especially at the high nanosilica concentration of 20 wt.%.

It has been demonstrated that thermoplastics, such as polysulfones (PSU), poly(ether imide)s (PEI) [48] and polyamides, can improve fracture toughness of thermosetting epoxy systems.

Pearson and Yee [49] applied thermoplastic poly(phenylene oxide) (PPO) as a toughening agent in epoxy. The fracture toughness was reported to increase linearly with PPO content. A maximum 63% increase in fracture toughness was observed by adding 17 wt.% of PPO into epoxy. Cardwell and Yee [50] used polyamide-12 as the toughener due to its excellent adhesion with epoxy. The fracture toughness of toughened epoxy was increased by 134% by adding 37 vol.% of toughener. Note, both works were only conducted using the unreinforced epoxy resin. The toughening mechanisms associated with inorganic nanoparticle or thermoplastic particle filled epoxy are focused on: 1) deflection of crack growth; 2) plastic deformation of thermoplastic particles [50]; 3) plastic deformation of the matrix around the particles; and 4) crack pinning [38].

Although the matrix toughening show that the fracture toughness of the neat resin systems can be enhanced significantly, the observed considerable increase in unreinforced resin is not transferred into composite due to fibre constraint suppressing into inelastic resin deformation at the crack front [31, 51]. Moreover, applications of matrix toughening to fibre reinforced composites have commonly encountered problems. Some mechanical properties of matrix modified composites are compromised, such as modulus, shear/compression properties. Additionally, adding thermoplastics into epoxy systems increases the viscosity of mixed blends, which is not ideal in terms of manufacturing.

1.2.4.2 Stitching

Stitching can provide through thickness reinforcement of a laminated composite to improve the delamination resistance [52]. Stitching usually uses high tensile strength and stiffness materials as thread to sew the laid-up laminates. Figure 1.8 shows an architectural sample of a stitched laminate. The stitching thread needs to be flexible and resistant to abrasion during stitching, and retained after the curing process [53]. Fritz Larsson [54] reported that the interlaminar fracture toughness of stitched CFRP laminates was 10 times higher than that of unstitched laminates. But the compression strength was reduced by 30%. Dransfield et al. [53] investigated the effect of stitching on G_{Ic} of CFRP laminates and found that the G_{Ic} of stitched laminates was improved up to 15 times. Dransfield et al. believe that the major contributing failure mechanisms are: 1) thread debonding from the matrix; 2) the elastic

stretching of the thread limits the crack propagation; 3) thread failure and pull-out from matrix provides an energy dissipation way. Yoshimura et al. [55] experimentally and numerically investigated the impact resistance of stitched CFRP laminates. The results demonstrated that the impact resistance of CFRP laminates was improved by stitching. The damage area of stitched laminate was approximately 60% smaller than that of unstitched laminate after an impact test (impact energy: 3.35 J/mm, normalised by the plate thickness). The energy absorption by the stitching threads which were located inside or around the delamination area is proposed as the cause of improvement in the damage resistance.

Although stitching offers some mechanical benefits to stitched laminates, the effect on the in-plane properties is a great concern of using this toughening technique. The reasons are as follows: 1) material discontinuity at the stitching point in the composite structure which can lead to high stress concentration; 2) the presence of the through thickness fibres creates resin rich pockets that reduce the in-plane fibre volume fraction; 3) the loops generated by the stitching process on the plane surface may result in kinking of the in-plane fibres [52]. In addition, the toughening effect of stitching depends on various factors such as the thread type, stitch density, composite type and the loading type. The complex combination of those factors make it hard to predict the final toughening efficacy. Therefore, it is difficult for industry to employ this toughening technique [56].

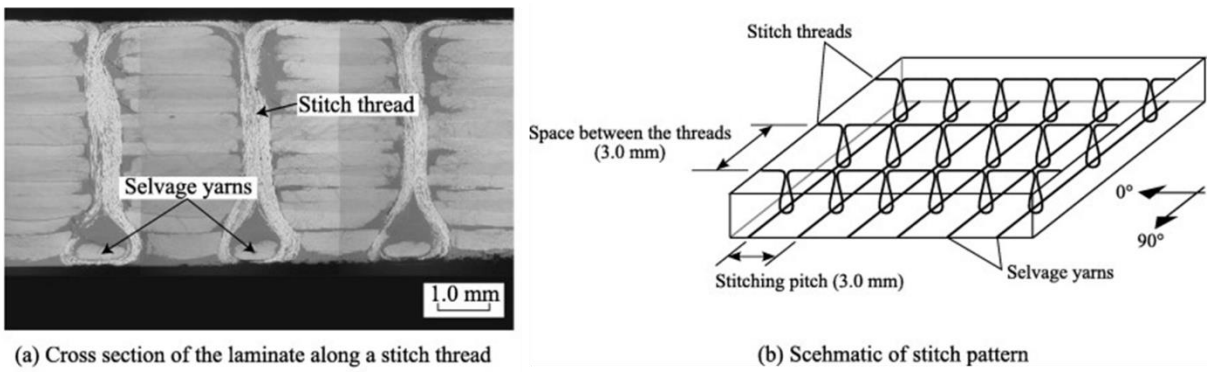

Figure 1.8 Stitching of CFRP laminate [55].

1.2.4.3 Interleaving

Instead of toughening the matrix where the toughening materials are mixed with the whole bulk matrix, toughening materials are placed onto crack favoured regions (Figure 1.9). As the crack tends to propagate between the laminated plies [52, 57], the placement of interleaved toughening material between plies (or interleaving) has been investigated. It has been demonstrated that the interlaminar fracture toughness of fibre reinforced composite laminates can be significantly enhanced by using various interleaves such as epoxy, carbon nanofiber/nanotube and Nylon 6,6. The interleaves usually have high toughness and shear strain, and remain as a discrete toughened layer between laminas after co-curing with the matrix resin. Therefore, the toughened layer arrests the crack propagation between laminate plies.

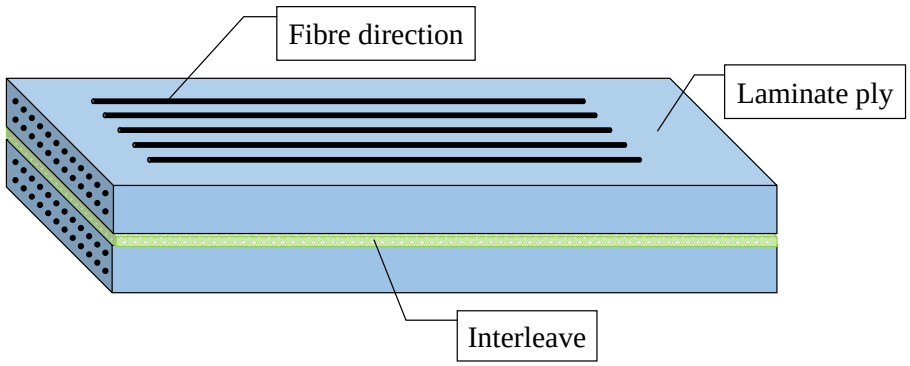

Figure 1.9 Schematic showing the interleaving system.

Arai et al. [58] used carbon nanofiber as an interlaminar toughener to toughen CFRP laminates. They manually applied the carbon nanofiber onto CFRP prepregs using a metal roller, and successfully increased the G_{Ic} and G_{IIc} of interleaved CFRP laminates by 50% and 300% respectively compared to their baseline. Similar work has been reported by White et al. [59] where a carbon nanotube/polyamide-12 epoxy thin film was used as a toughening interleave. An increase in G_{IIc} values nearly 2.5 times higher than the unmodified CFRP laminate was reported. Hojo et al. [60] used a self-same epoxy as the interleaf material by sequentially laying up the half-cured epoxy films and prepregs. It was reported that the G_{Ic} values of the laminates with the self-same epoxy interleaves were almost identical to those of the base laminates. However, the initial values and the propagation values of G_{IIc} of the

laminates with interleaves were 1.6 times and 3.4 times higher than those of the base CFRP laminate respectively. Hamer et al. [61] demonstrated a three-fold improvement in G_{Ic} values compared to the base laminate using an electro-spun Nylon 6,6 nano-fibrous mat as the interlaminar toughener.

Although interleaving improved the interlaminar fracture toughness to a greater or lesser extent, the continuous film inserted between the plies interfered with the chemical adhesion within the interlaminar region that is critical to the mechanical properties and the design criteria in the composite components. This interleaving method may compromise several aspects which are important to commercial manufacture. For example, minimum weight is required when considering whether to apply this toughened laminates to areas where weight is a critical key factor, therefore, the weight gain by using interleaves will need to be well considered. The additional interleaves increase thickness of final composite laminates, which may well be a problem for designing a delicate composite structure. In terms of mechanical properties, the addition of continuous interleaves decreases interlaminar shear properties which is also a vital aspect that needs to be considered when using interleaves as a toughening method.

1.2.5 Self-healing fibre reinforced composites

Repairable materials are able to heal microcracks either intrinsically or extrinsically. Intrinsic healing means materials can repair themselves without external assistances. Extrinsic healing means materials cooperating with healing agent can achieve healing via external stimulus. Numerous self-healing composite systems with different healing mechanisms have been reported to date. For example, hollow glass fibres (HGF) filled with self-healing agent have been embedded in CFRPs to provide a self-healing functionality. Once a breakage happens to these HGFs, the healing agent is released from the damaged HGFs and infiltrates damage site for subsequent curing and filling of the micro-cracks. Williams et al. [62] reported the self-healing carbon fibre reinforced composites with embedded HGFs can restore 97% of flexural strength of undamaged state and 89% of the baseline laminate performance. Figure 1.10 shows HGFs embedded within a CFRP laminate.

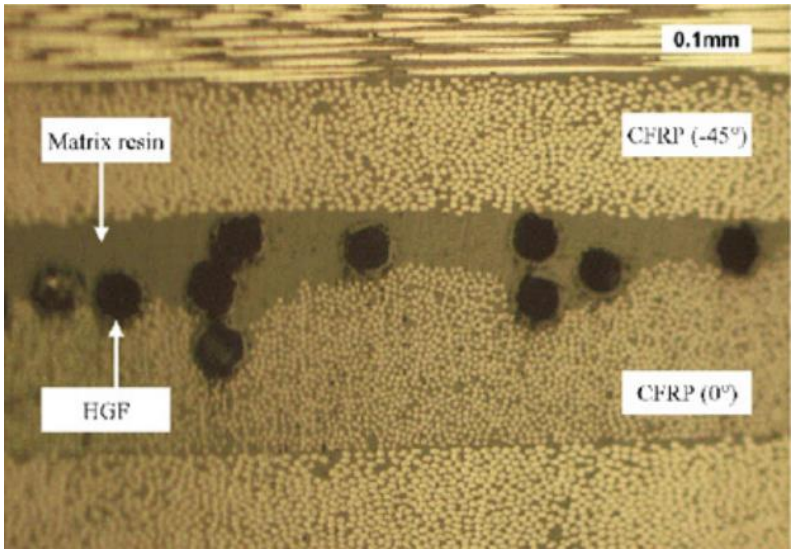

Figure 1.10 HGFs embedded in carbon fibre reinforced composite matrix [62].

However, this strategy has challenges. For example, how to effectively fill the brittle HGFs with self-healing agent remains an issue; the flowability of the healing agent released from the broken glass fibres inside the composites is a practical problem; the concentration of the healing fibres within the matrix and those fibres' geometrical distribution have to be optimised, because the addition of healing fibres tends to weaken the mechanical properties of the final composite [63].

Another extensively explored strategy to produce self-healing composite material is based on microencapsulated healing agent. Basically, the healing agent is microencapsulated and embedded with solid catalytic chemical materials within a polymer matrix. Upon damage, the microcapsules break to release healing agent into the damage sites. When the healing agent contacts the catalyst, polymerisation is triggered, therefore, cracks are healed by bonding crack surfaces closed. Brown et al. [64] demonstrated this technique in 2002 and they reported by optimising the concentration of catalyst and microcapsules, the system has over 90% of healing efficiency. Figure 1.11 schematically shows the self-healing mechanism based on microencapsulated healing agents.

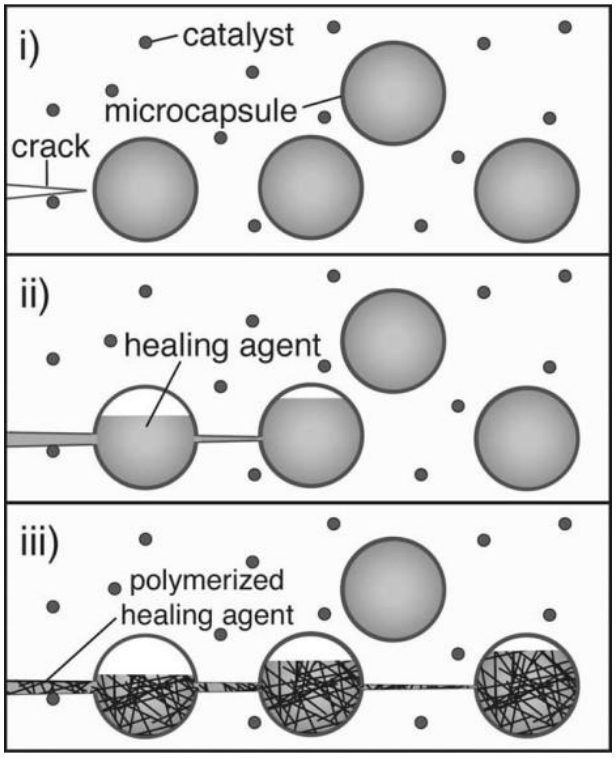

Figure 1.11 Schematic show of microencapsulated self-healing agents system [64].

Like the hollow glass fibre system, this technique has its own drawbacks. For example, the encapsulation should be compatible with the catalyst; the healing agent should be able to remain stable in microcapsules before cracks happen.

Although these two methods offer the self-healing function for composite materials, some desirable properties are compromised such as compression after impact (CAI) and toughness [63]. Finally, the extra weight introduced in composite may well be a problem especially in areas where weight is a crucial consideration, such as aerospace applications.

1.2.6 Applications of fibre reinforced composites

As fibre reinforced composites offer many attracting mechanical and physical properties such as high specific modulus, high specific toughness and light weight, applications of fibre reinforced composites to aeronautical, military, automotive structures have dramatically increased during the past three decades. The challenge for fibre reinforced composites is they

need reliable and better mechanical and physical properties compared to conventional metallic materials.

Currently fibre reinforced composites are mainly used in civil and military aircrafts to save bodyweight. For example, in the 90's Boeing started to use about 10% structural weight of carbon fibre reinforced epoxy composite in the 777. In their newest 787 Dreamliner, the amount of CFRPs used has increased to 50% by weight, which reduces the fuel consumption while increasing payload [60]. Airbus was the first manufacturer to use composites in their A310 aircraft in 1987. In their newest A380, up to 25% of its bodyweight materials are composites [9, 65] (Figure 1.12). The advantages of using fibre reinforced composites in aircraft are as follows: 1) saving weight: rising fuel costs and environmental issues increasingly attract the public's attention, greener aircrafts are needed in order to reduce the cost and emissions; 2) simplified manufacturing process: as fibre reinforced composite can be easily shaped and tailored to produce more efficient structural configurations, less components are needed when assembling aircraft. Additionally, the length of assembly time is reduced and the potential failure dangers around joints are reduced too. The key drawback of using (carbon) fibre reinforced composites is they are susceptible to delamination due to the inherent brittle nature of epoxy. Although several toughening techniques have proved to be effective, the extra weight gain and the compromised mechanical properties limits their applications in commercial products.

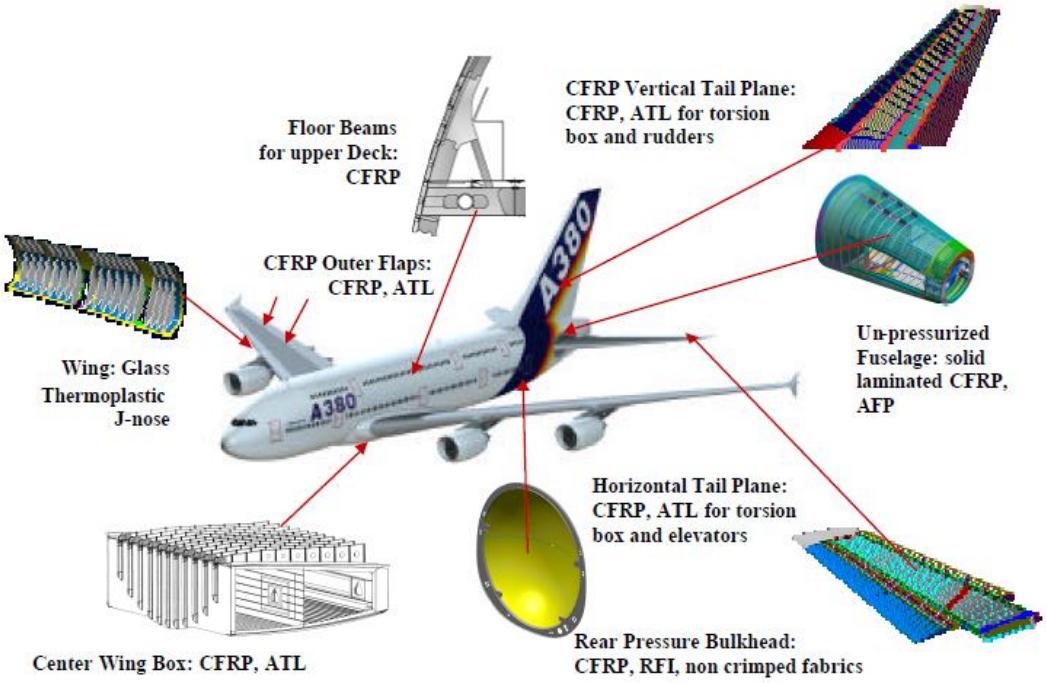

Figure 1.12 Composite materials used in Airbus A380 [65]. (ATL: **A**utomated **T**ape **L**aying; AFP: **A**utomated **F**ibre **P**lacement; RFI: **R**esin **F**ilm **I**nfusion)

Fibre reinforced composites are also widely used in automotive areas such as body, chassis and engine components. Glass fibre reinforced composite is the domain candidate used to replace metallic materials due to their low cost and desirable mechanical offers. However, carbon fibre reinforced composite is a promising candidate which can be used to build a stronger automobile body, and further reduce bodyweight of vehicles in order to improve fuel efficiency and therefore reduce emissions. This is because the carbon fibre reinforced composite offers the high specific modulus and strength, which is not achievable by using metallic materials.

1.3 Inkjet printing technique

1.3.1 Introduction

Inkjet printing is a computer-aided additive technology which is used to deposit liquid phase materials. These liquid materials, called inks, can undergo a phase change to leave behind a solid deposits [66]. Inkjet printing can selectively deliver pico-litre volume droplets as instructed from a computer file to form a two dimensional structure or stack droplets that solidify layer by layer to form 3D structure onto various substrates [67]. With the assistance of a computer, users can design various patterns for printing beforehand. As the time for changing patterns is short, downtime is minimised when printing. This eliminates the pre-mask step used in traditional printing methods, simplifying the manufacturing process and reducing costs of manufacture. Inkjet printing can either work with a one ink system or multiple ink system, both approaches can precisely print single/multiple materials at micrometre resolution with essentially no restrictions on the geometric complexity of the spatial arrangement. Also, the non-contact characteristic of inkjet printing minimises the risk of contamination in the final product, and waste of material is minimised. Inkjet printing is, therefore, an attractive technique for many research areas such as printed electronics [66, 68-70] and tissue engineering [71-80]. Recently researches [81, 82] have been used inkjet printing to print patterned toughening materials between laminate plies before curing process, which forms the main subject of this thesis.

There are two main forms of inkjet printing in terms of different droplet formation mechanisms: 1) continuous inkjet printing (CIJ) and 2) drop-on-demand inkjet printing (DOD). CIJ generates an electric charged stream of liquid phase materials through a small diameter nozzle. The Rayleigh instability is induced in the stream so that the break-up is repeatable to form uniform droplets [83]. Figure 1.13 shows the basic construction of CIJ. When droplets are charged electrically, they can be directed by an electrostatic or magnetic field to form a pre-defined structure. Those unwanted droplets are steered into a gutter and recycled [77]. CIJ has been widely used in commercial fields such as marking products and low resolution printing due to its fast deposition rate of ink. However, CIJ is limited by the risk of contamination of products and the electrically conductive inks.

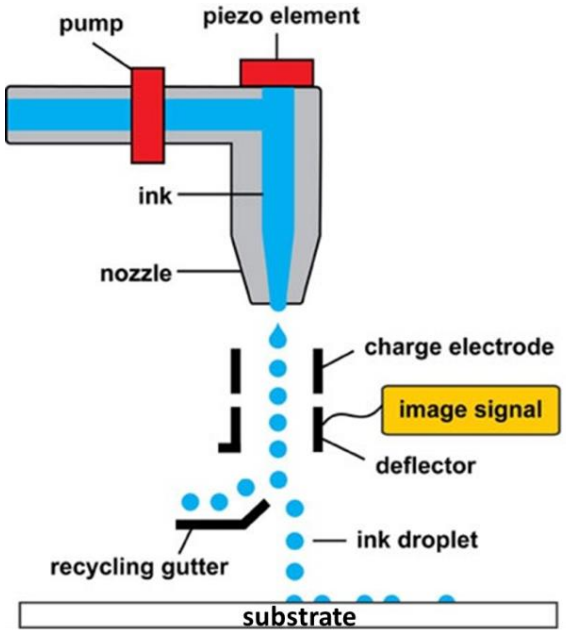

Figure 1.13 Continuous inkjet printing [84].

DOD inkjet printing, as shown in Figure 1.14, generates droplets only on required places by propagating a pressure pulse in a fluid filled chamber. Because droplets are only ejected when required, the material waste is minimised compared to CIJ. Both DOD and CIJ generate negligible waste compared to other fabrication methods, such as spin coating [85] and selective laser sintering [86, 87].

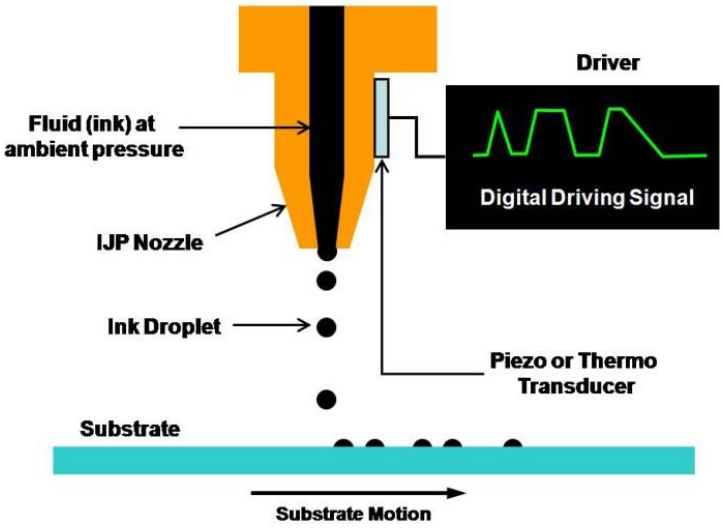

Figure 1.14 DOD inkjet printing [88].

DOD inkjet printing also minimises the risk of contamination of product because a recycling system is not needed, which means the ink used for DOD inkjet printing is always fresh. Moreover, DOD inkjet printing has the capability of using independent printheads to deliver different materials to fabricate structures without changing material during the printing. This advantage facilitates researchers to fabricate multi-functional structures which consist of different materials while minimising the contamination risk and fabrication time. For example, organ printing is seen as promising, because it combines direct printing technique to produce a scaffold which has desired shape and internal structures with incorporation of multiple living cell types to form a manually fabricated organ [89, 90]. The fundamental requirement of this strategy is printing tissue scaffolds and seeding cells on these printed scaffolds spontaneously.

There are two types of DOD inkjet printing: 1) thermal DOD inkjet printing. A bubble is generated by a heater/resister which can vaporise a small volume of the ink as shown in Figure 1.15 causing a droplet to be ejected; 2) piezoelectric DOD inkjet printing. Basically, piezoelectric DOD inkjet printing ejects a droplet by volume change of the ink chamber. In a piezoelectric DOD printhead, the formation of droplets is formed by mechanical actuation of the ink chamber, which is controlled by a pressure wave to form a pulse as shown in Figure 1.16. This sudden volume change of the ink chamber generates droplets. Figure 1.17 shows a typical pressure wave pulse generated in piezoelectric DOD printhead. Figure 1.18 shows stroboscopic images of droplets generated by a DOD printer. Droplets with 100 – 200 μm diameter can be seen from Figure 1.18(b).

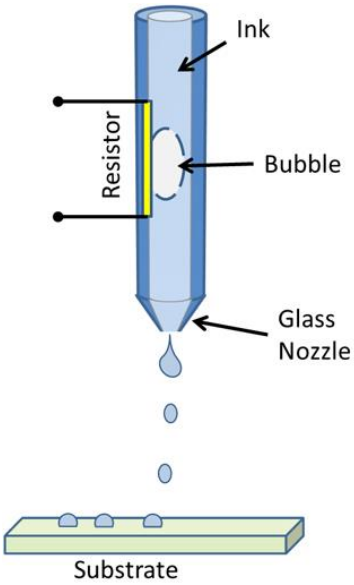

Figure 1.15 Droplet ejection by thermal DOD printer [91].

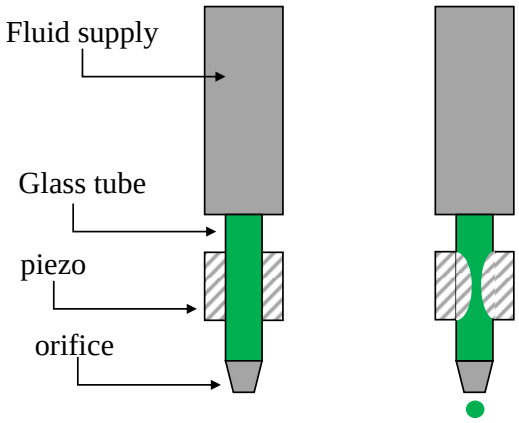

(a) Deactivated (b) Activated

Figure 1.16 Schematic of piezoelectric DOD printhead [92].

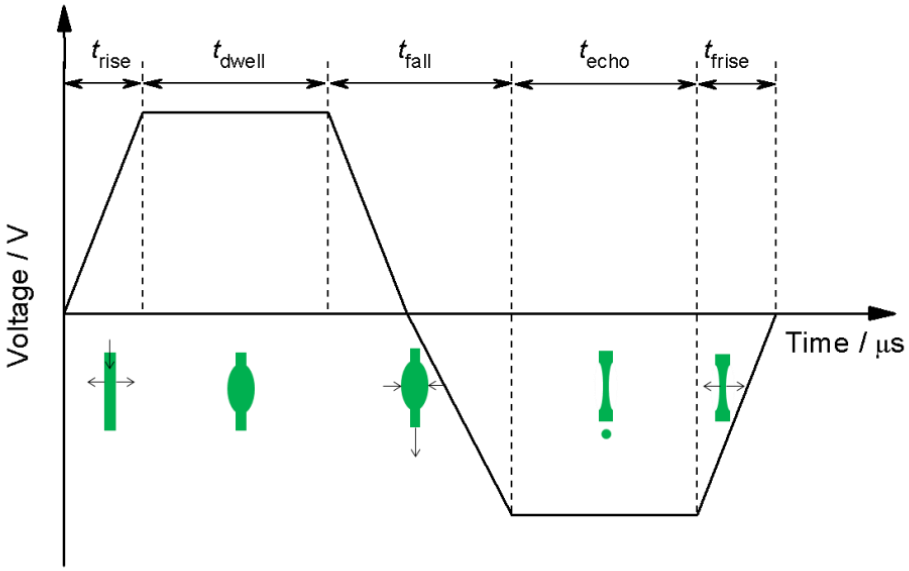

Figure 1.17 A typical pressure wave plus generated in piezoelectric DOD printhead and the droplet formation process.

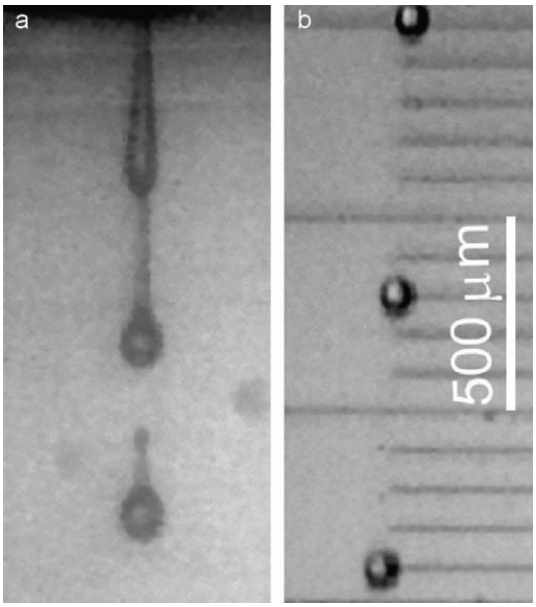

Figure 1.18 Stroboscopic images of the formation of droplets generated during printing. a) droplets formation near orifice; b) droplets in flight [83].

1.3.2 Fundamentals of inkjet printing of polymer solutions

To use inkjet printing, the primary parameters that have to be considered are the physical properties of the solutions, such as viscosity and surface tension [93-95], these two properties are the key factors which affect the behaviours of jetted stream and droplet. The viscosity should be suitable for printing (< 20 mPa·s), high viscosity inks cannot be ejected [94]. Surface tension controls the formation of droplet. Normally, the liquid phases tend to form a spherical shape which has the least surface energy. In order to form a stable spherical droplet for printing, the printing inks should possess suitable surface tensions. It has been demonstrated that the surface tension of inks which ranges from 28 mN m^{-1} to 350 mN m^{-1} can be printed [96]. The Ohnesorge number (*Oh*) which measures the ratio of the viscous and inertial resistances to spreading has been used to predict the printability of an ink (Equation 1.1) [83, 97, 98].

$$Oh = \frac{\eta}{\sqrt{\rho d \sigma}} \qquad 1.1$$

Where η is the viscosity, ρ is the density and σ is the surface tension of the ink, while d is the diameter of the orifice. In some literatures, Z (1/*Oh*) has been used to predict the printability of an ink [94, 98]. Researchers have found inks with $1 < Z < 10$ are commonly acceptable for printing [67, 83]. However, other work [99, 100] has reported that inks outside of this region are printable, suggesting that a high value of Z may not be a significant problem. This is because the Z number is an empirical calculation and based on Newtonian fluids. As the viscosity which is used to calculate the Z number is measured as a Newtonian fluid without subjecting any force, but the actual viscosity of a polymer solution jetted out of a nozzle may well not be as same as the measured one due to the shearing effect during jetting polymer solution. When polymer solution is jetted from a nozzle, the polymer chains are subjected to shear force which stretches the polymer chains from free coils to rearranged chains orientated to the shear direction [101]. Thus, the viscosity of polymer solution during jetting is different from the measured one, resulting in different Z numbers of polymer solutions during printing.

Polymer concentration and weight are also effects which can significantly influence the formation of jetted droplets and jetting process. Coil overlap concentration, C^*, is the point at which individual polymer chains in solution are just in contact. Four regimes are defined

in terms of droplet formation [96]. Regime I: low polymer concentration and/or weight, the filament is relatively long and breaks up to form satellite droplets. At this regime, because of the formation of satellite droplets, the resolution of printing is relatively low; Regime II: increasing polymer concentration and/or molecular weight reduces the formation of satellites at the end of filament; Regime III: further increasing polymer concentration and/or molecular weight can form a single droplet without filament which is ideal for printing, at this regime, the printing resolution is high; Regime IV: at a high polymer concentration and/or molecular weight, no droplet can be ejected from printhead as the viscosity of printing ink is too high to print [102].

Various materials have been used for inkjet printing, such as polymers [66, 81, 100, 103-106], ceramics [80, 107, 108], and metal nanoparticles [68-70, 109-111]. Polymers with a relatively low molecular weight, usually a few hundred g/mol, can be printed as a melt (e.g. melted wax printing). However, high molecular weight polymers (up to 100,000 g/mol) normally need to be dissolved in suitable solvents to form printable solutions. For solutions containing high molecular weight polymer, the concentration and molecular weight of the dissolved polymer determine the printability using DOD inkjet printing [102, 112]. Increasing concentration and/or molecular weight of polymer causes the viscosity of formed solutions increase. As mentioned above, solutions with high viscosity cannot be jetted, therefore, it is important to balance the viscosity and concentration of polymer solutions for inkjet printing.

1.3.3 Applications and limitations

As DOD inkjet printing has a high controllability of droplet placement, and minimizes the amount of materials needed for fabrication, it has been investigated for making a wide range of products which possess desired structures. For example, polymer inkjet printing has been widely used to print polymer light-emitting diode (PLED) displays. To print this display, different coloured electroluminescent polymers are used via individual printhead. Bharathan and Yang [113] fabricated a PLED device using a semiconducting aqueous polymer solution named poly(3,4-ethylenedioxythiophene) (PEDOT) as the printing ink. After printing, the device was spin-coated with an electroluminescent polymer buffer layer, the PEDOT layer

defined the emissive area. Zhang et al. [114] used a thermal DOD inkjet printer to synthesise a degradable polyurethane elastomer which possesses good anticoagulation properties and desired inner-structures.

As mentioned in Section 1.3.2, low molecular weight wax can be printed as a melt. The advantage of printing melted wax is that the solidification of melted wax occurs on the contact with the substrate. Thus, minimum droplet spreading is achieved yielding a fine printing finish. Thus, printing wax has been utilised to print masks for metal layer etching in the area of electronics, and the accuracy of droplet placement can be less than 1 μm [115].

Inkjet printing of polymer is also widely used in tissue engineering on account of its incorporation of computer design, non-contact approaches, precise deposition of material and minimum waste generated. Radulescu et al. [116] reported using inkjet printing to fabricate poly(D,L-lactide-co-ε-caprolactone) copolymer scaffolds for nerve regeneration. The cell test proved that the inkjet printed polymer scaffolds have the potential to be used in nerve repair.

Besides inkjet printing of polymer, nanoparticles/tubes has also been printed using inkjet printing. Walther et al. [117] used a piezoelectric DOD printer to print terahertz metamaterials using 20 wt.% suspension of silver nanoparticles as shown in Figure 1.19. Meier et al. [70] successfully used the same technique to print conductive silver lines with 25 μm width. A similar work was undertook by Schubert et al. [111] which showed silver lines fabricated using piezoelectric DOD inkjet printing have conductivity up to 23% of bulk silver. These researches indicate that the DOD inkjet printing can be applied as a method for manufacturing integrated electronics. Beyer et al. [118] reported using piezoelectric DOD inkjet printer to print single-wall carbon fibre nanotubes with controlled orientation and alignment as shown in Figure 1.20.

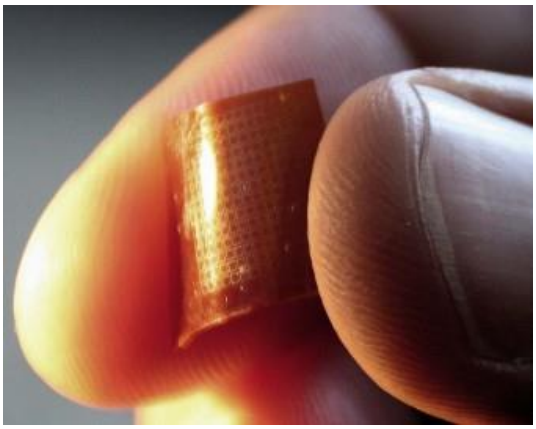

Figure 1.19 Inkjet printed terahertz metamaterial [117].

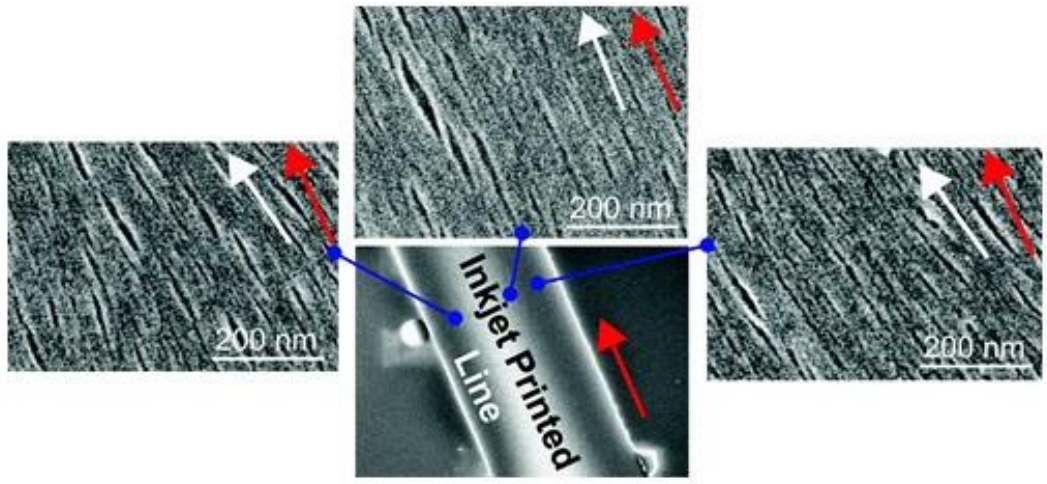

Figure 1.20 Surface morphology of inkjet printed lines with controllable carbon fibre nanotubes' orientations [118].

Although inkjet printing has been prevalently used to print text and pictures, and is increasingly used as a manufacturing method, its limitations are also need to be considered when employing it as a new fabrication route. Firstly, the printing inks should possess low viscosity in order to be jetted, therefore, solid materials either need to be melted or dissolved in solvent to enable a suitable viscosity for printing. For example, solid polymers usually need to be dissolved in suitable solvents to form printable solutions, and therefore, the polymer concentration/loading in solutions is usually low. Secondly, the resolution of inkjet

printed features depends on a verity of factors such as the accuracy of droplet deposition and the drying/solidification process after droplet printed on the substrate. As a result, the resolution of direct inkjet printed features is limited to a few tens of micrometres [119]. A better understanding and control of wettability of inks on different substrates will be helpful to increase the resolution.

1.4 Summary

Fibre reinforced composites are increasingly used to make high performance structures in aerospace or automotive industries due to their high specific strength and high specific modulus, which can lead to significant weight reductions. The aerospace industry has employed these promising materials into their commercial product to increase the fuel efficiency.

The major obstacle of applying these materials to more mechanically challenging areas such as primary structures of aeroplane is their susceptibility to delamination. Delamination is the most common failure in composite structures, and may result from various factors such as defects during manufacturing, impurities and mechanical damages during service. The brittle nature of epoxy matrix means the reinforced composites have low resistance to mechanical damages such as impact. Delamination starts from microcracks or barely visible impact damage (BVID) in composite structures. Unfortunately, the early stage of delamination is difficult to be detected. Therefore, it is difficult for engineers to identify the microcracked structures promptly, which can lead to catastrophic failure.

The development of toughened composites has a great potential for increasing the efficient applications of composite materials. Matrix toughening, stitching and interleaving are the most investigated toughening methods. All the toughening methods offer improvements in mechanical properties such as fracture toughness, impact resistance and compression after impact to some extent. However, applications of these methods to composites have commonly been accompanied by problems such as reduction in modulus and interlaminar strength.

Inkjet printing has been explored as a manufacturing technique due to its ability to precisely print patterned droplets according to predefined patterns without masks. The direct write ability of inkjet printing makes it an attractive method for various applications. As inkjet printing is a non-contact process, contamination is minimised. Additionally, the simplified fabrication processes and minimum waste generation of inkjet printing are advantages over conventional fabrication methods. The main consideration for using inkjet printing is in the physical properties of inks. Viscosity and surface tension are the most important factors which determine the printability of inks. Although inkjet printing has a promising potential which can be used in various applications, further researches need to be conducted to optimise its current limitations.

1.5 Scope and objectives of thesis

The use of thermoplastic polymers as toughening materials has been proven to be an effective method to toughen CFRP. Since the delamination tends to form between laminate plies, toughening materials are ideally placed onto the cracks favoured sites as a second phase to arrest crack propagation. The prevalent method of introducing a thermoplastic second phase are either adding thermoplastics into to the bulk matrix (matrix toughening) or inserting a toughening materials contained thin film between laminate plies co-curing with prepregs (interleaving). However, the matrix toughening is usually restricted to a low cross-linking density resin system, and the interleaving struggles to create an evenly distributed and constant morphology of the toughening materials. Moreover, the mechanical benefits are usually accompanied by other compromises, such as reduction in interlaminar shear strength.

Taking the abovementioned advantages of inkjet printing, it was interesting to employ inkjet printing to print discrete polymer deposits between laminate interfaces to improve the fracture toughness of modified CFRP laminates. Inkjet printing is capable of depositing highly dimension and volume controllable droplets onto targeted substrates. This also allows for much larger surface coverage of the toughening materials to be deposited onto wanted places without causing an uncontrollable formation of toughener between laminate plies.

To conduct the printing, the printability of polymer solutions (inks) needs to be characterised as reported in Chapter 3. The printer parameter settings and the efficiency of toughening

material usage is also described. In Chapter 4 and 5, the effect of different polymers, polymer loadings in printing solutions and different patterns on the mechanical performances are discussed based on the mechanical test results. The toughening mechanisms are discussed based on the observation of fracture surfaces of mechanically tested laminates and polymer deposits' formation surrounded by epoxy resin after heating. The thesis concludes in Chapter 6 by summarising the main results of this research together with a discussion of future research directions.

References

[1] D. Hull and T. Clyne, "An introduction to composite materials," *Cambridge university press*, 1996.

[2] ACSNHC. Landmarks, "High Performance Carbon Fibers," Accessed on 09/09/2013. Available:http://www.acs.org/content/acs/en/education/whatischemistry/landmarks/carbonfibers.html

[3] L. Pilato and M. Michno, "High Performance Fibers," in *Advanced Composite Materials*, ed: Springer Berlin Heidelberg, pp. 75-96, 1994.

[4] W. J. Cantwell and J. Morton, "The impact resistance of composite materials — a review," *Composites*, vol. 22, pp. 347-362, 1991.

[5] J. Summerscales and D. Short, "Carbon fibre and glass fibre hybrid reinforced plastics," *Composites*, vol. 9, pp. 157-166, 1978.

[6] P. Wambua, J. Ivens, and I. Verpoest, "Natural fibres: can they replace glass in fibre reinforced plastics?," *Composites Science and Technology*, vol. 63, pp. 1259-1264, 2003.

[7] A. P. Mouritz, C. Baini, and I. Herszberg, "Mode I interlaminar fracture toughness properties of advanced textile fibreglass composites," *Composites Part A: Applied Science and Manufacturing*, vol. 30, pp. 859-870, 1999.

[8] G. Dorey, G. R. Sidey, and J. Hutchings, "Impact properties of carbon fibre/Kevlar 49 fibre hydrid composites," *Composites*, vol. 9, pp. 25-32, 1978.

[9] P. K. Mallick, "Fibre-Reinforced Composites: Materials, Manufacturing, and Design," *CRC Press*, 2008.

[10] K. G. Satyanarayana, K. Sukumaran, P. S. Mukherjee, C. Pavithran, and S. G. K. Pillai, "Natural fibre-polymer composites," *Cement and Concrete Composites*, vol. 12, pp. 117-136, 1990.

[11] D. N. Saheb and J. Jog, "Natural fiber polymer composites: a review," *Advances in polymer technology*, vol. 18, pp. 351-363, 1999.

[12] S. Mishra, A. K. Mohanty, L. T. Drzal, M. Misra, S. Parija, S. K. Nayak, *et al.*, "Studies on mechanical performance of biofibre/glass reinforced polyester hybrid composites," *Composites Science and Technology*, vol. 63, pp. 1377-1385, 2003.

[13] H. N. Dhakal, Z. Y. Zhang, and M. O. W. Richardson, "Effect of water absorption on the mechanical properties of hemp fibre reinforced unsaturated polyester composites," *Composites Science and Technology,* vol. 67, pp. 1674-1683, 2007.

[14] A. K. Bledzki and J. Gassan, "Composites reinforced with cellulose based fibres," *Progress in Polymer Science,* vol. 24, pp. 221-274, 1999.

[15] C. Soutis, "Fibre reinforced composites in aircraft construction," *Progress in Aerospace Sciences,* vol. 41, pp. 143-151, 2005.

[16] A. Kelly, "Concise encyclopaedia of composite materials," *New York: Pergamon,* 1994.

[17] A. B. Strong, "Fundamentals of composites manufacturing: materials, methods and applications," *SMe*, 2008.

[18] G. Vunjak Novakovic and Wozney, "The fundamentals of tissue engineering: Scaffolds and bioreactors," *Novartis Found Symp,* vol. 249, pp. 34-51, 2003.

[19] C. Soutis, "Carbon fiber reinforced plastics in aircraft construction," *Materials Science and Engineering: A,* vol. 412, pp. 171-176, 2005.

[20] J. L. Thomason, "The interface region in glass fibre-reinforced epoxy resin composites: 1. Sample preparation, void content and interfacial strength," *Composites,* vol. 26, pp. 467-475, 1995.

[21] H. Albertsen, J. Ivens, P. Peters, M. Wevers, and I. Verpoest, "Interlaminar fracture toughness of CFRP influenced by fibre surface treatment: Part 1. Experimental results," *Composites Science and Technology,* vol. 54, pp. 133-145, 1995.

[22] J. George, M. Sreekala, and S. Thomas, "A review on interface modification and characterization of natural fiber reinforced plastic composites," *Polymer Engineering & Science,* vol. 41, pp. 1471-1485, 2001.

[23] F. L. Matthews and R. D. Rawlings, "Composite materials: engineering and science," *Elsevier*, 1999.

[24] I. Hamerton, "Recent developments in epoxy resins," *iSmithers Rapra Publishing*, vol. 91, 1996.

[25] B. L. Denq, Y. S. Hu, L. W. Chen, W. Y. Chiu, and T. R. Wu, "The curing reaction and physical properties of DGEBA/DETA epoxy resin blended with propyl ester phosphazene," *Journal of Applied Polymer Science,* vol. 74, pp. 229-237, 1999.

[26] H. A. Rijsdijk, M. Contant, and A. A. J. M. Peijs, "Continuous-glass-fibre-reinforced polypropylene composites: I. Influence of maleic-anhydride-modified polypropylene on mechanical properties," *Composites Science and Technology,* vol. 48, pp. 161-172, 1993.

[27] M. van den Oever and T. Peijs, "Continuous-glass-fibre-reinforced polypropylene composites II. Influence of maleic-anhydride modified polypropylene on fatigue behaviour," *Composites Part A: Applied Science and Manufacturing,* vol. 29, pp. 227-239, 1998.

[28] C. May, "Epoxy resins: chemistry and technology," *CRC Press*, 1987.

[29] K. Diamanti and C. Soutis, "Structural health monitoring techniques for aircraft composite structures," *Progress in Aerospace Sciences,* vol. 46, pp. 342-352, 2010.

[30] S. H. Lee, J. S. Jeong, Y. S. Lee, and S. K. Cheong, "Interlaminar fracture toughness characteristics of hybrid laminates with nonwoven carbon tissue under severe temperature conditions," *Journal of Composite Materials,* vol. 47, pp. 1865-1875, 2013.

[31] N. Sela and O. Ishai, "Interlaminar fracture toughness and toughening of laminated composite materials: a review," *Composites,* vol. 20, pp. 423-435, 1989.

[32] K. Diamanti, J. M. Hodgkinson, and C. Soutis, "Detection of Low-velocity Impact Damage in Composite Plates using Lamb Waves," *Structural Health Monitoring,* vol. 3, pp. 33-41, 2004.

[33] B. C. Kim, S. W. Park, and D. G. Lee, "Fracture toughness of the nano-particle reinforced epoxy composite," *Composite structures,* vol. 86, pp. 69-77, 2008.

[34] T. Yokozeki, Y. Iwahori, M. Ishibashi, T. Yanagisawa, K. Imai, M. Arai, *et al.*, "Fracture toughness improvement of CFRP laminates by dispersion of cup-stacked carbon nanotubes," *Composites Science and Technology,* vol. 69, pp. 2268-2273, 2009.

[35] J. Shi, B. Li, and T. Yen, "Mechanical properties of Al2O3 particle-Y-TZP matrix composite and its toughening mechanism," *Journal of Materials Science,* vol. 28, pp. 4019-4022, 1993.

[36] Y. Zeng, H. Y. Liu, Y. W. Mai, and X. S. Du, "Improving interlaminar fracture toughness of carbon fibre/epoxy laminates by incorporation of nano-particles," *Composites Part B: Engineering,* vol. 43, pp. 90-94, 2012.

[37] R. A. Pearson and A. F. Yee, "Influence of particle size and particle size distribution on toughening mechanisms in rubber-modified epoxies," *Journal of Materials Science,* vol. 26, pp. 3828-3844, 1991.

[38] A. C. Garg and Y. W. Mai, "Failure mechanisms in toughened epoxy resins—A review," *Composites Science and Technology,* vol. 31, pp. 179-223, 1988.

[39] H. Miyagawa, R. J. Jurek, A. K. Mohanty, M. Misra, and L. T. Drzal, "Biobased epoxy/clay nanocomposites as a new matrix for CFRP," *Composites Part A: Applied Science and Manufacturing,* vol. 37, pp. 54-62, 2006.

[40] H. Masaki, O. Shojiro, C. G. Gustafson, and T. Keisuke, "Effect of matrix resin on delamination fatigue crack growth in CFRP laminates," *Engineering Fracture Mechanics,* vol. 49, pp. 35-47, 1994.

[41] J. Scott and D. Phillips, "Carbon fibre composites with rubber toughened matrices," *Journal of Materials Science,* vol. 10, pp. 551-562, 1975.

[42] N. Chikhi, S. Fellahi, and M. Bakar, "Modification of epoxy resin using reactive liquid (ATBN) rubber," *European Polymer Journal,* vol. 38, pp. 251-264, 2002.

[43] R. A. Pearson and A. F. Yee, "Toughening mechanisms in elastomer-modified epoxies," *Journal of Materials Science,* vol. 24, pp. 2571-2580, 1989.

[44] T. K. Chen and H. J. Shy, "Effects of matrix ductility on rubber/matrix interfacially modified epoxy resins," *Polymer,* vol. 33, pp. 1656-1663, 1992.

[45] J. M. Scott, G. M. Wells, and D. C. Phillips, "Low temperature crack propagation in an epoxide resin," *Journal of Materials Science,* vol. 15, pp. 1436-1448, 1980.

[46] T. Hsieh, A. Kinloch, K. Masania, A. Taylor, and S. Sprenger, "The mechanisms and mechanics of the toughening of epoxy polymers modified with silica nanoparticles," *Polymer,* vol. 51, pp. 6284-6294, 2010.

[47] Y. Tang, L. Ye, D. Zhang, and S. Deng, "Characterization of transverse tensile, interlaminar shear and interlaminate fracture in CF/EP laminates with 10 wt% and 20 wt% silica nanoparticles in matrix resins," *Composites Part A: Applied Science and Manufacturing,* vol. 42, pp. 1943-1950, 2011.

[48] C. B. Bucknall and A. H. Gilbert, "Toughening tetrafunctional epoxy resins using polyetherimide," *Polymer,* vol. 30, pp. 213-217, 1989.

[49] R. A. Pearson and A. F. Yee, "Toughening mechanisms in thermoplastic-modified epoxies: 1. Modification using poly (phenylene oxide)," *Polymer,* vol. 34, pp. 3658-3670, 1993.

[50] B. Cardwell and A. F. Yee, "Toughening of epoxies through thermoplastic crack bridging," *Journal of materials science,* vol. 33, pp. 5473-5484, 1998.

[51] E. Woo and K. Mao, "Interlaminar morphology effects on fracture resistance of amorphous polymer-modified epoxy/carbon fibre composites," *Composites Part A: Applied Science and Manufacturing,* vol. 27, pp. 625-631, 1996.

[52] K. Dransfield, C. Baillie, and Y. W. Mai, "Improving the delamination resistance of CFRP by stitching—a review," *Composites Science and Technology,* vol. 50, pp. 305-317, 1994.

[53] K. A. Dransfield, L. K. Jain, and Y. W. Mai, "On the effects of stitching in CFRPs—I. mode I delamination toughness," *Composites Science and Technology,* vol. 58, pp. 815-827, 1998.

[54] F. Larsson, "Damage tolerance of a stitched carbon/epoxy laminate," *Composites Part A: Applied Science and Manufacturing,* vol. 28, pp. 923-934, 1997.

[55] A. Yoshimura, T. Nakao, S. Yashiro, and N. Takeda, "Improvement on out-of-plane impact resistance of CFRP laminates due to through-the-thickness stitching," *Composites Part A: Applied Science and Manufacturing,* vol. 39, pp. 1370-1379, 2008.

[56] A. Mouritz, K. Leong, and I. Herszberg, "A review of the effect of stitching on the in-plane mechanical properties of fibre-reinforced polymer composites," *Composites Part A: Applied Science and Manufacturing,* vol. 28, pp. 979-991, 1997.

[57] Y. Wang and T. H. Hahn, "AFM characterization of the interfacial properties of carbon fiber reinforced polymer composites subjected to hygrothermal treatments," *Composites Science and Technology,* vol. 67, pp. 92-101, 2007.

[58] M. Arai, Y. Noro, K. I. Sugimoto, and M. Endo, "Mode I and mode II interlaminar fracture toughness of CFRP laminates toughened by carbon nanofiber interlayer," *Composites Science and Technology,* vol. 68, pp. 516-525, 2008.

[59] K. L. White and H. J. Sue, "Delamination toughness of fiber-reinforced composites containing a carbon nanotube/polyamide-12 epoxy thin film interlayer," *Polymer,* vol. 53, pp. 37-42, 2012.

[60] M. Hojo, T. Ando, M. Tanaka, T. Adachi, S. Ochiai, and Y. Endo, "Modes I and II interlaminar fracture toughness and fatigue delamination of CF/epoxy laminates with self-same epoxy interleaf," *International Journal of Fatigue,* vol. 28, pp. 1154-1165, 2006.

[61] S. Hamer, H. Leibovich, A. Green, R. Intrater, R. Avrahami, E. Zussman, *et al.*, "Mode I interlaminar fracture toughness of Nylon 66 nanofibrilmat interleaved carbon/epoxy laminates," *Polymer Composites,* vol. 32, pp. 1781-1789, 2011.

[62] G. Williams, R. Trask, and I. Bond, "A self-healing carbon fibre reinforced polymer for aerospace applications," *Composites Part A: Applied Science and Manufacturing,* vol. 38, pp. 1525-1532, 2007.

[63] J. W. C. Pang and I. P. Bond, "A hollow fibre reinforced polymer composite encompassing self-healing and enhanced damage visibility," *Composites Science and Technology,* vol. 65, pp. 1791-1799, 2005.

[64] E. N. Brown, N. R. Sottos, and S. R. White, "Fracture testing of a self-healing polymer composite," *Experimental Mechanics,* vol. 42, pp. 372-379, 2002.

[65] J. Pora, "Composite materials in the airbus A380–from history to future," *Proceedings of ICCM13, Plenary lecture, CD-ROM,* 2001.

[66] E. Tekin, P. J. Smith, S. Hoeppener, A. M. J. van den Berg, A. S. Susha, A. L. Rogach, *et al.*, "Inkjet printing of luminescent CdTe nanocrystal-polymer composites," *Advanced Functional Materials,* vol. 17, 2007.

[67] J. T. Delaney, P. J. Smith, and U. S. Schubert, "Inkjet printing of proteins," *Soft Matter,* vol. 5, pp. 4866-4877, 2009.

[68] J. Perelaer, B. J. de Gans, and U. S. Schubert, "Ink-jet Printing and Microwave Sintering of Conductive Silver Tracks," *Advanced Materials,* vol. 18, pp. 2101-2104, 2006.

[69] M. Grouchko, A. Kamyshny, and S. Magdassi, "Formation of air-stable copper-silver core-shell nanoparticles for inkjet printing," *Journal of Materials Chemistry,* vol. 19, pp. 3057-3062, 2009.

[70] H. Meier, U. Löffelmann, D. Mager, P. J. Smith, and J. G. Korvink, "Inkjet printed, conductive, 25 μm wide silver tracks on unstructured polyimide," *physica status solidi (a),* vol. 206, pp. 1626-1630, 2009.

[71] Y. Zhang, C. Tse, D. Rouholamin, and P. Smith, "Scaffolds for tissue engineering produced by inkjet printing," *Central European Journal of Engineering,* vol. 2, pp. 325-335, 2012.

[72] T. Boland, T. Xu, B. Damon, and X. Cui, "Application of inkjet printing to tissue engineering," *Biotechnology journal,* vol. 1, pp. 910-917, 2006.

[73] K. Cai, H. Dong, C. Chen, L. Yang, K. D. Jandt, and L. Deng, "Inkjet printing of laminin gradient to investigate endothelial cellular alignment," *Colloids and Surfaces B: Biointerfaces,* vol. 72, pp. 230-235, 2009.

[74] C. Cook, T. Wang, and B. Derby, "Inkjet printing of enzymes for glucose biosensors," pp. 103-109, 2009.

[75] X. Cui and T. Boland, "Human microvasculature fabrication using thermal inkjet printing technology," *Biomaterials,* vol. 30, pp. 6221-6227, 2009.

[76] X. Cui, D. Dean, Z. M. Ruggeri, and T. Boland, "Cell damage evaluation of thermal inkjet printed Chinese hamster ovary cells," *Biotechnology and Bioengineering,* vol. 106, pp. 963-969, 2010.

[77] B. Derby, "Bioprinting: Inkjet printing proteins and hybrid cell-containing materials and structures," *Journal of Materials Chemistry,* vol. 18, pp. 5717-5721, 2008.

[78] M. Di Biase, R. E. Saunders, N. Tirelli, and B. Derby, "Inkjet printing and cell seeding thermoreversible photocurable gel structures," *Soft Matter,* vol. 7, pp. 2639-2646, 2011.

[79] A. Doraiswamy, T. M. Dunaway, J. J. Wilker, and R. J. Narayan, "Inkjet printing of bioadhesives," *Journal of Biomedical Materials Research - Part B Applied Biomaterials,* vol. 89, pp. 28-35, 2009.

[80] J. Ebert, E. Özkol, A. Zeichner, K. Uibel, Ö. Weiss, U. Koops, *et al.*, "Direct Inkjet Printing of Dental Prostheses Made of Zirconia," *Journal of Dental Research,* vol. 88, pp. 673-676, 2009.

[81] Y. Zhang, J. Stringer, R. Grainger, P. J. Smith, and A. Hodzic, "Improvements in carbon fibre reinforced composites by inkjet printing of thermoplastic polymer patterns," *physica status solidi (RRL) – Rapid Research Letters,* vol. 8, pp. 56-60, 2014.

[82] Y. Zhang, J. Stringer, R. Grainger, P. J. Smith, and A. Hodzic, "Fabrication of patterned thermoplastic microphases between composite plies by inkjet printing," *Journal of Composite Materials*, vol. 0, pp. 1-7, 2014.

[83] R. E. Saunders, J. E. Gough, and B. Derby, "Delivery of human fibroblast cells by piezoelectric drop-on-demand inkjet printing," *Biomaterials*, vol. 29, pp. 193-203, 2008.

[84] RIOT, "Inkjet," *Image Permanence Institute*, accessed on 07/08/2012. Available: http://www.dp3project.org/technologies/digital-printing/inkjet

[85] D. B. Hall, P. Underhill, and J. M. Torkelson, "Spin coating of thin and ultrathin polymer films," *Polymer Engineering & Science*, vol. 38, pp. 2039-2045, 1998.

[86] K. Tan, C. Chua, K. Leong, C. Cheah, P. Cheang, M. A. Bakar, *et al.*, "Scaffold development using selective laser sintering of polyetheretherketone–hydroxyapatite biocomposite blends," *Biomaterials*, vol. 24, pp. 3115-3123, 2003.

[87] J. M. Williams, A. Adewunmi, R. M. Schek, C. L. Flanagan, P. H. Krebsbach, S. E. Feinberg, *et al.*, "Bone tissue engineering using polycaprolactone scaffolds fabricated via selective laser sintering," *Biomaterials*, vol. 26, pp. 4817-4827, 2005.

[88] C. Z. Jun Xu, and Chun Fu, "Novel method for printing high-quality metal wires," *ed. Micro/Nano Lithography*, 2007.

[89] N. E. Fedorovich, J. Alblas, W. E. Hennink, F. C. Öner, and W. J. A. Dhert, "Organ printing: The future of bone regeneration?," *Trends in Biotechnology*, vol. 29, pp. 601-606, 2011.

[90] F. Marga, K. Jakab, C. Khatiwala, B. Shephard, S. Dorfman, and G. Forgacs, "Organ printing: A novel tissue engineering paradigm," pp. 27-30, 2011.

[91] "Thermal drop-on-demand inkjet printing", *webpage of Manchester university*, accessed on 15/03/2014. Available: http://www.eps.manchester.ac.uk/our-research/research-facilities/digital-fabrication/about-us/about-printing/

[92] L. Li, M. Saedan, W. Feng, J. Y. H. Fuh, Y. S. Wong, H. T. Loh, *et al.*, "Development of a multi-nozzle drop-on-demand system for multi-material dispensing," *Journal of Materials Processing Technology*, vol. 209, pp. 4444-4448, 2009.

[93] A. M. J. van den Berg, P. J. Smith, J. Perelaer, W. Schrof, S. Koltzenburg, and U. S. Schubert, "Inkjet printing of polyurethane colloidal suspensions," *Soft Matter*, vol. 3, 2007.

[94] P. Calvert, "Inkjet printing for materials and devices," *Chemistry of Materials,* vol. 13, pp. 3299-3305, 2001.

[95] M. J. Mondrinos, R. Dembzynski, L. Lu, V. K. C. Byrapogu, D. M. Wootton, P. I. Lelkes, *et al.*, "Porogen-based solid freeform fabrication of polycaprolactone–calcium phosphate scaffolds for tissue engineering," *Biomaterials,* vol. 27, pp. 4399-4408, 2006.

[96] B. J. de Gans, P. C. Duineveld, and U. S. Schubert, "Inkjet printing of polymers: state of the art and future developments," *Advanced Materials,* vol. 16, pp. 203-213, 2004.

[97] J. Perelaer, P. J. Smith, M. M. P. Wijnen, E. van den Bosch, R. Eckardt, P. H. J. M. Ketelaars, *et al.*, "Droplet Tailoring Using Evaporative Inkjet Printing," *Macromolecular Chemistry and Physics,* vol. 210, pp. 387-393, 2009.

[98] M. Singh, H. M. Haverinen, P. Dhagat, and G. E. Jabbour, "Inkjet Printing—Process and Its Applications," *Advanced Materials,* vol. 22, pp. 673-685, 2010.

[99] D. B. van Dam and C. Le Clerc, "Experimental study of the impact of an ink-jet printed droplet on a solid substrate," *Physics of Fluids (1994-present),* vol. 16, pp. 3403-3414, 2004.

[100] J. Perelaer, P. J. Smith, E. van den Bosch, S. S. C. van Grootel, P. H. J. M. Ketelaars, and U. S. Schubert, "The Spreading of Inkjet-Printed Droplets with Varying Polymer Molar Mass on a Dry Solid Substrate," *Macromolecular Chemistry and Physics,* vol. 210, pp. 495-502, 2009.

[101] M. B. Madec, P. J. Smith, A. Malandraki, N. Wang, J. G. Korvink, and S. G. Yeates, "Enhanced reproducibility of inkjet printed organic thin film transistors based on solution processable polymer-small molecule blends," *Journal of Materials Chemistry,* vol. 20, pp. 9155-9160, 2010.

[102] D. Xu, V. Sanchez-Romaguera, S. Barbosa, W. Travis, J. de Wit, P. Swan, *et al.*, "Inkjet printing of polymer solutions and the role of chain entanglement," *Journal of Materials Chemistry,* vol. 17, pp. 4902-4907, 2007.

[103] B. J. de Gans and U. S. Schubert, "Inkjet Printing of Well-Defined Polymer Dots and Arrays," *Langmuir,* vol. 20, pp. 7789-7793, 2004.

[104] R. K. Khillan, Y. Su, and K. Varahramyan, "High resolution polymer LEDs fabricated by drop-on-demand inkjet printing and reactive ion etching," pp. 59-65, 2005.

[105] P. Krober, J. T. Delaney, J. Perelaer, and U. S. Schubert, "Reactive inkjet printing of polyurethanes," *Journal of Materials Chemistry*, vol. 19, pp. 5234-5238, 2009.

[106] E. Tekin, P. J. Smith, and U. S. Schubert, "Inkjet printing as a deposition and patterning tool for polymers and inorganic particles," *Soft Matter*, vol. 4, pp. 703-713, 2008.

[107] B. Derby, "Inkjet printing ceramics: from drops to solid," *Journal of the European Ceramic Society*, vol. 31, pp. 2543-2550, 2011.

[108] B. Derby and N. Reis, "Inkjet printing of highly loaded particulate suspensions," *Mrs Bulletin*, vol. 28, pp. 815-818, 2003.

[109] T. Öhlund, J. Örtegren, S. Forsberg, and H. E. Nilsson, "Paper surfaces for metal nanoparticle inkjet printing," *Applied Surface Science*, vol. 259, pp. 731-739, 2012.

[110] P. J. Smith, D. Y. Shin, J. E. Stringer, B. Derby, and N. Reis, "Direct ink-jet printing and low temperature conversion of conductive silver patterns," *Journal of Materials Science*, vol. 41, pp. 4153-4158, 2006.

[111] T. H. J. van Osch, J. Perelaer, A. W. M. de Laat, and U. S. Schubert, "Inkjet Printing of Narrow Conductive Tracks on Untreated Polymeric Substrates," *Advanced Materials*, vol. 20, pp. 343-345, 2008.

[112] S. D. Hoath, O. G. Harlen, and I. M. Hutchings, "Jetting behavior of polymer solutions in drop-on-demand inkjet printing," *Journal of Rheology (1978-present)*, vol. 56, pp. 1109-1127, 2012.

[113] J. Bharathan and Y. Yang, "Polymer electroluminescent devices processed by inkjet printing: I. Polymer light-emitting logo," *Applied Physics Letters*, vol. 72, pp. 2660-2662, 1998.

[114] C. Zhang, X. Wen, N. R. Vyavahare, and T. Boland, "Synthesis and characterization of biodegradable elastomeric polyurethane scaffolds fabricated by the inkjet technique," *Biomaterials*, vol. 29, pp. 3781-3791, 2008.

[115] W. Wong, S. Ready, R. Matusiak, S. White, J. P. Lu, J. Ho, *et al.*, "Amorphous silicon thin-film transistors and arrays fabricated by jet printing," *Applied physics letters*, vol. 80, pp. 610-612, 2002.

[116] D. Radulescu, S. Dhar, C. M. Young, D. W. Taylor, H. J. Trost, D. J. Hayes, *et al.*, "Tissue engineering scaffolds for nerve regeneration manufactured by ink-jet technology," *Materials Science and Engineering: C*, vol. 27, pp. 534-539, 2007.

[117] M. Walther, A. Ortner, H. Meier, U. Löffelmann, P. J. Smith, and J. G. Korvink, "Terahertz metamaterials fabricated by inkjet printing," *Applied Physics Letters,* vol. 95, 2009.

[118] S. T. Beyer and K. Walus, "Controlled Orientation and Alignment in Films of Single-Walled Carbon Nanotubes Using Inkjet Printing," *Langmuir,* vol. 28, pp. 8753-8759, 2012.

[119] I. M. Hutchings and G. D. Martin, "Inkjet technology for digital fabrication," *John Wiley & Sons*, 2012.

Chapter 2

Experimental

This chapter gives details of the materials and equipment which were involved in the preparation of test samples. Material characterisation methods and mechanical test procedures which were adopted in this project are given. The printing parameters such as pattern dimensions are described.

2.1 Materials

2.1.1 Prepreg

Unidirectional carbon fibre pre-impregnated epoxy (prepreg) tape (CYCOM® 977-2-35-12KHTS-268-300, Cytec, USA) was used to fabricate CFRP laminates for testing. This carbon fibre/epoxy prepreg tape is 0.25 – 0.27 mm thick and 300 mm wide. It is a typical composite material widely used in civil and military aircraft industries. As mentioned in Chapter 1, carbon fibre dominates the load carrying in CFRP laminates, therefore the properties of the carbon fibre is of great importance to the mechanical properties of the final CFRP composite structures. In this specific prepreg, continuous high tensile strength carbon fibres were pre-impregnated unidirectionally into a toughened epoxy resin. Table 2.1 lists typical properties of the carbon fibre pre-impregnated in this prepreg. It can be clearly seen that the carbon fibre embedded in this type of prepreg has high specific strength and specific modulus compared to metallic materials such as aluminium alloy and stainless steel.

Table 2.1 Typical properties of the carbon fibre (in CYCOM® 977-2), aluminium alloy and stainless steel [1, 2].

Properties	Carbon fibre	Aluminium alloy	Stainless steel
Tensile strength / GPa	4.6	0.6	2.0
Specific strength / $kN \cdot mkg^{-1}$	2630	214	253
Elastic modulus / GPa	239	70	210
Specific modulus / $10^6\ m^2s^{-2}$	136	25	27
Average fibre diameter / μm	7.0	/	/
Density / g cm^{-3}	1.8	2.8	7.9

The resin used in CYCOM® 977-2 prepreg is a thermoplastic toughened epoxy resin with a 126 – 138 ℃ dry and 104 ℃ wet service capability. This resin is formulated for autoclave or hot press moulding with a 177 ℃ curing temperature. Typical properties of this toughened resin are shown in Table 2.2.

Table 2.2 Typical properties of CYCOM® 977-2 toughened epoxy resin. (Data was provided by Cytec Engineered Materials Ltd.)

Properties	Values
Tensile strength	81.4 ± 11.0 MPa
Tensile modulus	3.52 ± 0.14 GPa
Flexural strength	197 ± 7 MPa
Flexure modulus	3.45 ± 0.07 GPa
G_{Ic}	478 ± 84 J/m^2
T_g	212 ℃
Density	1.31 g/cm^3

By comparing Table 2.1 and Table 2.2, it can be seen that the mechanical properties of carbon fibre are superior to that of epoxy resin. However, the resin provides important functionalities

to the final composite. It holds the fibres in place to best carry the load and to protect the fibres from the environment. Also, the relatively high T_g of the resin ensures that this type of composite can be used under a relatively high temperature. This is a useful and critical factor as the dimension stability of structures is one of the key criteria that needs to be considered at the design stage.

2.1.2 Epoxy neat resin

Modified epoxy resin (CYCOM® 977-20 RTM resin, Cytec Engineered Materials Ltd., UK) was used to coat 76 mm × 26 mm microscope glass slides (Academy science Ltd., UK) for investigating the morphology of printed polymer deposits surround by epoxy resin before and after heating cycle. All glass slides were used without any pre-treatment. This epoxy resin is formulated as the resin transfer moulding version of Cytec's CYCOM® 977-2 toughened epoxy prepreg resin, it is a liquid clear resin at room temperature, therefore, the printed polymer deposits on this resin coated glass slide can be observed by optical microscope, and also the glass slides can be easily coated with this resin due to its relatively low viscosity.

2.1.3 Polymers and solvents for formulating solutions

2.1.3.1 Polyethylene glycol solutions

Polyethylene glycol (PEG, M_n ~ 20,000, Sigma Aldrich, UK) was dissolved in deionised water. The molecular weight distribution can be characterised by the ratio of polymer's weight average molecular weight (M_w) and its number average molecular weight (M_n), the ratio of which is called the polydispersity index (M_w/M_n). The polydispersity index of PEG (M_n ~ 20,000) is between 1.01 – 1.1 [3]. Pure ethanol (Fisher Scientific, UK) and 1-Propanol (propanol, Fisher Scientific, UK) respectively for printing (concentration varies). PEG can be dissolved in water at room temperature and forms a clear liquid solution (PEGw). A temperature controllable hot plate was used to heat up PEG/ethanol (PEGe) and PEG/propanol (PEGp) solutions to promote the dissolution of PEG. The temperatures used for both solutions was 60 ℃ until PEG was completely dissolved. After PEG had dissolved

in ethanol or propanol completely at elevated temperature, clear liquid solutions were formed. However, when these two solutions cooled down to room temperature, the clear liquid solutions turned to opaque "gels" due to the crystallization of PEG.

2.1.3.2 Poly(methyl methacrylate) solutions

Poly(methyl methacrylate) (PMMA, M_w ~ 15,000, Sigma Aldrich, UK) was dissolved into N,N-Dimethylformamide (DMF) to form printable solutions. The polydispersity index of PMMA typically is between 1.06 – 1.15 [4]. The poly 5 wt.%, 10 wt.% and 20 wt.% PMMA solutions were prepared. Ultrasonic bath was used to help the dissolution of PMMA in DMF at room temperature. The compositions of solutions for printing used in this project are detailed in Table 2.3.

In order to investigate the wetting behaviour of polymer deposits printed on prepreg before and after heating, 0.1 wt.% fluorescein (Sigma Aldrich, UK) was added into 5 wt.% PEG/ethanol solution and 5 wt.% PMMA solution respectively to improve the visibility of printed polymer deposits on prepreg.

Table 2.3 Summary of solutions' compositions.

Solutions	Solution Compositions		
	Solute	wt.%	Solvent
PEGw	PEG	5,10	Deionised water
PEGe	PEG	5	Pure ethanol
PEGp	PEG	5,10	1-Propanol
PMMA	PMMA	5,10,20	DMF

2.1.4 Viscosity and surface tension of solutions

The viscosity of printing solutions were measured at the temperature which was used to conduct the printing. Viscosity of PMMA and PEGw solutions were measured at room temperature, while PEGe and PEGp solutions were measured at 60 ℃. An A&D sine-wave

vibro viscometer (European Instruments, UK) was used to measure the viscosity. A KRÜSS K11 tensiometer (KRÜSS GmbH, Germany) was used to measure the surface tension of these printing solutions.

2.2 Inkjet printer

A drop-on-demand (DOD) inkjet printer (MicroFab IV, MicroFab Inc., USA) as shown in Figure 2.1 was used to conduct the printing works (Low temperature jet was installed). A low temperature piezoelectric printhead (diameter: 60 μm) (MicroFab Inc., USA) (Figure 2.2 (a)) was used to print solutions which can be printed at room temperature. In this work, all PMMA solutions and PEG/deionised water solutions were printed using a low temperature jet and printhead. This DOD single jet dispensing printhead is suited for dispensing droplets of aqueous and solvent-based fluids at up to 50 ℃.

A high temperature jet (polymer jet) (MicroFab Inc., USA) as shown in Figure 2.3 was used to print solutions which need a high temperature to maintain their printability. There are two different temperatures that can be controlled separately by using the high temperature jet. One is the reservoir temperature, and another one is the printhead temperature. In this project PEG/ethanol and PEG/propanol solutions were printed using this high temperature jet. The temperature which was used to control reservoir and printhead temperature were same (60 ℃). The high temperature jet equipped with a high temperature piezoelectric printhead (diameter: 60 μm) (MicroFab Inc., USA) (Figure 2.2, (b)). This DOD single jet dispensing printhead is suited for dispensing droplets of fluids such as adhesives, waxes, polymers and liquid metals up to 250 ℃.

Although PEG and PMMA can be melted below 250 ℃, the viscosities of these two melted polymers are still too high for this DOD printer to print. As mentioned in Chapter 1, the acceptable viscosity of inkjet printing is commonly less than 20 mPa s. Therefore, solvent based fluids are preferred in this work since a low viscosity solution can be obtained for printing. Also, as the droplets are printed onto prepreg in which the resin is still in B stage, high temperature droplets are best avoided to prevent the negative effects of localised high temperature on the B stage epoxy resin.

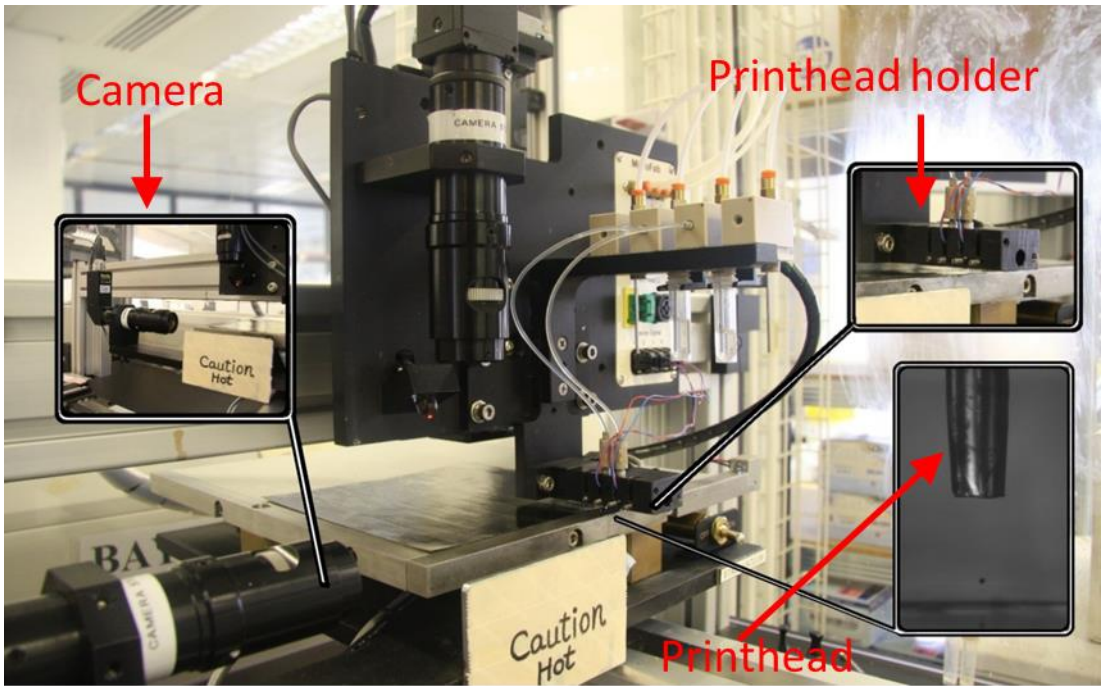

Figure 2.1 DOD piezoelectric inkjet printer used for the experiments.

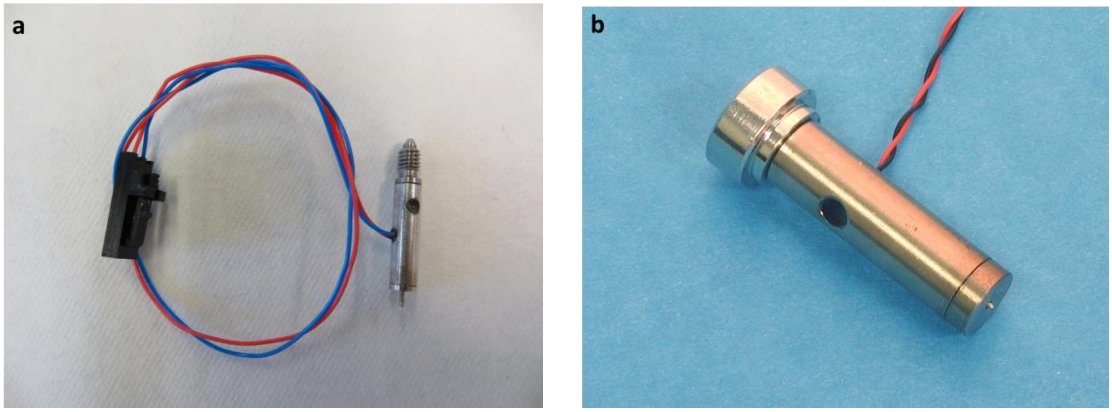

Figure 2.2 Printheads. (a) a low temperature printhead; (b) a high temperature printhead.

Figure 2.3 High temperature jet.

As shown in Figure 2.1, the inkjet printer can dispense up to four different solutions during one experimental session, this ability minimises the down time of changing solutions and reduces the risk of contamination during solution changing process. The printhead holder can hold up to four printheads which can be directly linked to different solution reservoirs, which reduces or eliminates the risk of cross contamination. The temperatures of substrate and printhead holder can be controlled separately.

Figure 2.4 shows the pneumatics controller which is used to control the air pressure applied to the solution reservoirs to push/suck solutions into/from printheads via polytetrafluoroethylene (PTFE) tubes. When the pressure applied to reservoir(s) is positive, the solution(s) will be pushed into printhead(s). When the pressure is negative, the solution will be held or sucked back into reservoir(s) depends on suction pressure.

The printing speed can be scripted as needed. The highest speed for this specific inkjet printer is 50 mm/s. Generally, using a lower printing speed helps to increase the resolution of printed features. However, the printing time is increased as a consequence. Therefore, the printing

speed and time length need to be balanced according to the specific requirements of printing work.

Figure 2.4 Pneumatics controller.

The operation program is designed to drive the printer. A graphical user interface is provided to set the operating parameters for piezoelectric dispensing devices (printheads). Figure 2.5 (left part) is a typical interface which is used to set up jetting parameters before and during printing in order to have an ideal printing condition. Dispensing a stable single droplet from the tip of printhead (Figure 2.5 right part) is of importance to a high resolution printing finish. Otherwise, if the main droplet is accompanied by satellite droplet(s) as shown in Figure 2.6, the printed feature will be interfered with by the satellite droplets. These parameters can be saved and retrieved interactively in a format fully compatible with the printing platforms.

A camera is used to help adjust droplet dispensing. Figure 2.5 (right part) shows the stroboscopic images of the formation of droplets generated during printing. Images can also be used in measuring the diameter of generated droplets with the appearance of ruler (blue scale in the Figure 2.5 right part).

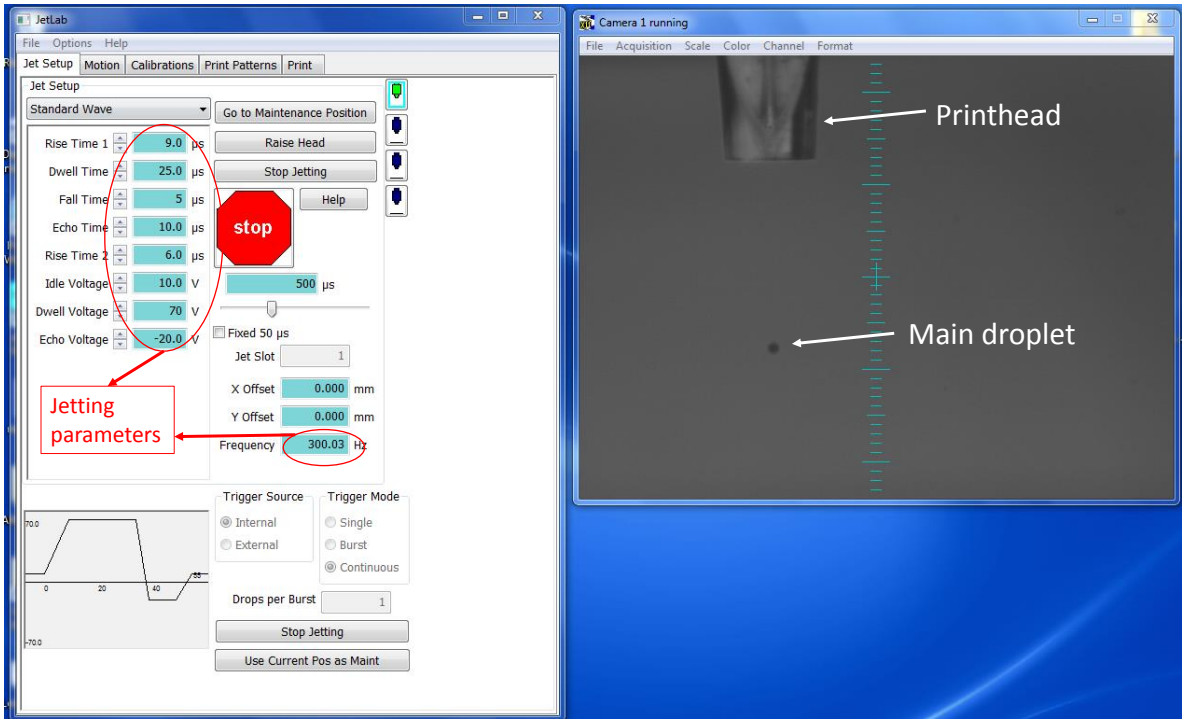

Figure 2.5 A typical interface of MicroFab IV inkjet printer.

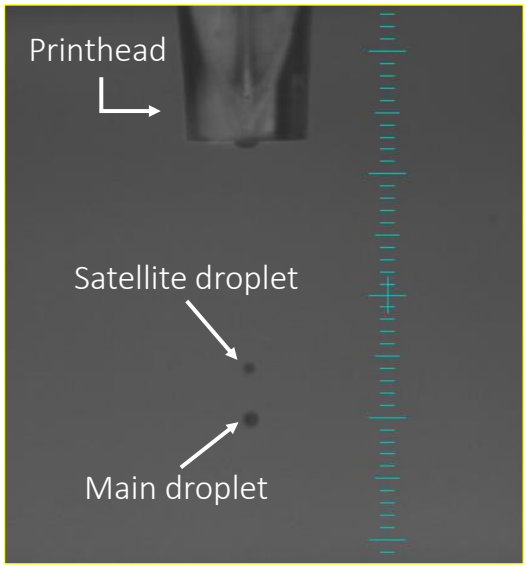

Figure 2.6 Stroboscopic images of the formation of main and satellite droplets generated during printing.

2.3 Printing pattern design

As mentioned in Chapter 1, the patterns used for inkjet printing can be pre-designed according to a user's requirements. Inkjet printing is a flexible printing technique as it can print various patterns and pictures without masks. Figure 2.7 shows the patterns that were designed for this work, *dx* is the distance between the adjacent dots' centres in *x* axis; *dy* is the distance between the adjacent dots' centres in *y* axis. *dx* and *dy* are important parameters for printing, because they are used to determine the size and shape of the pattern to be printed. By decreasing dot spacing (*dx* or/and *dy*), droplets will be more densely packed, and vice versa. When drop spacing is smaller than the diameter of the polymer deposit on the substrate, droplets will be overlapped. For example, when *dx* is smaller than the deposit diameter while *dy* is larger than the deposit droplet, a line pattern can be formed. Pattern density means the surface coverage of polymer deposits in a unit area. It can be seen in Figure 2.8 that same number of droplets deposited in different sizes of unit area, the right one has a higher pattern density.

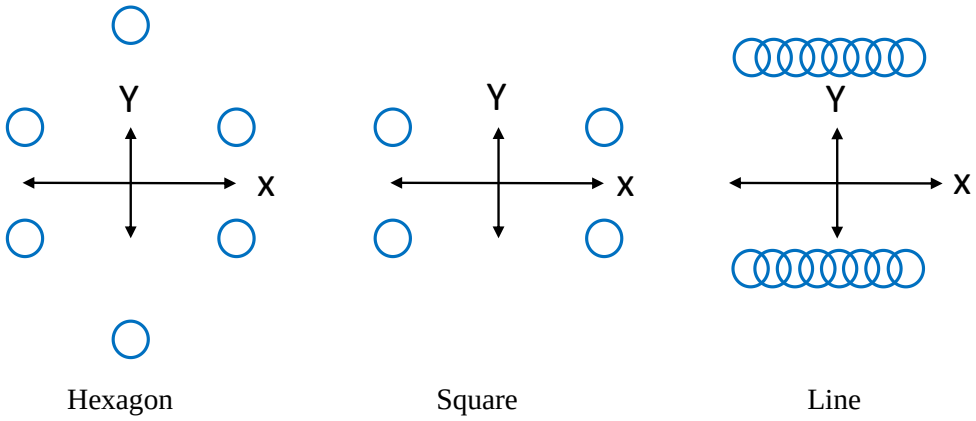

Figure 2.7 Patterns used for printing in this work.

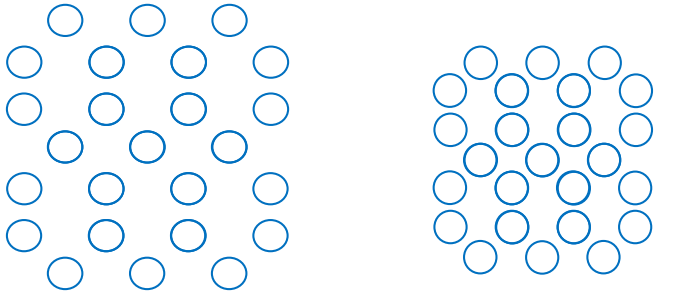

Figure 2.8 Different pattern densities.

Although polymer solutions can be deposited between layers where delamination is prone to occur, the directions which microcracks are going to propagate between laminate plies are not predictable. Therefore, several different patterns, different pattern densities and pattern directions were used to prepare test samples in order to find out the potential effect on the mechanical properties of final CFRP laminates.

2.4 Preparation of neat resin coated glass slides with printed polymer deposits

Neat CYCOM® 977-20 resin was defrosted the day before use. Microscope glass slides were coated with a thin layer of liquid state resin of about 50 μm thickness. All glass slides were used without any pre-treatment. A pre-heat procedure was used to partially cure the coated liquid resin to simulate the B-stage of epoxy in actual CYCOM® 977-2 prepreg. All fresh coated glass slides were heated to 120 ℃ (2 ℃/min) for 2 hours using a temperature controllable oven to achieve this. After heating, the thickness of the resin layer became uneven because the liquid resin tends to contract under high temperature.

PMMA and PEG solutions with various concentrations were used to print several different patterns such as hexagon, lines and continuous films onto the partially cured epoxy coated glass slides. All printed glass slides were left to dry for 24 hours at room temperature before covering with another partially cured epoxy coated glass slide for the subsequent heating.

Figure 2.9 schematically shows the preparation steps of the epoxy coated glass slides with printed polymer deposits.

All "sandwich" samples were then put into a temperature controllable oven to heat up to 160 ℃ (2 ℃/min) for 30 minute with pressure provided by a steel block, then cooling down (2 ℃/min) to room temperature for microscopy analysis. As any change of the morphology of deposited polymer and coated resin occurs when they are both in a low viscosity stage, considering the cross-linking of epoxy, the best temperature range for a good wetting is between 60 – 85°C (suggested by provider). After that point, the epoxy will gradually achieve a quite high viscosity due to cross-linking, which means there is a minimum movement of deposited polymer, therefore, a full curing of the epoxy resin in this experiment is not necessary.

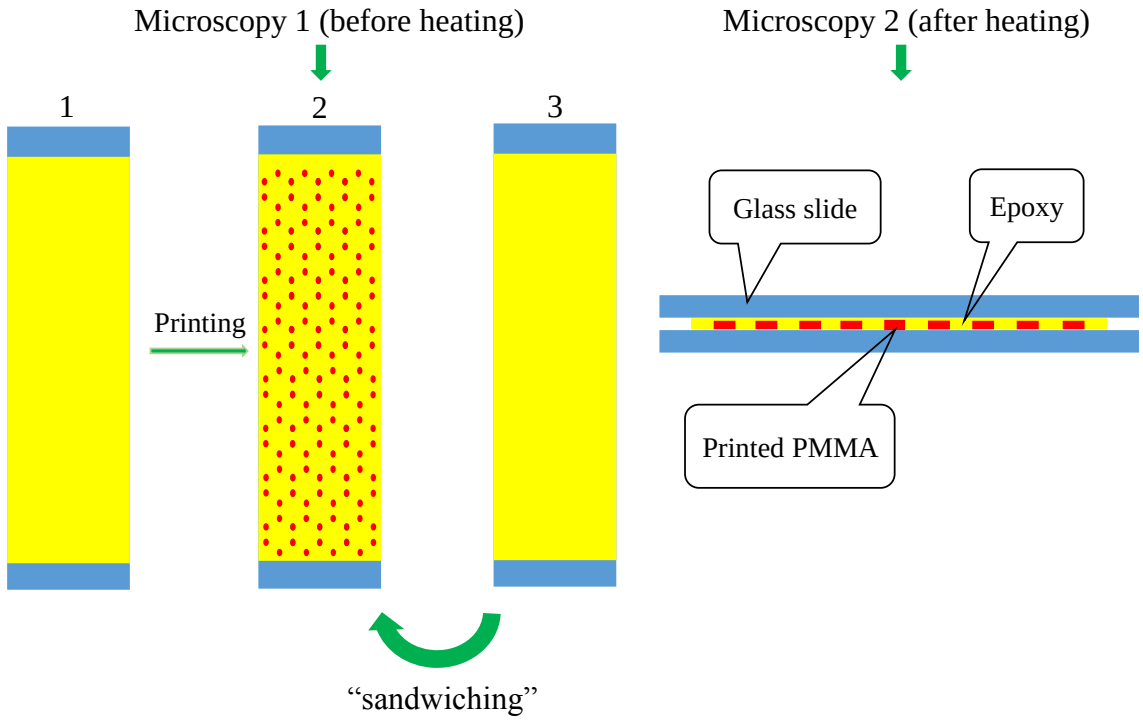

Figure 2.9 Schematically show the preparation of epoxy coated glass slide with inkjet printed polymer deposits.

2.5 Printing on prepreg

Prepreg tape was defrosted in a sealed bag for 12 hours before cutting into 150 × 140 mm and 100 × 100 mm sheets for printing. According to the tests' geometrical requirement, two different sizes of printing areas were printed as shown in Figures 2.10 and 2.11, where *d* shows the trim area after curing. Two different thicknesses of panels were prepared with 8-ply (100 × 100 mm) and 12-ply (150 × 140 mm) of prepreg sheets respectively, and the thickness of these two cured panels were about 2.1 ± 0.1 mm and 3.1 ± 0.1 mm respectively. Within the 8-ply panel, 7 out of 8 prepreg sheets were printed with polymer deposits, which means the every interface between laminate plies contained the printed polymer deposits. For the 12-ply panel, only the mid-plane sheet was printed with polymer deposits as the subsequent test aims to test that specific interface. All fresh printed prepreg were stored in separate tray and sealed in plastic bags to protect the printed patterns. Normally, the printed prepreg sheets were laid up on the following day after printing. Otherwise, the sealed prepreg sheets were stored in freezer until the day before lay-up.

As mentioned in Section 2.2, the speed limitation of this inkjet printer is 50 mm/s. Using a slow printing speed can help to increase the definition of the printed feature at the expense of printing time. Therefore, the printing speed and time length need to be balanced according to the requirements of the experiment and the available time scale. As the printed areas in this work were relatively large, the speed of printing was set as 30 mm/s which was good enough in terms of pattern definition. The time length for printing one prepreg sheet with Figure 2.10 and 2.11 sized area were about 50 min and 40 min respectively.

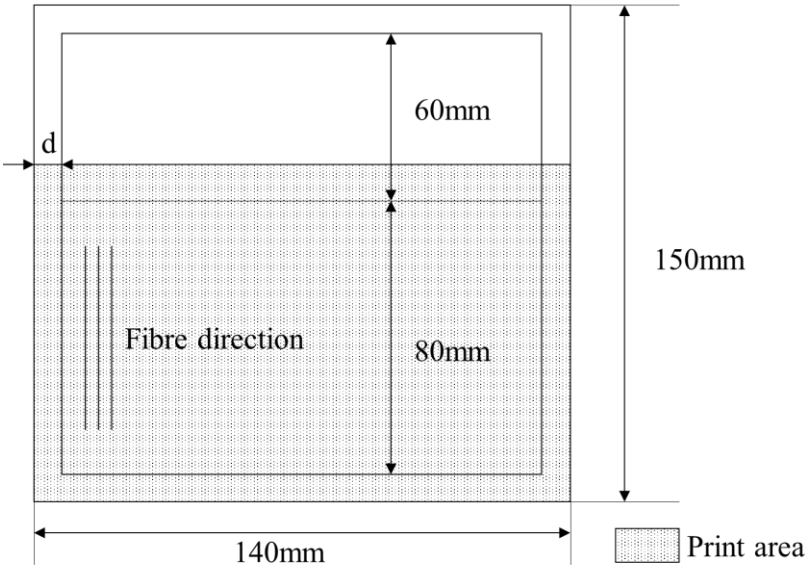

Figure 2.10 Dimensions of printing area for DCB samples.

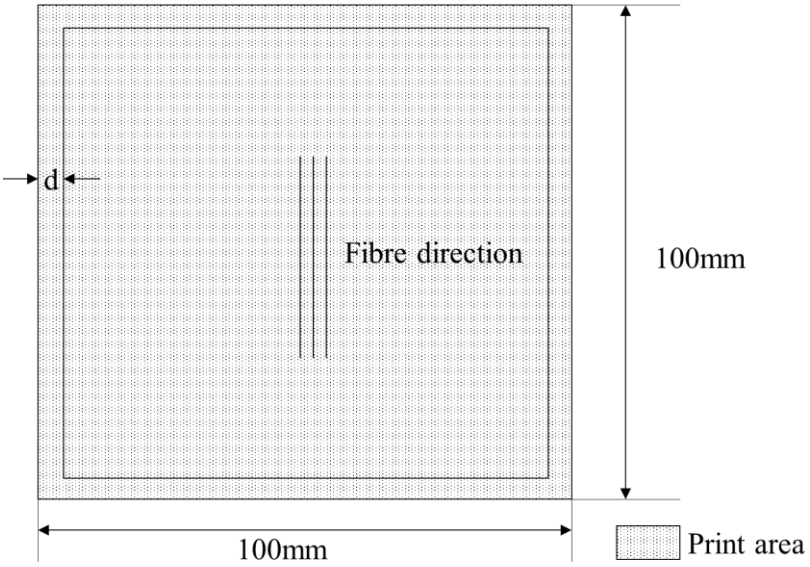

Figure 2.11 Dimensions of printing area for SBS samples.

2.6 Lay-up and curing

All printed prepreg sheets were hand laid up unidirectionally. A blunt plastic tool was used to consolidate the panels during lay-up with the aim of eliminating the air between plies as

much as possible. Then the laid up panels were vacuum bagged before curing in an autoclave (Premier Autoclave Ltd., UK). Figure 2.12 schematically shows the vacuum bag system.

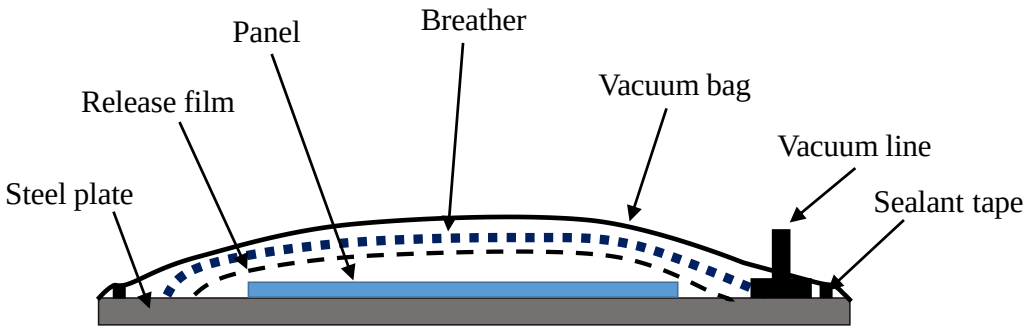

Figure 2.12 Schematic vacuum bag.

Transformation of partially cured epoxy based prepregs into composite laminates involves curing materials at elevated temperatures and pressures for a pre-determined length of time. As the resins of different prepregs vary, they need different curing cycles which include temperature cycles and pressure cycles to make the final composites. For CYCOM® 977-2 carbon fibre reinforced epoxy, Table 2.5 shows the cycles that were used to make the final composite laminates as suggested by the company.

Table 2.4 Curing cycles used to cure laid-up panels.

	Cycle 1: ramp	Cycle 2: dwell	Cycle 3: ramp
Temperature	177 ℃ (2 ℃/min)	180 min	20 ℃ (2 ℃/min)
Pressure	90 psi (5 psi/min)	300 min	0 psi (5 psi/min)

2.7 Mechanical test

2.7.1 Double cantilever beam test

A double cantilever beam (DCB) test standard (BS ISO 15024:2001) [5] was adopted to evaluate the mode I interlaminar fracture toughness (G_{Ic}) of polymer printed CFRP laminates. 5 test samples were wet-cut from each 12-ply cured parent laminate using a diamond saw.

Then, the wet-cut samples were polished with 600 grade SiC sand paper to eliminate the free edge effects. Figure 2.13 shows the sample configuration suggested in the standard, where a polytetrafluoroethylene (PTFE) film was placed inside the laminate's mid-plane during lay-up to simulate a crack.

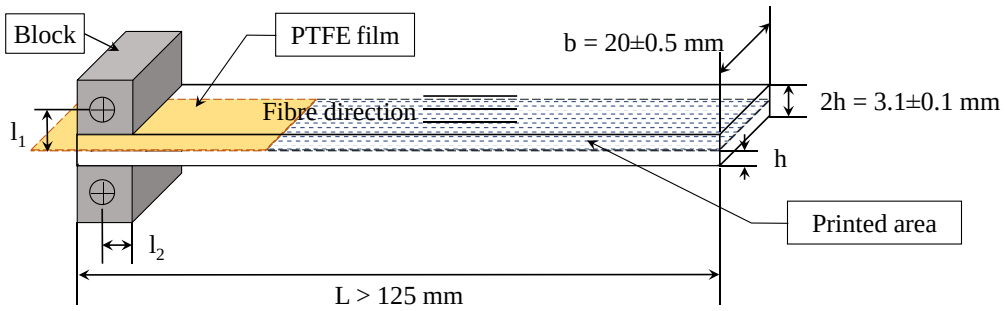

Figure 2.13 Schematic showing a DCB test sample.

The polished test samples were left to dry at room temperature for about 6 hours. After drying, two 11.9 × 11.9 mm centre-drilled aluminium blocks were bonded to each PTFE-insert sample ends using epoxy adhesive (Araldite®, Velcro Ltd., UK) as shown in Figure 2.13. Then epoxy adhesive needs 12 hours to dry and form strong bonding to the samples. In order to make a good contrast for the following test video recording, each sample edge were painted with a white fluid (Tipp-Ex, Société Bic, France). After painting, all samples were left to dry at room temperature for about 15 hours before test.

A tensometer equipped with a 500 N load cell (TA500 Texture Analyser, Lloyd Instruments, UK) was used to conduct the DCB test. The speed of cross head was set as 5 mm/min according to the test standard. A high definition camcorder (HC-X920M Panasonic, Japan) was used to record the crack growth under loading. Figure 2.14 shows a DCB test sample (left) and the DCB test setup (right).

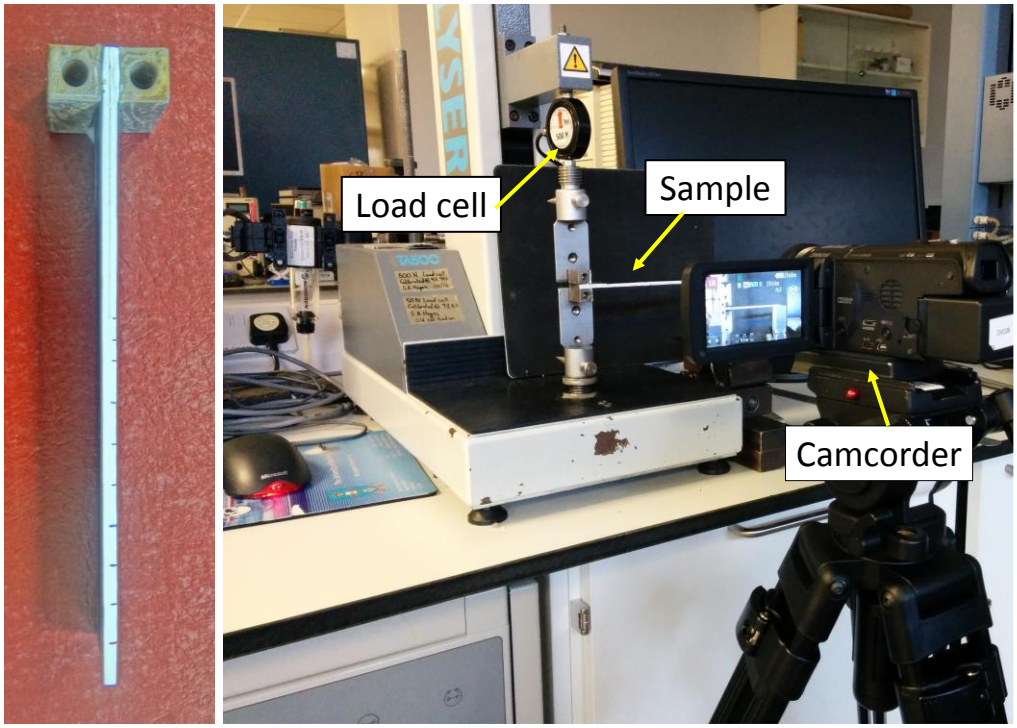

Figure 2.14 A DCB test sample with load blocks (left) and test set up (right).

2.7.2 Short beam shear test

A short beam shear (SBS) test standard [6] were used to evaluate the apparent interlaminar shear strength (ILSS) of polymer printed CFRP laminates. 9 – 12 SBS test samples were wet-cut from each 8-ply cured parent laminate using the diamond saw which was used to cut DCB samples. All fresh cut samples were polished with 600 grade SiC sand paper to eliminate the free edge effects. Figure 2.15 shows the configuration used for SBS test samples. All polished samples were left to dry at room temperature at least 15 hours before test.

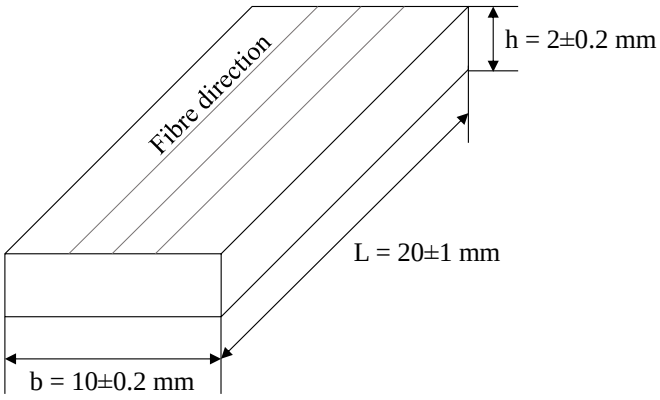

Figure 2.15 Schematic showing a SBS test sample.

The test was carried out using a benchtop tester (H25KS, Tinius Olsen Ltd., UK) equipped with a 25 KN load cell. The speed of cross head of SBS tests was set as 1 mm/min. The distance between two supporters was 10 mm, the span/thickness ratio was 5 which was recommended by the SBS test standard to encourage the shear failure. Figure 2.16 shows the SBS test setup and a test sample.

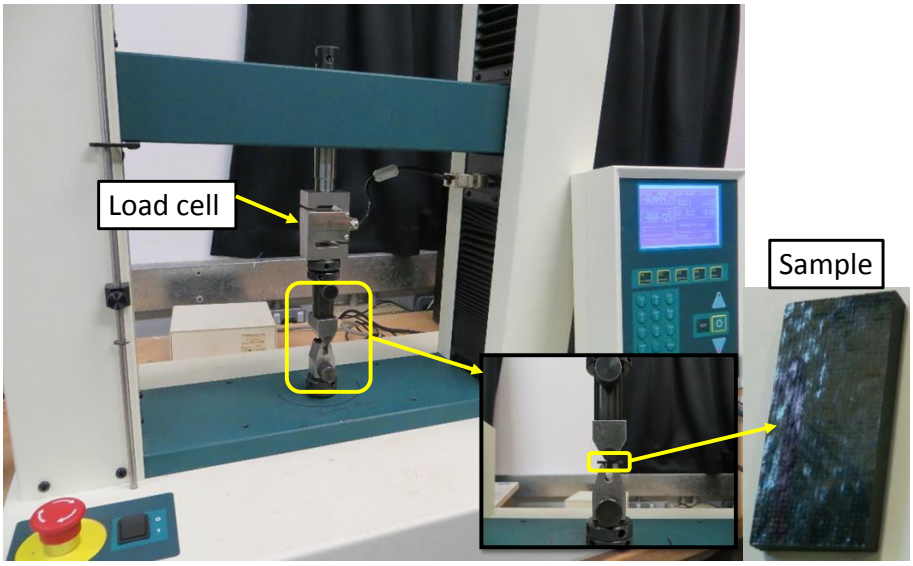

Figure 2.16 SBS test setup and a test sample.

In order to validate the shear test, only those samples with single or multiple shear failure (Figure 2.17) were accepted for the following data interpretation.

Figure 2.17 Acceptable shear failure [6].

2.8 Dynamic mechanical analysis

Dynamic mechanical properties of inkjet printed CFRP laminate samples were collected with a DMA 8000 (PerkinElmer Inc., UK) operating in the three-point bending mode at an oscillation frequency of 1.0 Hz. The amplitude and the static force were 20 μm and 5.0 N, respectively. Data were collected from − 50 ℃ to 200 ℃ at a scanning rate of 2 ℃/min. A minimum of three specimens of each group were tested.

2.9 X-ray tomography

In order to investigate the damage tolerance of CFRP laminates with printed polymer deposits between plies, two 100 × 100 mm 8-ply CFRP laminates were prepared for subsequent impact. One was a non-printed laminate, and the other one was printed using the 20 wt.% PMMA solutions, the PMMA deposits were patterned in hexagon (*dx/dy* = 0.4/0.2 mm) between every ply. A drop weight tower was used to introduce the impact damage to these laminates. 1 J impact energy were used to impact two laminates respectively. Five positions were impacted within a laminate, then three 100 × 10 mm strips were cut from the original impacted laminates for X-ray inspection. Figure 2.18 schematically shows the impact places and cutting dimensions.

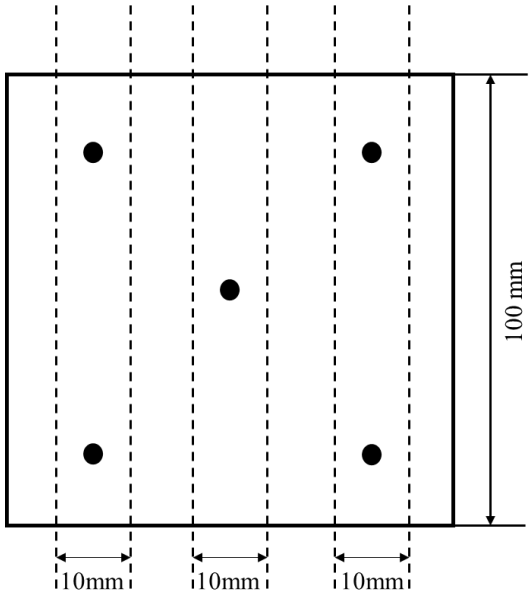

Figure 2.18 Schematically shows the impact positions and cutting dimensions.

A custom design Nikon/Metris dual source high energy micro-focus walk-in room system at The University of Southampton was used to conduct non-destructive X-ray tomography analysis of the three impacted CFRP laminates. The scan used the 225 kV source with 1621 PerkinElmer caesium-iodide detector. The current was set at 157 uA (8.6W), the distance between the cut strips and the source-imaging was about 700 mm.

2.10 Microscopy

Scanning electron microscope (SEM) (Camscan Mk2, Germany) was used to investigate the fracture surfaces of DCB tested samples, the surfaces and edges of drilled holes. Optical microscope (CK40-SLP, Olympus, Japan) was used to take optical images of plain glass slides and epoxy coated glass slides with printed polymer deposits. A fluorescence microscope (Axon Instruments Inc., USA) was used in conjunction with a fluorescein-doped sample of polymer solutions to elucidate information about the flow of polymer within the composite upon heating.

2.11 Water aging test

In order to evaluate the effect of the printed polymer deposits between CFRP laminate plies on the moisture absorption of the final composite, three groups of polymer printed CFRP samples with the same size as SBS test samples were soaked in water bath for 31 days. One group was non-printed samples, the other two groups of samples were printed with 10 wt.% and 20 wt.% PMMA solutions with a hexagon pattern (*dx/dy* = 0.7/0.35 mm) respectively.

All soaked samples were taken out from water bath on the 1st, 3rd, 6th, 20th and 31st day, then quickly dried with lab tissue without any apparent water marks on sample surfaces. Then weight each sample and record the results accordingly.

References

[1] A. Jumahat, C. Soutis, F. R. Jones, and A. Hodzic, "Fracture mechanisms and failure analysis of carbon fibre/toughened epoxy composites subjected to compressive loading," *Composite structures*, vol. 92, pp. 295-305, 2010.

[2] Webpage, "Vectran fibre tensile properties," *Vectran*, accessed on 09/08/2013. Available: http://www.vectranfiber.com/BrochureProductInformation/TensileProperties.aspx

[3] R. I. Mahato, "Biomaterials for delivery and targeting of proteins and nucleic acids," *CRC Press*, 2004.

[4] Webpage, "Polymer Reference Materials-Poly(Methyl Methacrylate)," *polymer sources*, Available: http://polymersource.com/ReferenceMaterial/Polymethyl%20Methacrylate.pdf

[5] Standard, "Fibre-reinforced plastic composites. Determination of mode I interlaminar fracture toughness," ed: BS ISO, 15024:2001.

[6] Standard, "Fibre-reinforced plastic composites. Determination of apparent interlaminar shear strength by short-beam method," ed: BS EN ISO 14130:1998.

Chapter 3

Investigation into polymer solution printability and behaviour on substrates

This chapter introduces basic information about the polymers, poly(methyl methacrylate) (PMMA) and polyethylene glycol (PEG), which were used as toughening materials in this work. Viscosity and surface tension of printing solutions made from these two polymers were characterised to predict their printability. Microscopy was conducted to determine the repeatability of different patterns printed on different substrates, and morphology of polymer deposits embedded in resin matrix after curing. Material usage is also calculated to show the efficiency by using inkjet printing.

3.1 Introduction

Poly(methyl methacrylate) (PMMA, M_w ~ 15,000) is a linear, amorphous thermoplastic polymer, whose molecular structure is shown in Figure 3.1. It is a tough and lightweight material that has high mechanical strength, high Young's modulus and good impact strength (Table 3.1) compared to some engineered polymers such as polystyrene. As discussed in Chapter 1, CFRP has desirable physical and mechanical properties, and has been commonly used wherever high specific strength and high rigidity are required. However, the tendency for CFRP to delaminate limits the efficient applications of this promising material due to the brittle nature of matrix [1]. For the present study, the reasons for choosing PMMA as toughening material were as follows: 1) PMMA which is blended with epoxy and hardener tends to form discrete small particles after curing which can act as fillers to toughen epoxy resin system [2, 3]; 2) PMMA has a melting point which is close to the curing temperature of this specific epoxy resin system, which enables the PMMA added epoxy resin to retain the toughening effectiveness at a relatively high temperature in service; 3) PMMA possesses low moisture and water absorption, which is of importance if it is to be used in CFRP composites.

This thesis investigated the utilisation of PMMA as one of toughening materials, the toughened CFRP material with better damage resistance is expected.

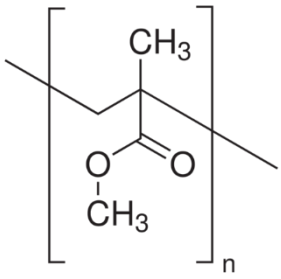

Figure 3.1 A PMMA molecular structure.

Table 3.1 Physical and mechanical properties of PMMA and PEG (M_n ~ 20,000) [4, 5].

Properties	PMMA	PEG
Density / g cm^{-3}	1.15 – 1.19	1.19
Glass transition temperature (T_g) / ℃	105 (midpoint)	/
Water absorption / wt.%	0.3 – 0.4	Soluble in water
Tensile strength, Ultimate / MPa	47 – 79	1.5
Young's modulus / GPa	2.2 – 3.8	1.3
Impact strength (Izod, Unnotched) / kJ m^{-2}	11	/

PMMA can be dissolved in various organic solvents such as N,N-Dimethylformamide (DMF), toluene and acetone, which provides the opportunities for inkjet printing. A suitable solvent will allow the PMMA to be easily dissolved in solvent for inkjet printing, and provide a suitable evaporation rate minimising any solvent residue on the prepreg before subsequent lay-up. However, this does not mean the most volatile solvent is the best, the evaporation rate of the solvent needs to be balanced with the printability of the formed solution. If the solvent is too volatile, the solute will accumulate quickly at the printhead tip, causing printhead clogging. Therefore, DMF was chosen to dissolve PMMA as it satisfies these two requirements.

Polyethylene glycol (PEG, M_n ~ 20,000) is a linear, crystalline polymer (Figure 3.2) that is commercially available in a wide range of molecular weights. The degree of crystallisation increases as the molecular weight of PEG increases [6]. Previous researches reported that PEG has good miscibility with epoxy, and the addition of a small amount of crystalline polymer can toughen the brittle epoxy resin by plasticisation [7, 8]. Therefore, it is quite interesting to find out whether this good compatibility and mechanical enhancement can be imparted to CFRP composite by using inkjet printing. Unlike the approach employed by Carfagna et al. [8], who mixed toughening material with epoxy in bulk resin, in this work the toughening material will be deposited by inkjet printing at locations where damage is most likely to happen. Therefore, the toughening is more targeted and the negative effect(s) of added polymer on the mechanical performance is eased. Furthermore, as the inkjet printing is flexible to deposit materials, the processing is relatively simple.

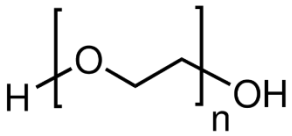

Figure 3.2 PEG molecular structure.

Since the mechanical properties of PEG are not as good as PMMA as shown in Table 3.1, it is worth comparing the results of polymer added CFRP using these two different types of polymers as toughening materials. This comparison would provide a potential explanation of how the inkjet printed polymers between laminate plies would affect the mechanical properties of final laminates.

3.2 Calculation of *Z* number

PMMA and PEG solutions were characterised for viscosity (η) and surface tension (σ) for calculating *Z* number, ultimately to predict the printability of these solutions. Table 3.2 lists these parameters and calculated *Z* numbers.

Table 3.2 Characterisations of solutions used in this project.

Solution	wt.%	T / ℃	η / mPa s	σ / mN m^{-1}	Z
PMMA/DMF	5	20	1.30	36.69	35.36
PMMA/DMF	10	20	2.05	36.43	22.49
PMMA/DMF	20	20	6.32	36.46	7.39
PEG/deionised water	5	20	5.06	59.12	11.85
PEG/ethanol	5	60	1.97	19.20	15.54
PEG/propanol	5	60	2.05	20.45	15.54
PEG/propanol	10	60	5.86	20.11	5.4

It can be seen from Table 3.2, the viscosity of the PMMA solutions increases as the concentration of PMMA increases. The viscosity not only depends on the concentration of dissolved polymer, but also depends on the viscosity of solvent and the measuring temperature. Unlike viscosity, the surface tension of the three PMMA solutions were quite close and similar to that of pure DMF (37.1 mN m^{-1}, 20 ℃). This could be because the added solute (PMMA) decreases the surface tension of solvent (DMF), and the minimum surface tension was reached even when the concentration of PMMA was 5 wt.%. Therefore, no additional effect of PMMA on the surface tension of 10 wt.% and 20 wt.% PMMA/DMF solutions was observed. Z number was calculated using parameters in Table 3.2 and the equation presented in Chapter 1, although the calculated Z numbers of the solutions were not all in the defined range which is $1 < Z < 10$, those solutions still can be printed by optimised combination of printing settings. Other work [9, 10] has also reported that solutions outside of the defined region are printable. As explained in Section 1.3.2, the polymer chains were subjected to shear force which causing the rearrangement of polymer chains, thus the viscosity of polymer solution during jetting was different from the one measured without applied force. Therefore, the actual Z number was different from the calculated Z number.

3.3 Settings of inkjet printer

Different fluids have their own physical properties such as viscosity and surface tension. In order to jet a single stable droplet of solution for a high resolution printing finish, different parameter combinations of printer settings should be used. The size of droplet can not only be adjusted by using printhead with different diameters, but also can be controlled by voltage applied to printhead and the distance between the printhead and substrate [11, 12]. In this work, once the printing system was installed, the distance between printhead and substrate is a constant which is approximately 1 mm, with variation due to textured surface of the prepreg. Changing size of droplet can be achieved by changing the voltage applied to the printhead.

In order to generate a stable droplet stream for printing, different parameter combinations were used for different solutions' printing. Generally speaking, the 'Rise time 1', 'Dwell time', 'Fall time' and 'Dwell voltage' were the main parameters which were used to generate an constantly sized droplet, values range from 42 to 90 V. During printing, parameters varied in a very small range to maintain the stability of droplets stream. Table 3.3 summarises the parameters for all solutions used in this work.

Table 3.3 Summary of the printing parameters for all solutions used in this work.

Solution	Rise time 1 (μs)	Dwell time (μs)	Fall time (μs)	Echo time (μs)	Rise time 2 (μs)	Idle Voltage (V)	Dwell Voltage (V)	Echo Voltage (V)
5wt.%PEGw	16.0	30.0	5.0	5.0	5.0	0.0	72.0	-6.0
5wt.%PEGe	3.0	7.0	5.0	9.0	9.0	0.0	16.0	0.0
5wt.%PEGp	5.0	30.0	4.0	10.0	5.0	0.0	55.0	-20.0
10wt.%PEGp	5.0	30.0	5.0	7.0	5.0	0.0	90	-15.0
5wt.%PMMA/DMF	4.0	4.0	4.0	6.0	8.0	0.0	47.0	0.0
10wt.%PMMA/DMF	4.0	6.0	4.0	5.0	5.0	0.0	60.0	0.0
20wt.%PMMA/DMF	5.0	6.0	4.0	4.0	2.0	0.0	90.0	0.0

3.4 Pattern repeatability

3.4.1 Polymer deposits printed on glass substrate

PMMA/DMF and PEG/deionised water solutions were deposited on glass substrates to determine the repeatability of the printed patterns. Figure 3.3 shows optical images of PMMA and PEG deposits printed on glass substrates with different patterns. It can be seen that the patterns can be repeatedly printed on glass substrates with controllable dimensions.

As the wetting ability of the different solutions on glass slide varies due to the different energy between liquid and solid surface, therefore, the deposits' diameter of different polymer solution printed on glass slide is different. The diameters of PMMA and PEG deposits printed on glass slide were approximately 100 – 140 and 85 – 100 μm respectively, indicating the PMMA/DMF solution has a better wettability on glass slide than PEG/deionised water solution.

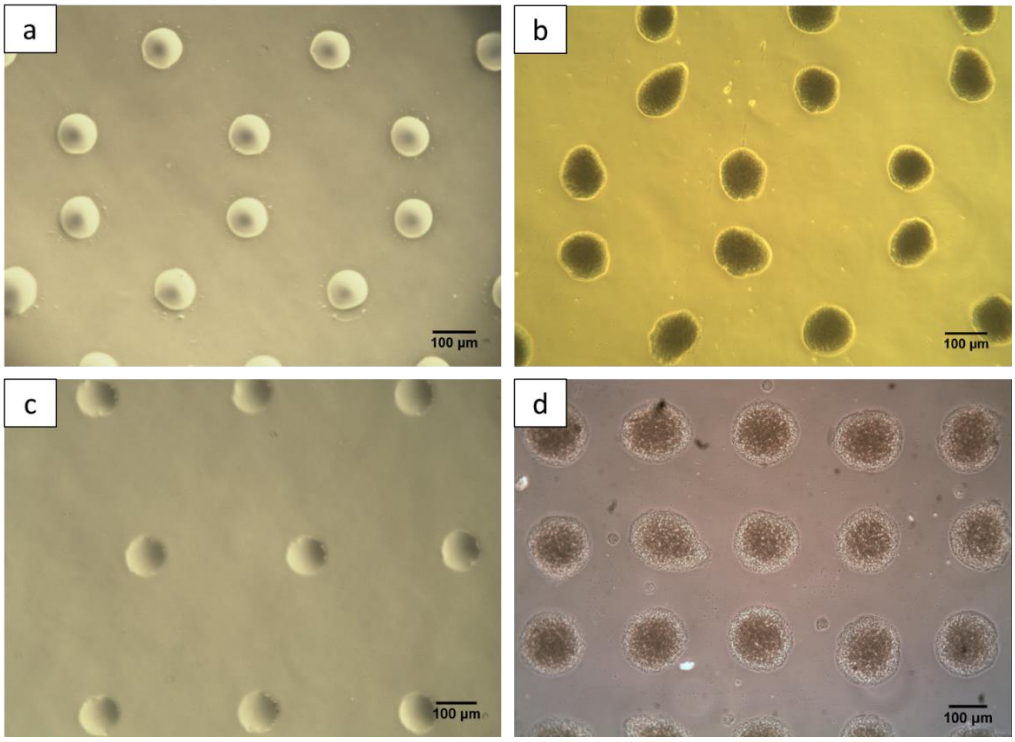

Figure 3.3 Optical images of polymer deposits patterned on glass substrates. a) 5 wt.% PEG/deionised water, hexagon (*dx/dy* = 0.4/0.2 mm); b) 10 wt.% PMMA, hexagon (*dx/dy* = 0.4/0.2 mm); c) 10 wt.% PEG/deionised water, parallelogram (*dx* = *dy* = 0.4 mm); d) 5 wt.% PMMA, square (*dx* = *dy* = 0.3 mm).

This observed difference of deposit size on the same substrate can be explained by Young's equation for contact angle is as follows:

$$\gamma_{sg} - \gamma_{sl} - \gamma_{lg} \cdot \cos\theta = 0 \quad (3.1)$$

Where γ_{sg} is the solid-vapor interfacial energy, γ_{sl} is the solid-liquid interfacial energy, γ_{lg} is the liquid-vapor interfacial energy, and θ is the contact angle. In Section 3.2, the surface tension of DMF based solutions have lower surface tension than that of deionised water based solutions. According to equation 3.1, the contact angle of DMF based solutions is smaller than that of deionised water based solutions, indicating DMF based solution has a better wetting ability than deionised water based solution. This conclusion agreed with the observation in Figure 3.3 that the diameter of PMMA deposits on glass slide was larger than that of PEG deposits.

3.4.2 Polymer deposits printed on prepreg

PMMA/DMF and PEG/ethanol solutions were also printed on prepreg to confirm the repeatability of printed patterns. In order to increase the contrast of transparent polymer deposits on black prepreg, 0.1 wt.% of fluorescein was added into PEG/ethanol and PMMA/DMF solutions to help locating the polymer deposits after printing. As shown in Figure 3.4, designed patterns can be repeatedly printed on prepreg with controllable pattern dimensions. The diameter of both PEG and PMMA deposits printed on prepreg was larger than that of PEG and PMMA deposits printed on glass substrates, measured as approximately 190 – 200 μm for both solutions.

In this case, using prepreg as substrate is more complex than using a glass slide as the presence of carbon fibres. The interfacial force between liquid and solid still affects the wetting ability of solutions, however, the presence of carbon fibres causes the capillary flow of the printed solution as shown in Figure 3.4a. Thus, the size of deposit printed on prepreg is a combination result of different factors.

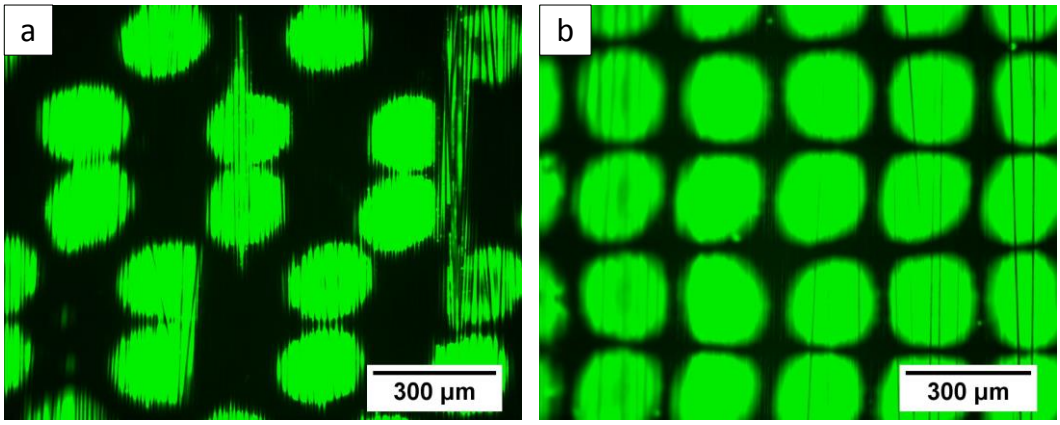

Figure 3.4 Polymer deposits (with fluorescein) printed on prepreg before curing. a) 5 wt.% PEG/ethanol, hexagon (*dx/dy* = 0.4/0.2mm); b) 5 wt.% PMMA, square (*dx* = *dy* = 0.3 mm).

As the fluorescein barely dissolved in deionised water, the patterns printed on prepreg using the PEG/deionised water solution was imaged by optical microscope as shown in Figure 3.5. The diameter of PEG deposits was smaller than that of PEG printed using ethanol based solution, suggesting the solvents play an important role in wetting ability of solutions on the same solid surface. In addition to that, the wettability of polymer solutions will also be influenced by the strongly textured surface of the prepreg [13]. It can be seen from Figure 3.4, the printed deposits tended to extend on fibre direction.

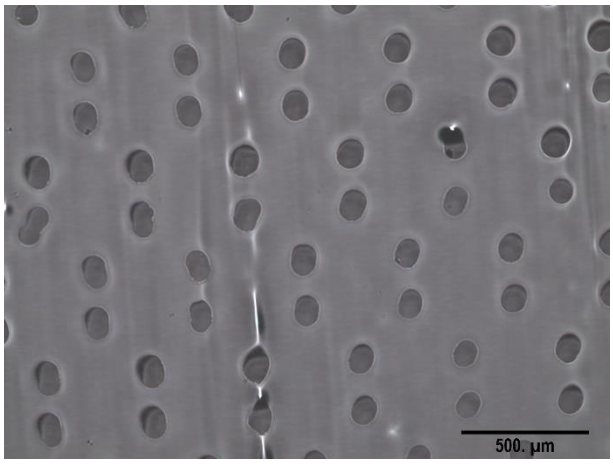

Figure 3.5 PEG deposits printed on prepreg (5 wt.% PEG/deionised water, hexagon, *dx/dy* = 0.4/0.2 mm).

3.5 Material usage

As mentioned in Chapter 1, the amount of toughening materials added into composites plays an important role in the success of toughened composites. Because the toughening effectiveness ideally is not achieved at the expense of weight increasing. Especially in the aerospace area, materials' weight is a critical consideration. Inkjet printing has the ability to constantly generate pico-litre volume droplet, and deposit them into highly controllable patterns with the assistance of a computer. Therefore, the deposits can be precisely printed into close or loose packed patterns to vary the coverage of the printed deposits on substrates to optimise the toughening efficiency. In this work, different patterns and pattern densities were involved, thus, the surface coverage and volume fractions of printed polymer depositions in final CFRP laminates were different accordingly.

3.5.1 Surface coverage of polymer deposits

As mentioned in Chapter 1, the toughening agent is designed to be deposited into discrete regions along specific interfaces, aiming to achieve toughening while easing the problems associated with other toughening methods. Hypothetically, the toughening effectiveness would increase as the toughening agent printed area increase, in this case, these printed deposits should be close packed but minimise contacting with each other. Therefore, it is helpful to know the surface coverage by printed deposits. A ratio of surface coverage of polymer depositions on prepreg (ξ) was defined as the area of the repeating unit cell with the pattern divided by the area of the unit cell (Figure 3.6). The measured deposit diameter was used to calculate deposits area within one repeating unit cell and the pattern dimension was used to calculate the repeating unit area, Equation 3.1 was used to calculate the coverage.

$$\xi = \frac{S_{printed}}{S_{unit}} = \frac{nd^2\pi}{4dxdy} \times 100\% \qquad 3.1$$

Where ξ is the surface coverage, $S_{printed}$ is the area of the repeating unit cell with the pattern and S_{unit} is the area of the repeating unit cell. n is the number of deposit within a unit area; d is the diameter of deposit, dx and dy are the pattern dimensions.

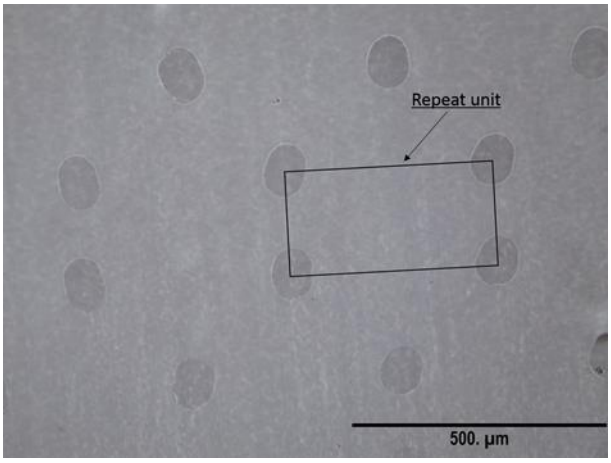

Figure 3.6 Illustration of the defined surface coverage [14]. (PEG/deionised water printed on prepreg with a hexagon pattern, *dx/dy* = 0.4/0.2 mm)

As discussed in Section 3.4.2, droplets of solutions with different surface tensions spread onto the prepreg surface forming different sized polymer deposits, which affects the surface coverage of deposits. And the pattern dimensions also influence the surface coverage. For example, the deposit diameter of PMMA/DMF solution printed on prepreg is about 195 µm, if the PMMA droplets patterned in two different sized hexagon patterns, *dx/dy* = 0.4/0.2 mm and 0.7/0.35 mm, according to Equation 3.1, the surface coverages are about 37.5% and 12.2% respectively. Table 3.4 lists surface coverages of varying solutions and patterns.

3.5.2 Volume fraction of polymer deposits

Volume fraction of polymer used in one test sample was defined as the volume of toughening materials deposited per unit volume of sample, *V*, and was calculated using Equation 3.2 and 3.3, which are based on the diameter of the jetted droplet (D_0), the pattern dimensions (*dx* and *dy*), the volume fraction of polymer in the solutions (*f*) and the dimensions of the sample (length, *l*, width, *b*, thickness, *t*). Assuming the droplet generated by inkjet printing is a perfect sphere, and the diameter equals to the diameter of printhead, the volume of a single droplet (V_0) can be calculated straightway (Equation 3.3). Note, the calculation of volume fraction is based on short beam shear (SBS) test samples prepared according to the test

standard, because the toughening materials were printed between every adjacent laminate ply, thus, the material usage is a maximum scenario.

$$V = \frac{V_{printed}}{V_{sample}} = \frac{7V_0 f}{dxdyt} \times 100\% \quad 3.2$$

$$V_0 = \frac{\pi D_0^3}{6} \quad 3.3$$

Table 3.4 lists volume fraction of varying solutions and patterns. It can be concluded that the surface coverage is determined by both the diameter of deposit and pattern dimensions, while the volume fraction are determined by pattern dimensions and the polymer concentrations in printing solutions.

Table 3.4 Calculation of surface coverage and volume fraction (polymer concentration: 5 wt.%).

Pattern (dimension / mm)	Unit area / mm^2	ξ / %		V / %
		DMF based solutions (d ~ 195 μm)	Water based solutions (d ~ 98 μm)	
Hexagon, *dx/dy* = 0.4/0.2	0.08	37.5	10.0	0.025
Hexagon, *dx/dy* = 0.7/0.35	0.25	12.2	3.3	0.008
Square, *dx* = *dy* = 0.3	0.09	33.3	8.9	0.022
Line, *dx/dy* = 0.8/0.1	0.08	24.3	12.3	0.025
Film, *dx/dy* = 0. 1	/	100	100	0.200

Note: the volume fraction was calculated based on SBS test sample, as polymer deposits were printed between every layer of laminate, therefore, the volume fraction is a maximum.

The calculations of surface coverage and volume fraction indicate that a significant surface coverage of polymer deposits on prepreg can be obtained by using inkjet printing of a very small amount of material. For ease of comparison with previous work looking at interleaved thermoplastic films, this would correspond to an interleaved film thickness of approximately 140 nm (calculated based on using 10 wt.% PMMA solution, and hexagon pattern, *dx/dy* = 0.4/0.2 mm). A film of this thickness would be difficult to handle with conventional interleaving techniques, showing that inkjet printing can deposit amounts of thermoplastic toughening material at the interface between composite plies that would be unachievable by conventional methods.

3.6 Morphology of polymer deposits embedded in epoxy resin

3.6.1 PMMA deposit

Although session 3.4.2 shows that the polymer solutions can be deposited on prepreg with controllable pattern dimensions, i.e. forming discrete dot regions. It is of great interest to know the behaviours of polymer deposits between laminate plies after curing. Moreover, since the high temperature and pressure during composite curing may influence the formation of polymer deposits, the new morphology or structure formation of the polymer deposits surrounded by epoxy resin and carbon fibre are critical to the damage mechanism. Unfortunately, the black background and fibrous texture of CFRP make the observation of printed polymer deposition between laminate plies extremely difficult. Therefore, glass substrates were coated with a thin layer of epoxy resin to mimic the matrix of prepreg as the potential behaviours of polymer depositions are mainly involved with the epoxy resin.

Firstly, the polymer deposits printed in discrete dot pattern was investigated. Three different PMMA concentrations (5, 10 and 20 wt.%) of printing solutions were used to print a same dimensional hexagon pattern to see any potential difference associated with polymer concentration. Figure 3.7 shows the optical microscope images of patterns printed on epoxy coated glass substrates before and after heating cycle. As can be seen, the printed PMMA deposits tended to form spherical particles due to lack of compatibility between epoxy, hardener and PMMA, while keeping the hexagonal pattern after heating cycle. Note, some

of the deposits shifted positions due to the fluidity of the epoxy/PMMA systems under high temperature, and because there was no fibre in this situation, the flowability of epoxy/PMMA was not constrained by the fibres, thus, the shift of pattern was prone to happen.

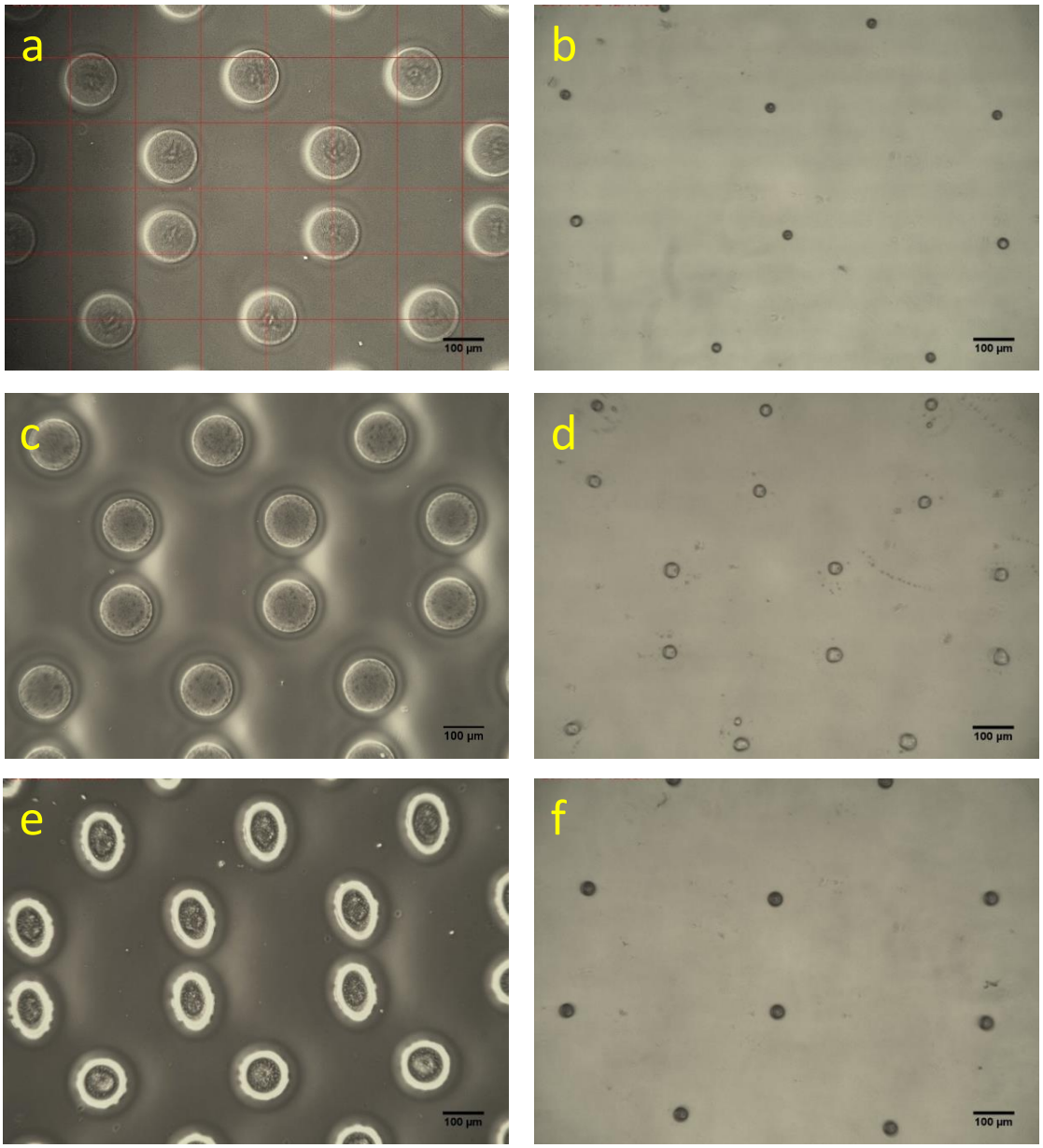

Figure 3.7 Optical images of epoxy coated glass substrates with printed PMMA deposits (hexagon, *dx/dy* = 0.4/0.2 mm). a), c) and e) 5, 10, and 20 wt.% PMMA deposits before heating cycle; b), d) and f) 5, 10 and 20 wt.% PMMA deposits after heating cycle.

Also note that the epoxy in both prepreg and neat resin is not a pure epoxy, it represents a mixture containing other additions such as hardeners. Previous researchers [2, 15] reported that PMMA was miscible with pure epoxy but not with the hardener. When curing the blends which containing epoxy, hardener and PMMA at a high temperature, phase separation occurred: blends formed discrete small particles (Figure 3.8, especially, resin system showed in graph (a) and system adopted in this thesis used the same hardener). Similarly, when curing the PMMA deposited epoxy system at high temperature, spherical particles formed, these particles may not be pure PMMA, they could be PMMA domains containing other additions such as hardener. For simplicity, PMMA particle(s) are used to represent these PMMA-domain spherical particles in the following discussion. However, a detailed examination of these particles' composition has not been performed in this work due to the limited time.

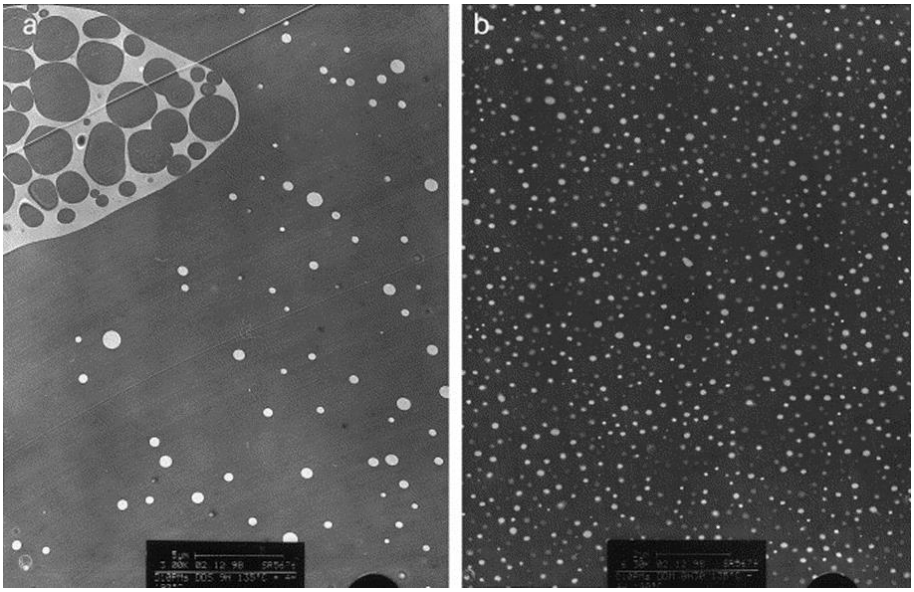

Figure 3.8 Transmission electron micrographs of PMMA-hardener-epoxy blends [15]. (a and b used two different hardeners respectively).

Although a retained print pattern can be observed after heating, this observation does not necessarily imply that the printed pattern between CFRP laminate plies is also perfectly kept after curing, due to the complicated fibrous texture of CFRP laminate. However, because the prepreg plies were tightly pressed with each other during lay-up, and they are more flexible than glass slide, the printed polymer deposits may have limited movability between plies,

therefore, the shift of pattern should not be severe between plies. Based on the above observations, it is reasonable to conclude that the PMMA deposits with controllable size can be printed on the crack favoured interface between laminate plies, and the PMMA deposits remain as discrete thermoplastic regions evenly distributed along the printed area thanks to the versatile inkjet printing.

The diameters of PMMA deposits printed on the epoxy coated glass substrates of three solutions with different PMMA concentrations were quite similar before heating. However, the diameters of PMMA particles after heating depended on the PMMA concentration in solutions. In other words, the diameter of PMMA particles depends on the amount of PMMA deposited during printing. As shown in Figure 3.9, the diameter of PMMA particles increases as the PMMA concentration/amount increases after heating, and the percentage of decrease in deposit diameter decreases as the PMMA concentration/amount increases.

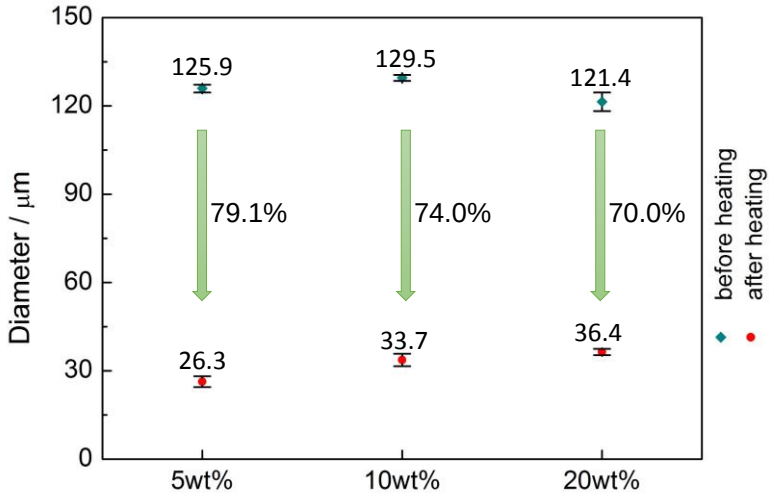

Figure 3.9 Percentage changes of PMMA deposits' diameter after heating cycle. (Error bar represents standard deviation, n = 10)

In order to confirm that the amount of PMMA at a single printing location affects the diameter of PMMA particles after heating, multilayer printing was conducted to increase the amount of PMMA at a single location by increasing the number of printing layers instead of using a higher PMMA concentration solution. A 10 wt.% PMMA solution was used to print a hexagon pattern (*dx/dy* = 0.4/0.2 mm) twice. Figure 3.10 shows the printed pattern before

and after the heating cycle. As expected, the printed PMMA deposits formed particles after heating while retaining the hexagon pattern. The diameter of the PMMA deposits after double printing was slightly larger than that of single layer printing, this was because more solution was packed up at a same location after double printing. As a result, the diameter of deposit expands to a small amount. In terms of the diameter of PMMA particles, theoretically, the diameter of PMMA particles printed using 10 wt.% PMMA solution should be equal to that of PMMA particles printed using 20 wt.% PMMA solution. The results highly agreed with the expectation. Table 3.5 lists the statistic results of this comparison.

There were some "rings" around the main PMMA particles after heating, this was because of the multilayer printing, when the second PMMA deposit hit the same printing location, as shown in Figure 3.10(a), the edge part of the deposit has relatively more PMMA than the region between the middle and the edge of deposit. Therefore, PMMA at the edge of a deposit tended to break up from the main part and form particles itself due to the interfacial tension forces.

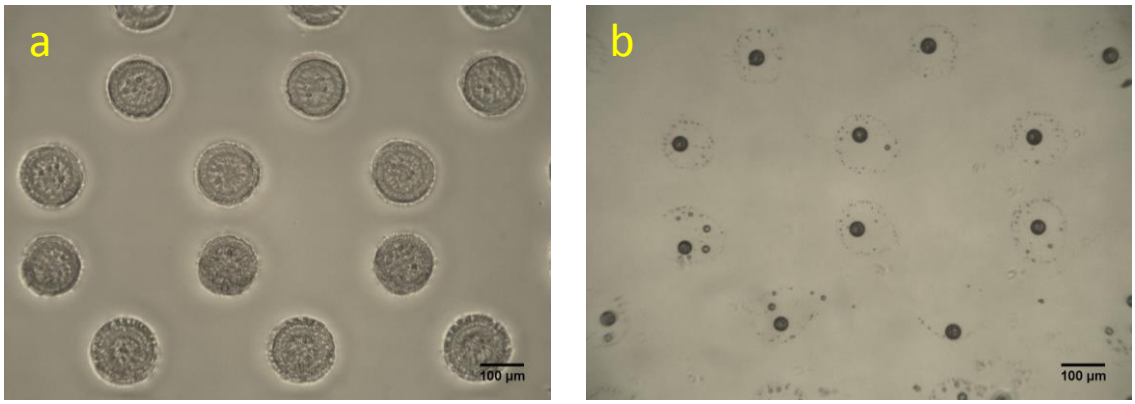

Figure 3.10 Optical images of epoxy coated glass slides with printed 10 wt.% PMMA deposits twice before (a) and after (b) heating cycle.

Table 3.5 Diameters of PMMA deposits/particles before and after heating cycle.

Solution	Before heating / μm	STDEV	After heating / μm	STDEV
10 wt.%	129.5	1.0	33.7	2.1
10 wt.% twice	147.4	3.3	36.8	2.0
20 wt.%	121.4	3.1	36.4	1.1
Note: STDEV represents standard deviation, n = 10				

Secondly, the 10 wt.% PMMA solution was used to print a line pattern to observe the possible changes after heating cycle. Figure 3.11 shows the printed lines before and after heating. It can be seen that the continuous lines broke down into unevenly sized particles, but these particles still partially lined up. This result suggests that the continuous phase of PMMA cannot be retained after curing. Unlike the case of discrete dot pattern, the amount of PMMA at every printed position was about the same, therefore, the size of PMMA particles after heating was about the same with a small variation. However, the size of PMMA particles formed from a continuous phase, lines here, was not controllable as observed.

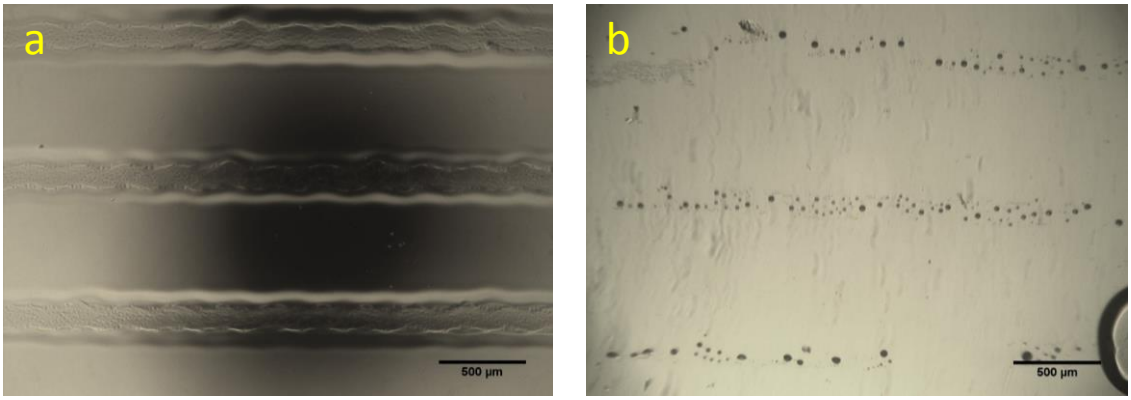

Figure 3.11 Optical images of epoxy coated glass substrates with printed PMMA lines before (a) and after (b) heating.

Lastly, a thin film was printed using 10 wt.% PMMA solution onto the epoxy coated substrate to repeat the above experiment. Figure 3.12 shows the printed PMMA thin film broke down into randomly distributed particles with a wide range of diameters.

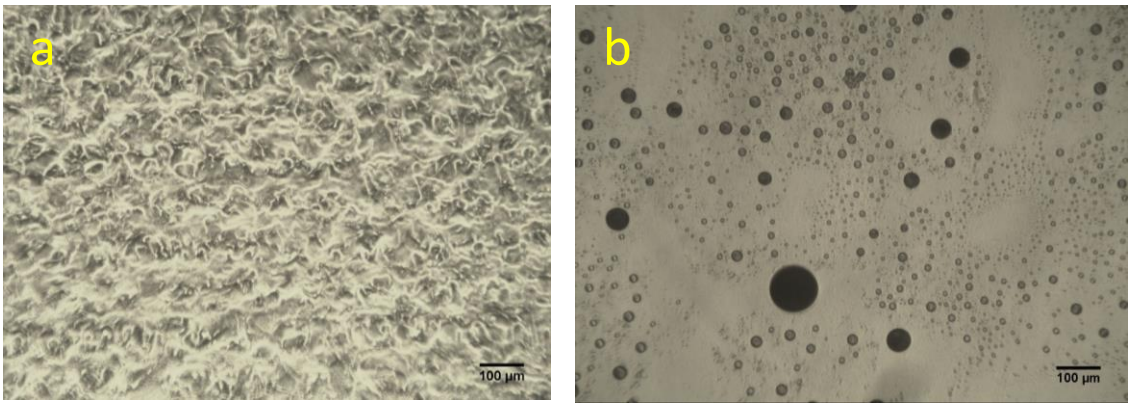

Figure 3.12 Optical images of epoxy coated glass slides with printed PMMA thin film before (a) and after (b) heating.

3.6.2 PEG deposit

10 wt.% PEG/deionised water solution was also used to print a hexagon pattern on the epoxy coated glass slide to investigate the deposits formation surrounded by epoxy before and after heating. Figure 3.13 shows that the PEG deposits, unlike PMMA deposits, did not bead up to form micro-sized particles. Instead, the PEG deposits seemed miscible with the epoxy resin after heating. The printed pattern was still identical as shown in Figure 3.13(b), suggesting the PEG deposits may not significantly diffuse into the whole epoxy resin, but formed PEG dissolved regions kept in the initial printed pattern.

Based on the above observations, printed PMMA formed the discrete polymer regions evenly distributed along the targeted area by using a discrete dot pattern, which is the ideal situation proposed in Chapter 1. Moreover, the size of formed PMMA particles after heating is quite uniform when printed as discrete dots, which may benefit the toughening in the composite. Although the PEG printed system seemed to form PEG-contained regions, the actual formation of PEG embedded in epoxy resin after heating is not quite clear compared to PMMA printed system. Therefore, the following works were focused on printing of PMMA.

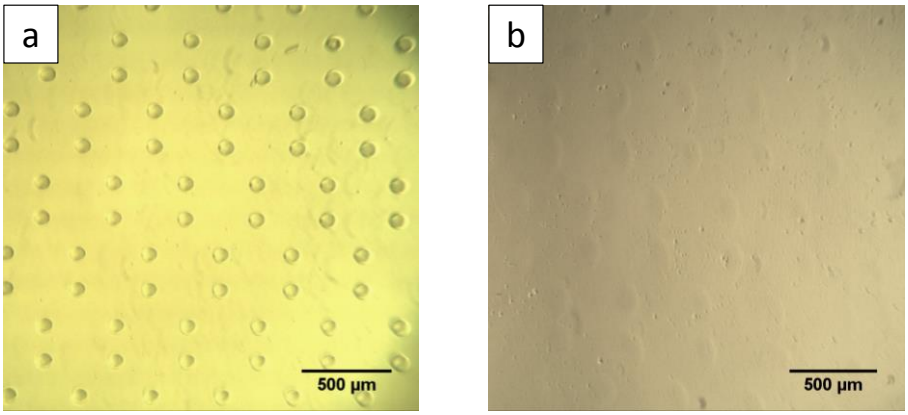

Figure 3.13 Optical images of epoxy coated glass slides with printed PEG deposits before (a) and after (b) heating.

3.7 Conclusions

PMMA and PEG can be dissolved in suitable solvents to form printable solutions for inkjet printing. The printer needs to be suitably adjusted to print different solutions due to their different physical properties (e.g. viscosity and surface tension). Microscopy showed that the polymer deposits can be repeatedly printed into various patterns on different substrates (glass slide and prepreg). The diameter of polymer deposits varies on different substrates because of the following reasons: 1) different forces formed on the interface between different solutions and substrates; 2) different surface tensions of solutions; 3) different surface roughness of the substrates, i.e. glass surface is smooth and impenetrable, but prepreg surface is quite rough due to the presence of fibres and is penetrable compared to glass surface.

The surface coverage of polymer deposits depends on the pattern dimensions. Among those designed discrete dot patterns used in this work, hexagon pattern (*dx/dy* = 0.4/0.2 mm) has the highest surface coverage which is 37% with only 0.025 vol.% of toughening material. The printed PMMA deposits tended to form spherical particles after co-curing with epoxy resin. Generally, the diameter of PMMA particles increased as the percentage of PMMA in printing solution increased. Continuous features such as line and film tended to break up into spherical particles with a wide range of diameters. By depositing discrete dot pattern, the distribution and size of PMMA particles were more controllable. Although by using a continuous pattern (e.g. line and film), the surface coverage can be increased dramatically,

the formation of polymer particles is not controllable in terms of particle size and geometrical distribution. PEG deposits seemed miscible with the epoxy resin as no noticeable micro-sized phases was observed, however, the printed pattern still can be identified indicating the PEG did not completely diffuse into the whole resin, forming PEG dissolved epoxy regions instead. Whether the different formation of polymer deposits after curing would make any effect on toughening will be investigated in the next two chapters.

References

[1] N. Sela and O. Ishai, "Interlaminar fracture toughness and toughening of laminated composite materials: a review," *Composites,* vol. 20, pp. 423-435, 1989.

[2] C. M. Gomez and C. B. Bucknall, "Blends of poly (methyl methacrylate) with epoxy resin and an aliphatic amine hardener," *Polymer,* vol. 34, pp. 2111-2117, 1993.

[3] S. Ritzenthaler, E. Girard-Reydet, and J. Pascault, "Influence of epoxy hardener on miscibility of blends of poly (methyl methacrylate) and epoxy networks," *Polymer,* vol. 41, pp. 6375-6386, 2000.

[4] M. Koleva, "Poly(methyl methacrylate) (PMMA)," accessed on 24/08/2014. Available: http://webhotel2.tut.fi/projects/caeds/tekstit/plastics/plastics_PMMA.pdf

[5] M. A. Nasassrah, F. Podczeck, and J. M. Newton, "The effect of an increase in chain length on the mechanical properties of polyethylene glycols," *European Journal of Pharmaceutics and Biopharmaceutics,* vol. 46, pp. 31-38, 1998.

[6] Y. Li, Q. Ma, C. Huang, and G. Liu, "Crystallization of Poly (ethylene glycol) in Poly (methyl methacrylate) Networks," *Materials Science,* vol. 19, pp. 147-151, 2013.

[7] Y. Fang, H. Kang, W. Wang, H. Liu, and X. Gao, "Study on polyethylene glycol/epoxy resin composite as a form-stable phase change material," *Energy Conversion and Management,* vol. 51, pp. 2757-2761, 2010.

[8] C. Carfagna, L. Nicolais, E. Amendola, and A. Filippov, "Toughening epoxy resins by liquid crystalline polymers," *Journal of applied polymer science,* vol. 44, pp. 1465-1471, 1992.

[9] D. B. van Dam and C. Le Clerc, "Experimental study of the impact of an ink-jet printed droplet on a solid substrate," *Physics of Fluids (1994-present),* vol. 16, pp. 3403-3414, 2004.

[10] J. Perelaer, P. J. Smith, E. van den Bosch, S. S. C. van Grootel, P. H. J. M. Ketelaars, and U. S. Schubert, "The Spreading of Inkjet-Printed Droplets with Varying Polymer Molar Mass on a Dry Solid Substrate," *Macromolecular Chemistry and Physics,* vol. 210, pp. 495-502, 2009.

[11] E. Tekin, P. J. Smith, and U. S. Schubert, "Inkjet printing as a deposition and patterning tool for polymers and inorganic particles," *Soft Matter,* vol. 4, pp. 703-713, 2008.

[12] J. Perelaer, P. J. Smith, M. M. Wijnen, E. van den Bosch, R. Eckardt, P. H. Ketelaars, *et al.*, "Droplet tailoring using evaporative inkjet printing," *Macromolecular Chemistry and Physics*, vol. 210, pp. 387-393, 2009.

[13] J. Perelaer, B. J. de Gans, and U. S. Schubert, "Ink-jet Printing and Microwave Sintering of Conductive Silver Tracks," *Advanced Materials*, vol. 18, pp. 2101-2104, 2006.

[14] Y. Zhang, J. Stringer, R. Grainger, P. J. Smith, and A. Hodzic, "Fabrication of patterned thermoplastic microphases between composite plies by inkjet printing," *Journal of Composite Materials*, vol.0(0), pp.1-7, 2014.

[15] S. Ritzenthaler, E. Girard-Reydet, and J. P. Pascault, "Influence of epoxy hardener on miscibility of blends of poly(methyl methacrylate) and epoxy networks," *Polymer*, vol. 41, pp. 6375-6386, 2000.

Chapter 4

Influence of inkjet printed polymer on mode I interlaminar fracture toughness of CFRP

This chapter firstly introduces the main information about the double cantilever beam (DCB) test which was used to determine the mode I interlaminar fracture toughness (G_{Ic}) of unidirectional fibre reinforced plastic composites. The test results of samples with addition of PMMA and PEG deposits respectively are then provided. An approximately 40% increase in G_{Ic} was observed of sample printed with PMMA deposits patterned in a hexagon discrete dot pattern. Although laminates with printed PMMA film showed the highest improvement in G_{Ic}, the crack propagation is instable. Microscopy of fracture surfaces of DCB tested samples is provided. Therefore, the possible toughening mechanisms and explanations for the improved G_{Ic} are discussed.

4.1 Introduction

While CFRP laminate composites have made a remarkable breakthrough in industries on account of their favourable mechanical properties, a major problem of using these composites is their low interlaminar properties. As mentioned in Chapter 1, the CFRP multi-layered laminates is prone to delaminate due to lack of through thickness reinforcement. Various external and internal factors such as impact damage during service, impurities, voids and fabrication defects accumulated during processing can lead to delamination which considerably reduces the mechanical integrity of CFRP laminates. Therefore, it is of great importance to improve the interlaminar damage tolerance for laminated composites.

As the cracks tend to grow along the interface region between adjacent plies [1], toughening materials were printed in a pre-defined array pattern onto prepreg. A series of printed prepreg layers were then laid up and cured to produce a composite consisting of carbon fibre embedded in a thermoset epoxy resin with discrete micro-sized regions of polymer located

in the interlaminar region. The ability to deposit toughening material exclusively on the interface region between carbon fibre reinforced prepreg layers means that overall volume fraction of toughening materials can be reduced, thus, the toughened laminates gain as little weight as possible.

Mode I interlaminar fracture toughness, G_{Ic}, is one of the common indicators which can be used to quantify the resistance to delamination of laminated materials. Double cantilever beam (DCB) test is prevalently used to characterise the interlaminar fracture toughness in mode I loading (Figure 4.1). All the DCB tests were based on BS ISO 15024:2001 [2] in this thesis.

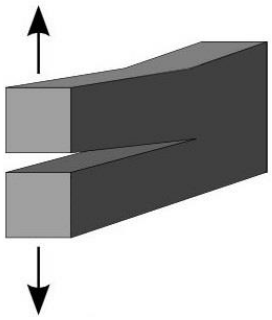

Figure 4.1 Mode I loading (opening).

As introduced in Chapter 3, PMMA and PEG possess quite different mechanical and chemical properties, they both have been used to toughen epoxy resins and the results showed a promising toughening effectiveness previously [3-5]. In addition to that, those two polymers are dissolvable in organic or/and inorganic solvents to form printable solutions for inkjet printing. Thus, PMMA and PEG were chose as the toughening materials in this work.

4.1.1. Principle

A mode I double cantilever beam (DCB) sample is used to determine G_{Ic} which is the critical energy release rate or interlaminar fracture toughness of fibre reinforced plastic composites. The test is limited to zero-degree unidirectional lay-up only. Data interpretation yields

initiation and propagation values of G_{Ic} for mode I fracture toughness. Initiation refers to the region between the start of cracks and the start of steady crack propagation; propagation refers to the steady growth of cracks. An R-curve is generated by plotting G_{Ic} as a function of delamination length. Figure 4.2 is a typical R-curve obtained from DCB test, showing increasing delamination resistance with delamination length before reaching a plateau (steady crack propagation stage).

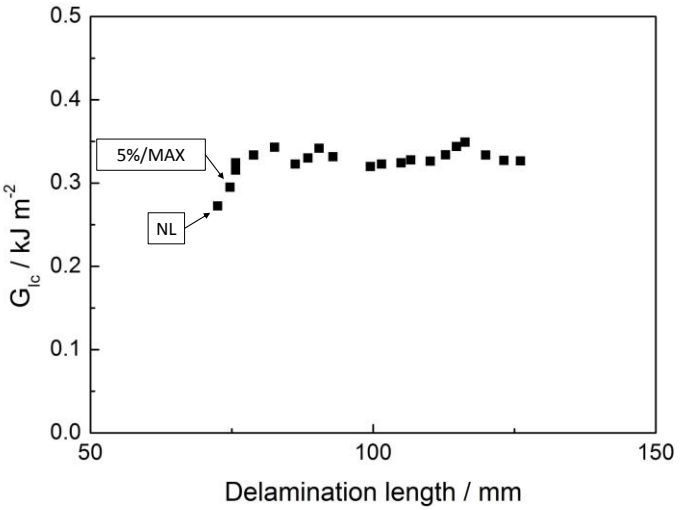

Figure 4.2 A typical R-curve deduced from the DCB test.

A crack-opening load is applied to the DCB sample, perpendicular to the plane of delamination, through load blocks under extension control at a constant rate. The sample is firstly pre-cracked by loading (mode I) the DCB sample immediately after the first increment of delamination growth from an insert which is a thin, non-adhesive film embedded at the mid-thickness of laminated sample. The purpose of this step is to create a sharp crack tip to minimise the resin rich pocket effect. The DCB sample is then reloaded while recording the delamination initiation and propagation. In order to obtain G_{Ic}, three parameters, including time, load (P), and load line extension (δ) should be recorded by the test machine. The delamination length (a) is recorded by the camcorder.

4.1.2 Definitions of interpreted points

In order to evaluate the effect of inkjet printed polymer deposits between CFRP laminates' layers by using this DCB test, the following point(s) are monitored and interpreted for result interpretation:

Non-linear (NL) point – the point of deviation from linearity on the load versus extension trace.

5 % / MAX point – the point which occurs first on loading the sample between:

a) The point of 5 % increase in compliance ($C_{5\%)}$ from its initial value (C_0);

b) The maximum load point.

PROP points – are determined for each discrete delamination length during steady crack propagation (NL and 5% / MAX points are excluded from PROP points). Average value of these points is used to present crack propagation.

Note, the NL and 5%/MAX points are used to present the initiation of crack growth. The PROP points are used to represent the propagation of crack.

Figure 4.3 is a typical load-extension curve for the DCB test showing initiation from the resulting mode I precrack followed by crack propagation and unloading. The load-extension curve has three major parts. In the first part, the load is increased with respect to extension linearly until the NL point where the cracks starts. The second part is the propagation part and has non-linear behaviour between NL point and peak load, which is a result of bridging of carbon fibres [6-9]. This is a common phenomenon in unidirectional laid-up sample for DCB test, as all fibres aligned in the same direction, it is unavoidable that the fibres cross the delamination plies. When fibre bridging happens, the observed fracture toughness values are higher than that of delamination within matrix alone, because more fracture energy is needed to break the bridged fibres. In this work, the precracking process is conducted to effectively remove most of the bridged fibres in order to generate a truly sharp crack tip with limited fibre bridging. The third part is the load is decreased with respect to extension after peak load, which shows the steady crack propagation, the propagation G_{Ic} values are calculated from this part.

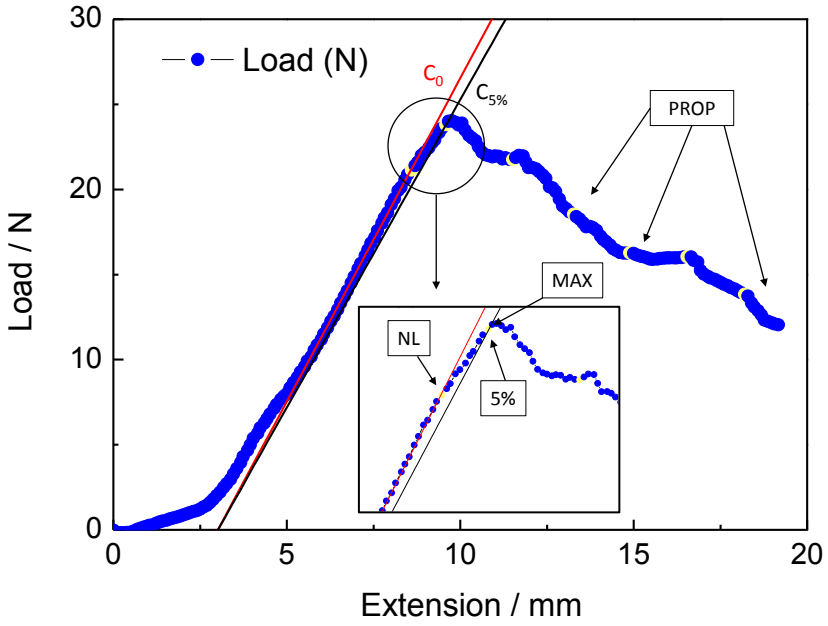

Figure 4.3 Load-extension curve of a DCB test.

4.1.3 G_{Ic} calculation

As suggested in the standard, corrected beam theory (CBT) is used to calculate G_{Ic} values. The equation is as follows:

$$G_{Ic} = \frac{3P\delta}{2b(a+|\Delta|)} \times \frac{F}{N} \tag{4.1}$$

Where P is the load, δ is the load curve displacement, b is the specimen width, a is the total delamination length, Δ is calibration parameter which can be determined by plotting the cube-root of compliance $(C = \delta/P)$, $(C/N)^{1/3}$ (load blocks are being used), as a function of delamination length a, Δ is the absolute value of the horizontal axis intercept of the $(C/N)^{1/3} - a$ curve. F is the large-displacement correction which is calculated by equation (4.2) and N is the load block correction which is calculated by equation (4.3):

$$F = 1 - \frac{3}{10}\left(\frac{\delta}{a}\right)^2 - \frac{2}{3}\left(\frac{\delta l_1}{a^2}\right) \tag{4.2}$$

$$N = 1 - \left(\frac{l_2}{a}\right)^3 \frac{9}{8}\left[1 - \left(\frac{l_2}{a}\right)^2\right]\frac{\delta l_1}{a^2} - \frac{9}{35}\left(\frac{\delta}{a}\right)^2 \quad (4.3)$$

Where l_1 is the distance from the centre of the loading pin to the mid-plane of the specimen beam and l_2 is the distance from the loading-pin centre to its edge (Figure 2.10).

4.2 Test results

As inkjet printing is a flexible deposition technique which can print different patterns easily and change between different printing inks (solutions) with negligible downtime, the effect of different toughening materials and printing patterns on G_{Ic} were investigated. Firstly, different toughening materials (i.e. PMMA and PEG) were tried with the aim to select the best one to continue the investigations. Secondly, the effect of deposited polymer amount on G_{Ic} was explored. Thirdly, different printing patterns were employed to prepare test samples to investigate their potential influence. Finally, the effect of pattern density (close or loose packed) was also studied.

4.2.1. Variation of polymer solute

5 wt.% PMMA/DMF and 5 wt.% PEG/deionised water (PEGw) solutions were printed in a hexagon pattern (*dx/dy* = 0.4/0.2 mm) onto prepreg respectively. This test aimed to investigate how the different polymers affect G_{Ic} of CFRP laminates. Figure 4.4 shows samples with printed polymer deposits have improved G_{Ic} compared to non-printed samples (NP). Error bar represents the standard deviation over the five samples of each group according to the test standard. Samples with printed PMMA have a higher improvement in G_{Ic} than samples with printed PEG in terms of crack initiation, while the crack propagation was enhanced about the same of these two groups. Note, the samples used in this set of test were made from an old batch of prepreg, as it was out of date for quite a long time, the properties of that batch of prepreg were unpredictable and unstable because the resin was gradually cured over a long period of time. As a consequence, the laminates made from the old prepreg processed deteriorating and unpredictable interlaminar properties which were not

observed in the following tests (a new batch of same type prepreg was used). Based on the results, PMMA was chosen as the primary toughening material in the following investigations.

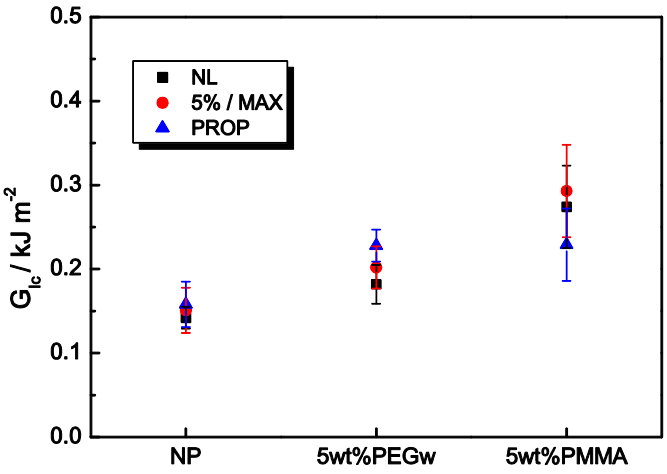

Figure 4.4 G_{Ic} comparison between non-printed (NP), 5 wt.% PEGw and 5 wt.% PMMA printed samples (n = 5).

4.2.2 Variation of PMMA amount at printed positions

It can be seen from Section 4.2.1 that samples with printed PMMA deposits showed better performance than samples with printed PEG regarding G_{Ic} improvement. This improvement was further optimised by increasing the amount of PMMA that was deposited into CFRP samples using a control pattern. There are two ways to increase the overall amount of PMMA deposited at every single printed place: 1) increasing concentration of PMMA in the solutions for printing; 2) increasing the number of printing layers (overlapping). By using a control pattern, the surface coverage of PMMA deposits before curing hardly changed as shown in Chapter 3. The amount of PMMA only increased at each localised PMMA regions. The aim of this test was to find out how the amount of localised PMMA affected the interlaminar fracture toughness of PMMA printed laminates.

4.2.2.1 Variation of PMMA concentration in solutions

Figure 4.5 shows the G_{Ic} comparison of samples with different amounts of localised PMMA deposits that were patterned using a control pattern and pattern density in each group (hexagon, *dx/dy* = 0.4/0.2 mm and rectangle, *dx/dy* = 0.4/0.2 mm). It can be clearly seen that samples with printed PMMA deposits possessed higher G_{Ic} at their respective NL point, 5%/MAX point and the PROP points. Especially, in hexagon pattern group, printed samples using 10 wt.% and 20 wt.% PMMA solutions showed a similar improvement in G_{Ic} but higher than that of the other groups (NP and 5 wt.%). Statistic data are shown in Table 4.1. In the rectangle group, samples with addition of PMMA depositions also benefited from printing. Samples were prepared using 10 wt.% and 20 wt.% PMMA solutions had a similar increase in G_{Ic} compared to the NP group as shown in Table 4.2.

This increase is of a similar magnitude to that observed in previous work where thermoplastic toughening materials have been applied [10]. However, the usage of toughening materials as discussed in Chapter 3 is considerably lower than that of other toughening methods such as interleaving and matrix toughening. The thickness of interleaves normally ranges from tens to hundreds microns [10-15], but the material usage in this work would correspond to an interleaved film thickness of about 0.07 – 2.30 μm (calculated based on cases investigated in this work). The film with this thickness would be very difficult for handling. Matrix toughening using even more toughening material as the toughening material is diffused into the resin matrix in bulk. The volume fraction of toughening material normally ranges from 2 vol.% – 50 vol.% [3, 16, 17] which is significantly larger than that of this work (0.025 vol.% – 0.8 vol.%, calculated based on cases investigated in this work). Therefore, using inkjet printing to deposit toughening materials not only can place them into pre-defined patterns precisely onto prepreg, but also can highly control the overall amount of material in order to minimise the weight gain of the toughened composites.

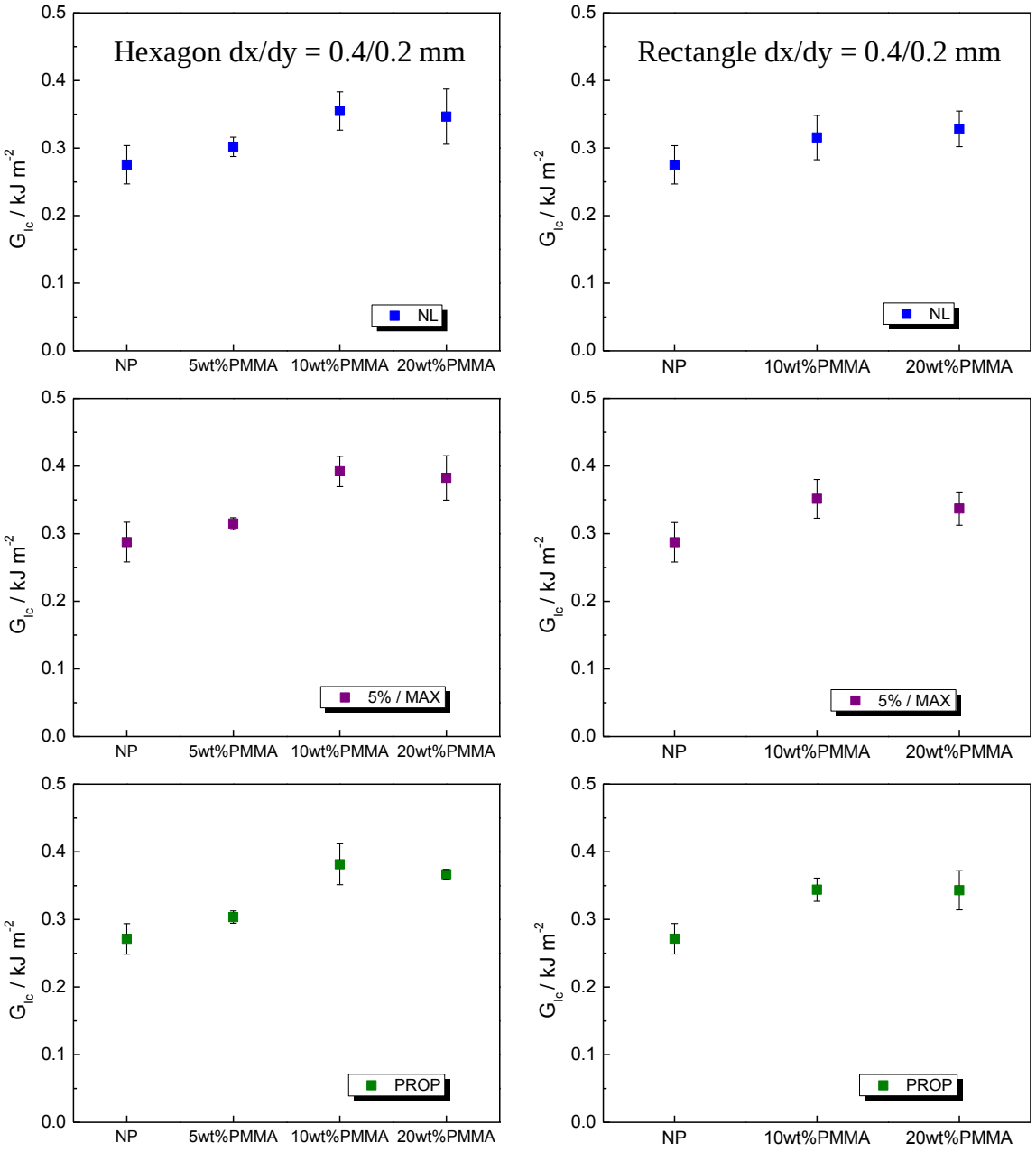

Figure 4.5 G_{Ic} comparison of samples prepared using different PMMA concentrations in the printing solutions (n = 5).

However, the increased G_{Ic} values did not follow a linear increasing trend as expected. It seems like the concentration of toughening material in printing solution has an optimum point,

less or more than that would yield a lower or equal toughening efficiency. Although the optimised concentration has not been identified, 10 wt.% of PMMA loading in the printing solution seemed the most optimised at the present time.

Table 4.1 DCB test results of samples printed with hexagon pattern using different PMMA concentration solutions.

Group	G_{Ic} / kJ m^{-2}			Increase / %
	NL	5% / MAX	PROP	
NP	0.275	0.288	0.271	–
5 wt.%	0.302	0.315	0.303	9 ~ 11%
10 wt.%	0.355	0.392	0.382	29 ~ 41%
20 wt.%	0.347	0.383	0.367	26 ~ 35%

Table 4.2 DCB test results of samples printed with rectangle pattern using different PMMA concentration solutions.

Group	G_{Ic} / kJ m^{-2}			Increase / %
	NL	5% / MAX	PROP	
NP	0.275	0.288	0.271	–
10 wt.%	0.316	0.351	0.344	15 ~ 27%
20 wt.%	0.328	0.337	0.343	19 ~ 27%

Tables 4.1 and 4.2 showed that samples printed with 10 wt.% and 20 wt.% PMMA solutions had a higher improvement in G_{Ic} than that of samples printed with 5 wt.% PMMA solutions and NP. However, no significant difference was observed between 10 wt.% and 20 wt.% groups, suggesting the toughening efficiency of 10 wt.% PMMA solution is the highest at the present time.

4.2.2.2 Variation of number of printing layers

Figure 4.6 shows the G_{Ic} comparison of samples with different number of printed PMMA layers using a control pattern (rectangle, *dx/dy* = 0.4/0.2 mm). As expected, the G_{Ic} values of PMMA printed samples were higher than that of NP group. Theoretically, the group with two printed 10 wt.% PMMA layers should have the same amount of PMMA depositions as the group with one printed 20 wt.% PMMA layer. The results agreed with the expectation that the increases in G_{Ic} of these two groups were about the same as shown in Table 4.3. However, like observed in Section 4.2.2.1, doubling the amount of PMMA usage did not give a doubled toughening efficiency. Therefore, the results from increasing PMMA concentration in printing solutions and double the printed layers of PMMA depositions indicate that adding more toughening material while keeping a same coverage (using a same pattern) does not necessarily mean the toughening efficiency could be increased if the optimum is achieved.

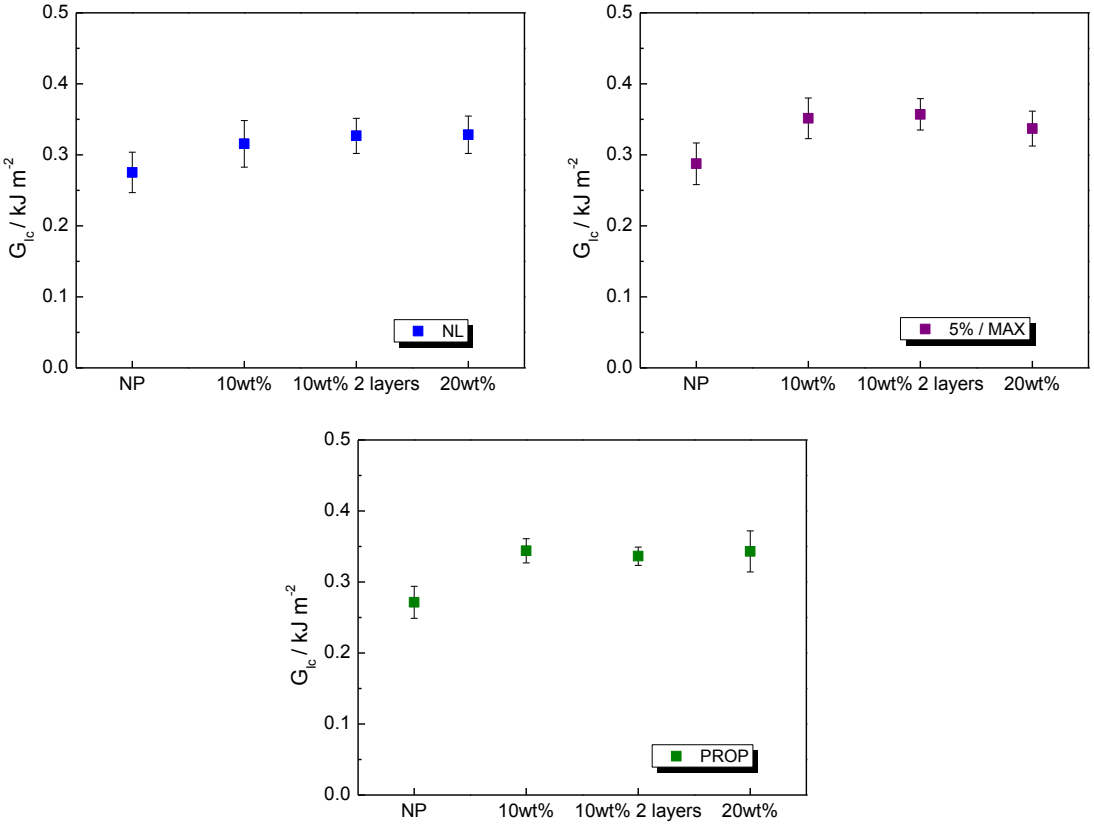

Figure 4.6 G_{Ic} comparison of samples printed with different amounts of PMMA at localised regions (n = 5).

Table 4.3 DCB test results of samples printed with different amounts of PMMA at localised regions.

Group	G_{Ic} / kJ m^{-2}			Increase / %
	NL	5% / MAX	PROP	
NP	0.275	0.288	0.271	–
10 wt.%	0.316	0.351	0.344	15 ~ 27%
10 wt.% 2 layers	0.327	0.357	0.336	19 ~ 24%
20 wt.%	0.328	0.337	0.343	19 ~ 27%

This is an encouraging result, because it illustrates that the improvement in G_{Ic} of CFRP laminates with inkjet printed polymer deposits does not simply depend on the amount of toughening material added. From the above variations in the amount of toughening material deposited, it is reasonable to conclude that the G_{Ic} values of polymer printed CFRP laminates can be increased proportionally by increasing the amount of toughening material deposited regardless of pattern or pattern density. However, when an optimum amount of material deposited between laminate plies was reached, the G_{Ic} values were not affected further by the amount of toughening material (based on the investigated cases in this thesis). Thus, whether other variations such as pattern shape and pattern density would make any difference to G_{Ic} values of polymer printed CFRP laminates were of great interests to investigate further.

As demonstrated in Chapter 1, drop-on-demand (DOD) inkjet printing can deposit material on specific/favoured locations without mask. This flexibility allows various patterns can be printed, and the change of patterns is simple and fast. Therefore, it is feasible and reasonable to vary the pattern shape and pattern density to explore their potential effects on the G_{Ic} of final composites.

4.2.3 Variation of printing patterns

4.2.3.1 Discrete dot pattern and line pattern

We know increasing the amount of PMMA deposits between laminate plies leads to an increase in G_{Ic}, up to about 41% as observed in Section 4.2.2.1. In this section, different discrete dot patterns, line patterns were employed to investigate their potential effect on the G_{Ic} values of polymer printed laminates. Since the previous experiments showed that samples prepared using 10 wt.% PMMA solution performed the best among the groups, it was chosen as the printing solution to conduct this sectional experiments. Four different patterns with the same material usage per unit area were designed to be printed. Figure 4.7 schematically shows these four different patterns with their respective dimensions.

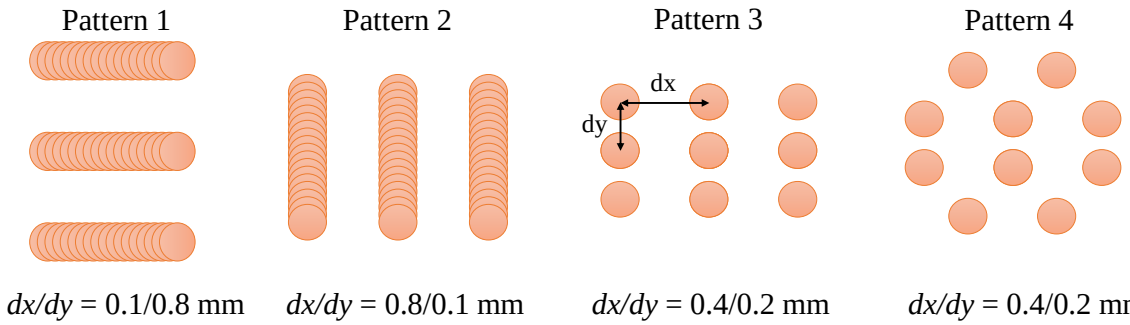

Figure 4.7 Schematically show the four different patterns for printing with their respective dimensions.

It can be found from Figure 4.8 that all the four groups with printed PMMA deposits had improved G_{Ic} as expected. Especially, groups 3 and 4 with printed discrete patterns have higher G_{Ic} values compared to that of samples with printed line patterns (pattern 1 and 2). The group with printed hexagon pattern (pattern 4) showed the highest improved G_{Ic} corresponding to both crack initiation and propagation. Table 4.4 gives the statistical results of these tests. Although these four groups had the same amount of PMMA deposited between plies, the distribution of formed PMMA particles of line printed groups was not as even as groups with discrete dots. Additionally, the size of PMMA particles formed from printed

PMMA line was neither even. These two differences could contribute to the lower increases in G_{Ic} of PMMA line printed samples.

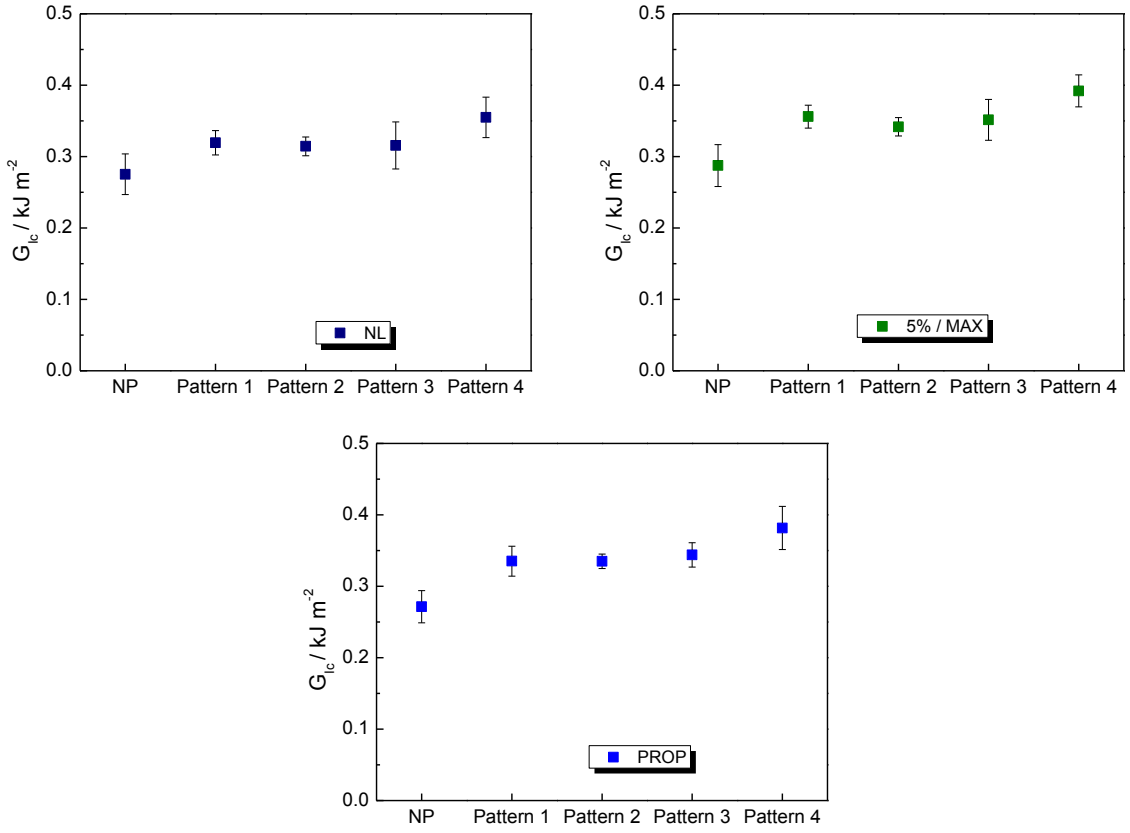

Figure 4.8 G_{Ic} comparison of samples with different printing patterns (n = 5).

Table 4.4 DCB test results of samples printed with different patterns.

Groups	G_{Ic} / kJ m^{-2}			Increase / %
	NL	5%/MAX	PROP	
NP	0.275	0.288	0.271	–
Pattern 1	0.319	0.355	0.335	16 ~ 24%
Pattern 2	0.314	0.342	0.334	14 ~ 23%
Pattern 3	0.316	0.351	0.344	25 ~ 27%
Pattern 4	0.355	0.392	0.382	29 ~ 41%

4.2.3.2 Continuous thin film

It has been extensively reported that using interleaves to toughen laminate composites is an effective method, although inherent drawbacks exist, such as weight penalty [18], decrease in modulus and interlaminar shear properties [15]. In order to investigate the effect of a discrete dot pattern and a continuous thin film of toughening materials on the G_{Ic} of final CFRP laminates, 20 wt.% of PMMA solutions were used to print a thin film at the mid-thickness ply of DCB samples. The thickness of the printed thin film theoretically ranges from 0.6 – 2.3 μm (based on cases investigated in this work) depends on the polymer concentration in printing solutions. When a continuous thin film instead of a discrete dot pattern was printed between laminate plies, the surface coverage increases to 100%, while only about 37% area was printed using a discrete dot pattern (hexagon, dx/dy = 0.4/0.2 mm). Although the surface coverage of PMMA deposited as a thin film increased more than twice that in the discrete dot pattern system, the increased G_{Ic} values in the former case was not twice that of the latter as shown in Figure 4.9. This result suggests the toughening efficiency does not only depend on the surface coverage of toughening material.

Comparing the two systems regarding to the amount of the deposited PMMA, the 20 wt.% film group has eight times PMMA usage compared to the 20 wt.% discrete dot pattern group, however, the G_{Ic} values of samples with printed thin film were only about 0.3 – 0.6 times higher than that of samples with printed discrete dot pattern as shown in Table 4.5. Moreover, the crack propagation of the samples with printed thin film was unstable, even though the average G_{Ic} values were higher than that of samples with printed discrete dot pattern. Figure 4.10 shows the G_{Ic} against delamination length of every test sample within the three groups, it can be seen that the cracks that developed in every thin film printed sample were “jumpy”, and this large degree of variability is not ideal for applications in industry. On the contrary, the discrete dot pattern group showed a steady crack propagation. As shown in Chapter 3, the printed PMMA film broke up into randomly sized and distributed PMMA particles embedded in resin after curing, this lack of control over the distribution/size of toughening material regions after co-curing with the laminate is believed to be the reason for the large error observed in film printed group.

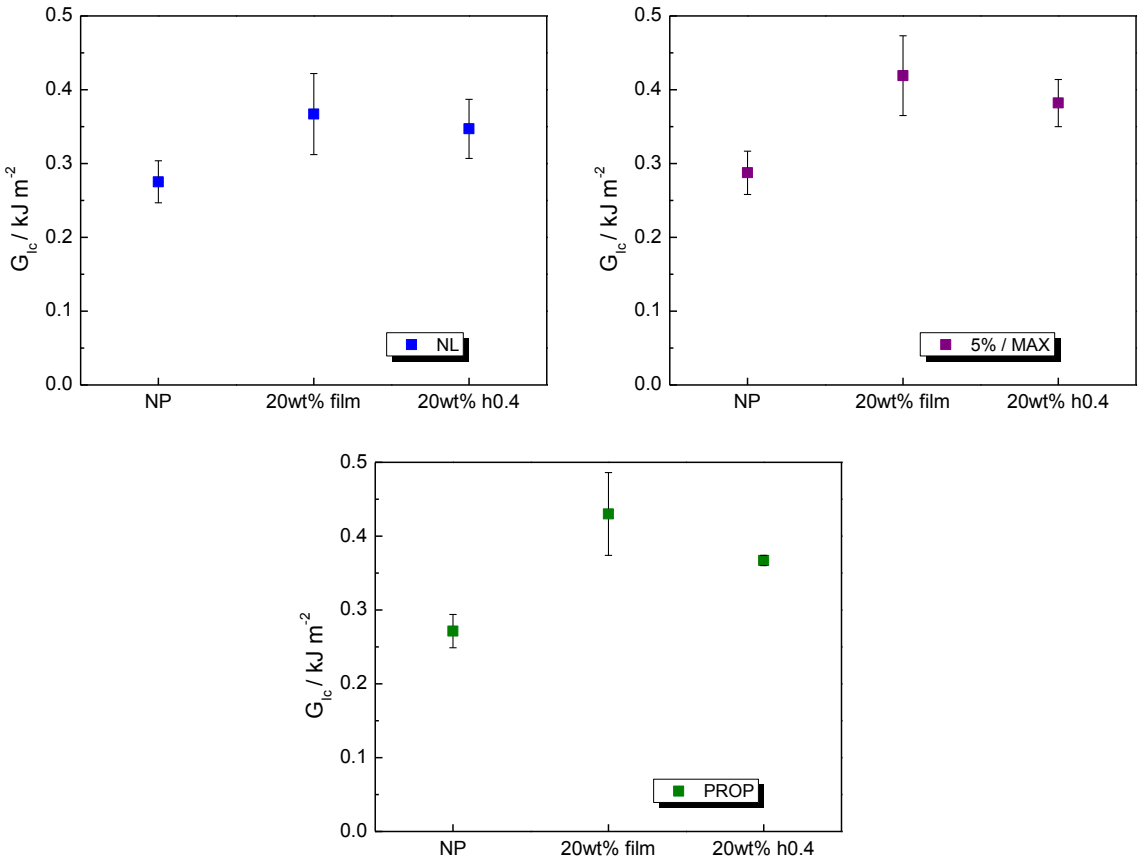

Figure 4.9 G_{Ic} comparison of samples with printed thin film and discrete dot pattern ("h0.4" represents hexagon, *dx/dy* = 0.4/0.2 mm; n = 5).

Table 4.5 DCB test results of samples with printed thin film and discrete dot pattern using the same PMMA solution.

Group	G_{Ic} / kJ m^{-2}			Increase / %
	NL	5% / MAX	PROP	
NP	0.275	0.288	0.271	–
20 wt.% film	0.367	0.419	0.430	33 ~58 %
20 wt.% h0.4	0.347	0.383	0.367	26 ~ 35%

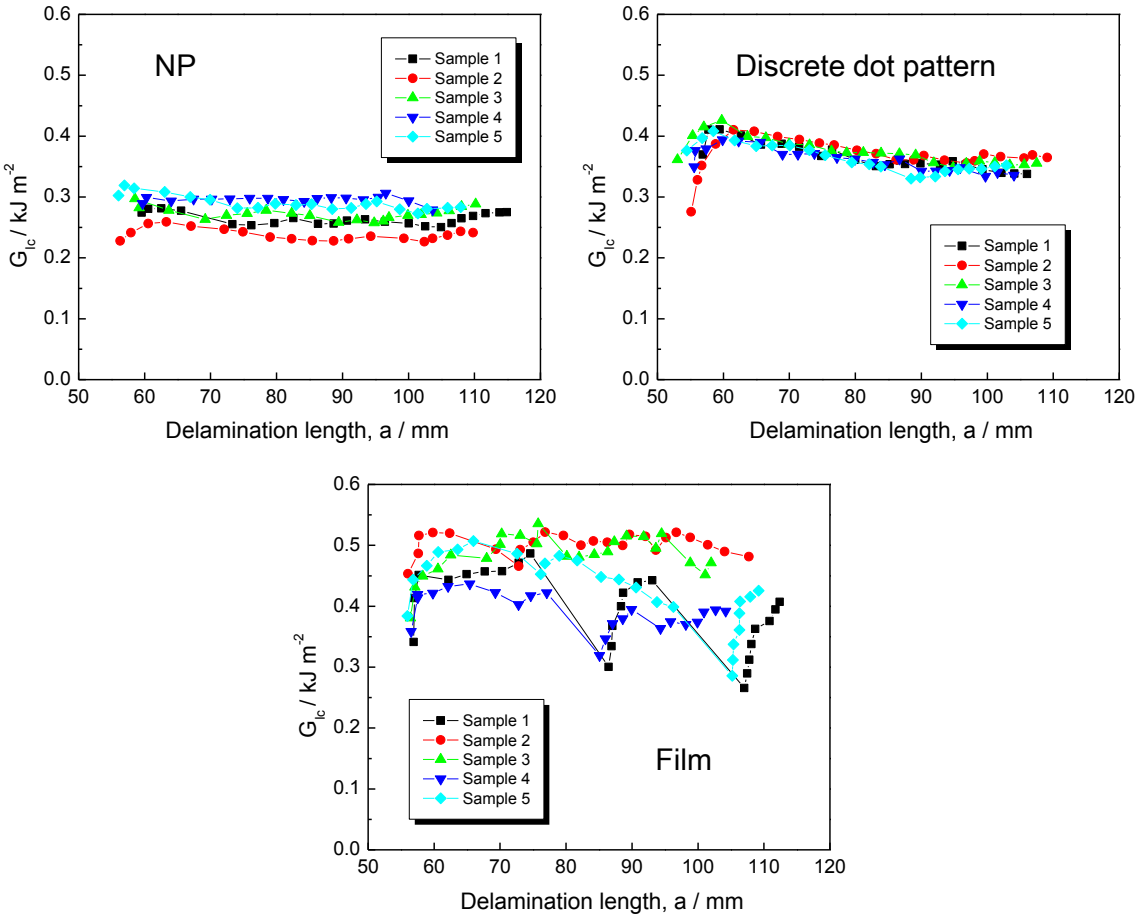

Figure 4.10 The crack propagation comparisons of samples without printing and printed with a discrete dot pattern and a thin film (n = 5).

The above comparisons indicate that the efficiency of material usage of inkjet printing is high due to the highly controllable printing pattern dimensions. Evenly distributed discrete dot pattern can be achieved by inkjet printing, and the above DCB test results demonstrated that the toughening materials patterned in a discrete dot pattern can improve the G_{Ic} of CFRP laminates more efficiently in terms of material usage. Although laminate printed with a thin film of toughening material had a higher improvement in G_{Ic}, the crack propagation was unstable that is not ideal for commercial products.

4.2.4 Variation of pattern density

As discussed in Chapter 2, pattern dimensions *dx* and *dy* can be varied to determine the pattern density deposited on a substrate. With smaller *dx* and/or *dy*, the pattern can be close packed and vice versa. The ultimate result of this variation is the different surface areas of PMMA particles embedded in resin matrix and different toughening material usages. Figure 4.11 schematically shows two different pattern densities using the same printing pattern.

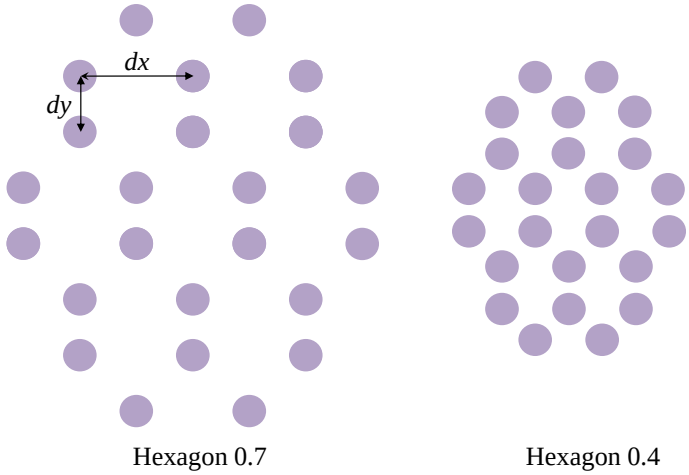

Figure 4.11 Two pattern densities with same pattern shape (Hexagon 0.7: *dx/dy* = 0.7/0.35 mm; Hexagon 0.4: *dx/dy* = 0.4/0.2 mm, n = 5).

The 10 wt.% of PMMA solution was used to print the above two pattern densities for preparing DCB samples. It can be seen from Figure 4.12 that samples prepared using the 'Hexagon 0.4' pattern possessed higher G_{Ic} than that of samples printed using the 'Hexagon 0.7' as expected. Higher pattern density means more toughening material is deposited per unit area onto a specific interface where the cracks are expected to propagate, requiring more energy to fracture numerous discrete toughed zones.

This method of increasing the amount of toughening material is different from the one used in Section 4.2.2. By close packing deposits, both the overall amount of material deposited and the surface covered by polymer deposits are noticeably increased. However, by increasing the concentration of solute in printing solution or/and increasing the number of printing layer overlapping at the same deposited position can noticeably increase the amount

of material deposited, but the surface area of polymer deposits can only be increased to a very small amount. For examples, by increasing the concentration of PMMA from 10 wt.% to 20 wt.% in solutions, although the material usage was doubled, the diameter of formed PMMA particles was slightly increased from 33.7 μm to 36.8 μm, accordingly, the surface area of PMMA particles was increased by 0.2 times. However, by close packing the PMMA dots as shown in Figure 4.11, the surface area of PMMA particles was increased by about 2 times with 1.75 times increase in material usage. Therefore, the noticeably increased PMMA surface area which acts as toughening area is assumed as the main reason for the enhanced toughness. Table 4.6 provides the statistic results of this set of test.

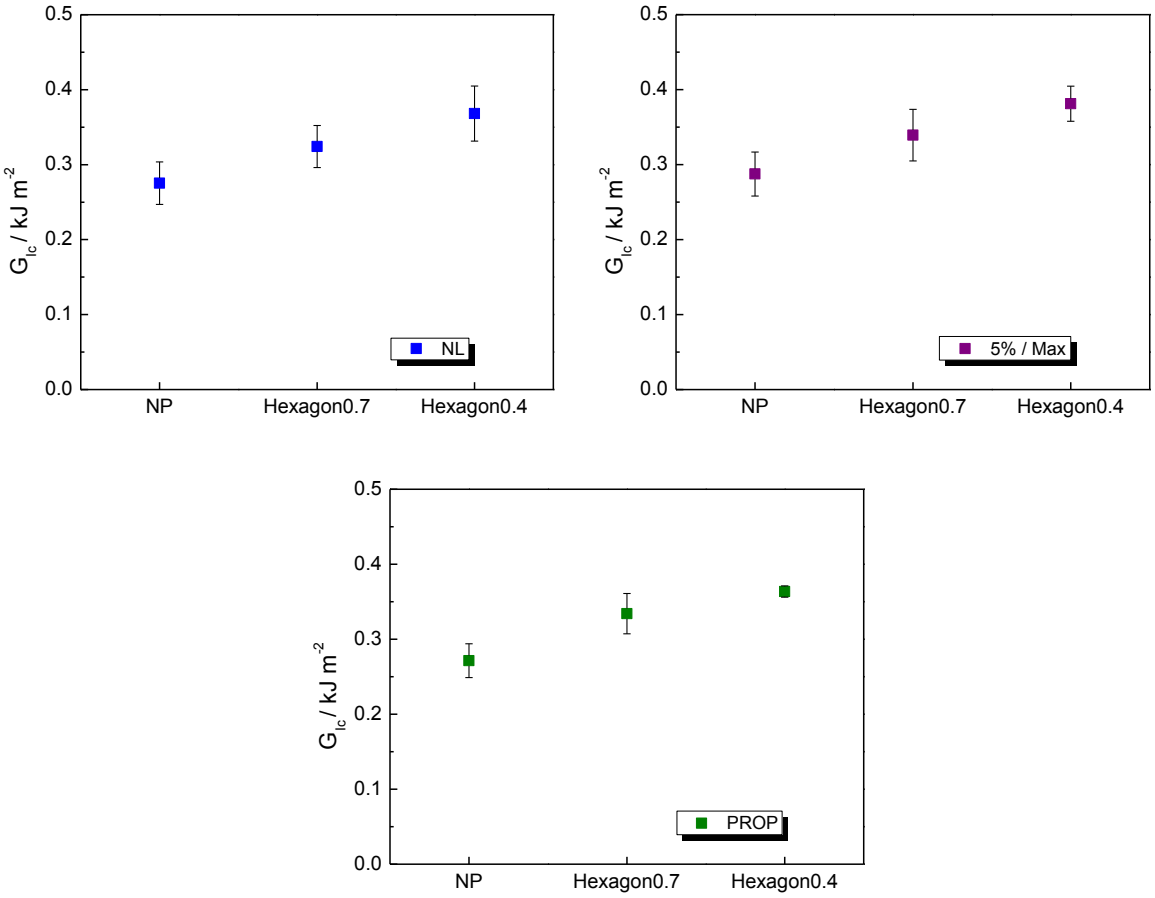

Figure 4.12 G_{Ic} comparison of samples printed with different pattern densities (n = 5).

Table 4.6 DCB test results of samples printed with different pattern densities using the same PMMA solution.

Group	G_{Ic} / kJ m^{-2}			Increase / %
	NL	5% / MAX	PROP	
NP	0.275	0.288	0.271	–
Hexagon 0.7	0.324	0.339	0.334	18 ~ 24%
Hexagon 0.4	0.355	0.392	0.382	29 ~ 41%

4.3 Selective printing

Inkjet printing is a flexible method which can deposit material at specific places on a substrate. This advantage can be utilised to achieve selective toughening which means the toughening materials are only applied to critical regions that have potential failure crisis. Some places within a structure are likely to be stress concentration points such as holes, bindings and corners. Toughening structures which have complex shapes and/or inner-structures such as holes and corners can be challenge. Ideally, the material of these places needs to be stronger than that of other places. Common ways to achieve this are to use different materials to make different parts of a structure, or add more/different materials at these specific places. Although these methods can achieve the selective toughening, they are not efficient in terms of material usage, manufacturing process and time. Moreover, if using different materials to make a structure, the joins between different materials is likely to be weak points which could lead to potential mechanical failure in future service.

By using inkjet printing to deposit toughening material(s) at targeted places where mechanical failures are prone to happen, a solution to the above problem can be provided, this process is named selective printing. Selective printing can toughen material locally, this will reduce the manufacturing cost and time, weight gain or/and minimises any side effects of introducing toughening materials, if at all.

In order to verify the effect of selective printing, 10 wt.% PMMA solution was used to prepare two different sets of DCB samples as shown in Figure 4.13. For the type A sample, the second half of the test area was printed with PMMA. For the type B samples, the first half of test area was printed with PMMA, the remaining half was left with no printing. Unlike the previous experiments, where the difference of printed and unprinted was between different samples, but in this experiment, the difference was generated within one sample, therefore, the potential G_{Ic} is expected to change within a single G_{Ic}-Delamination curve.

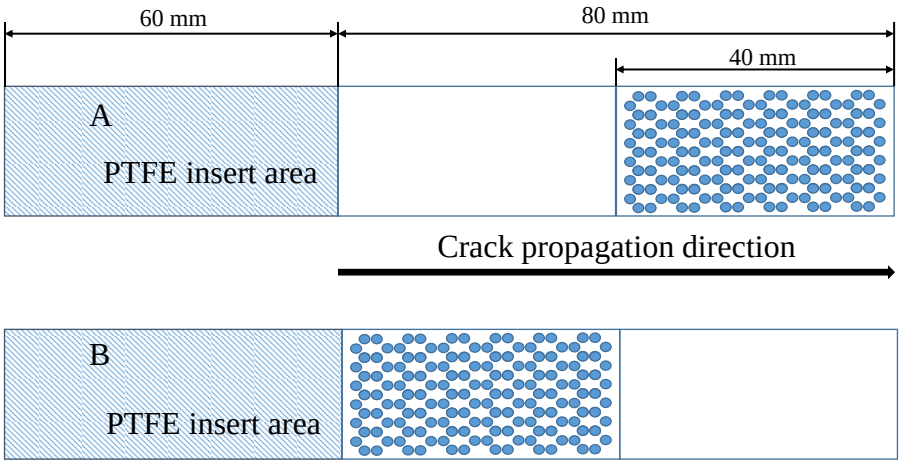

Figure 4.13 The two types of DCB samples. In sample A, the crack propagates into a non-printed zone then a printed zone. In samples B, the crack front encounters a printed region first then a non-printed zone.

As can be seen in Figure 4.14, the printed part within every test sample had higher G_{Ic} than that of the unprinted part. Figure 4.15 shows the average G_{Ic} values of each group (A and B), the printed part had an approximately 15% increase in G_{Ic} compared to that of non-printed part, indicating more energy was needed to propagate the PMMA toughened zone. This result indicates that the selective printing is feasible by inkjet printing, as the printing pattern can be pre-designed via software, complex patterns/shapes are easily obtained, therefore, if the stress concentration points can be identified from a structure, these areas can be selectively printed with different or more toughening materials to make them tougher without introducing overweight toughening material.

Another advantage of selective toughening is that the cure process of the original resin system can still be preserved without excessive interruption, therefore, the resin matrix still possesses good mechanical properties, and the negative effect of the introduced toughening material on the mechanical performance can be reduced to minimum.

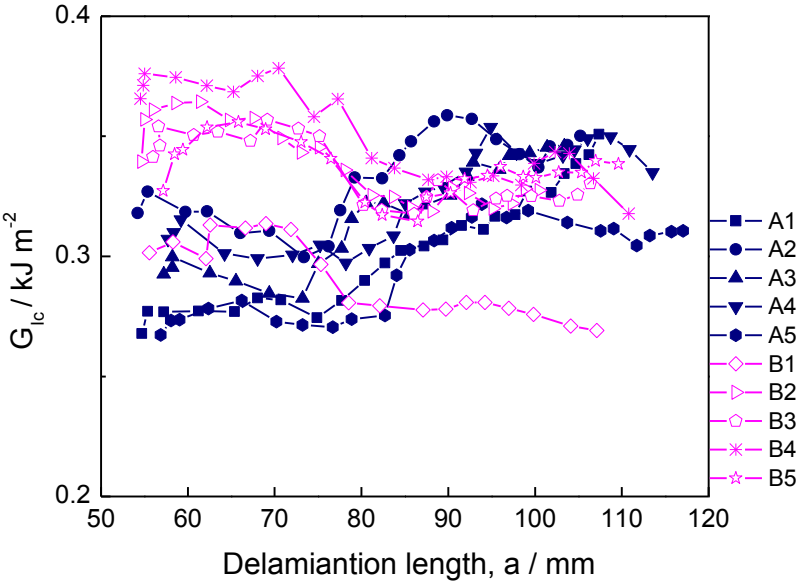

Figure 4.14 G_{Ic}-Delamination curves of type A and B samples (n = 5).

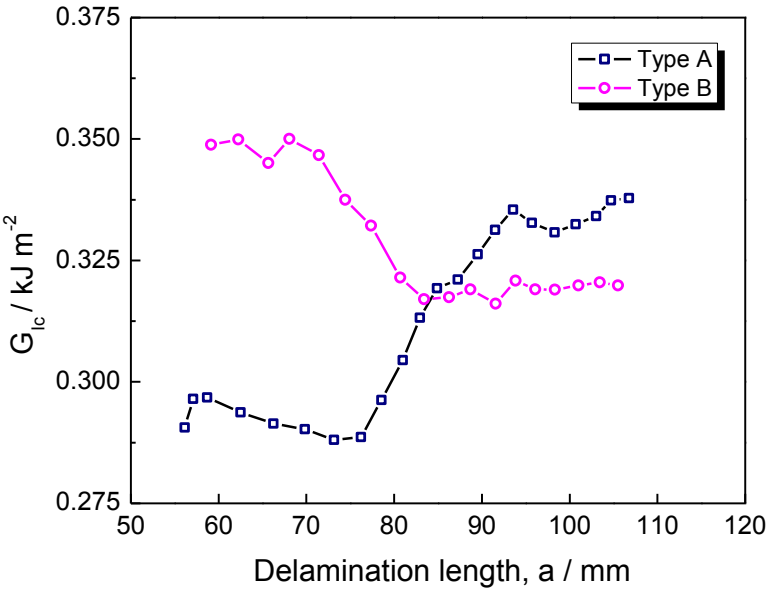

Figure 4.15 G_{Ic}-delamination curves (average value) comparison between type A and B samples (n = 5).

4.4 Discussion

The above experiments showed that the CFRP laminates with inkjet printed polymer deposits had better mode I delamination resistance compared to the non-printed ones. The improvement ranged from 9% to 58% and depended on parameters associated with the pattern dimensions, polymer concentrations and polymer natures. Overall, the addition of polymer deposited between laminate plies contributes the improvement in interlaminar properties. The following microscopy was conducted to investigate the possible explanations for the mechanical improvement of the engineered CFRP laminates.

4.4.1 Microscopy of fracture surfaces of DCB tested samples

The DCB test results suggest that the interface with printed polymer depositions is important in determining the improved mechanical property. The observations of polymer morphology showed in Chapter 3 suggests that the printed PMMA deposits formed particles embedded in epoxy resin after curing. Therefore, it is necessary to know the morphology of polymer deposits in composite after curing by investigating the fracture surfaces of DCB tested samples. Figure 4.16 shows the fracture surfaces of non-printed (NP) samples and samples with printed PMMA line patterns. The printed PMMA lines can be visualised with the naked eye, which again proves that different patterns can be printed with controllable dimensions and the printed patterns can be kept relatively within designed position. Unfortunately, the discrete dot pattern cannot be seen due to the destructive failure nature of the DCB test, it is difficult to identify the micro-sized individual particle in patterns on the rough fracture surfaces.

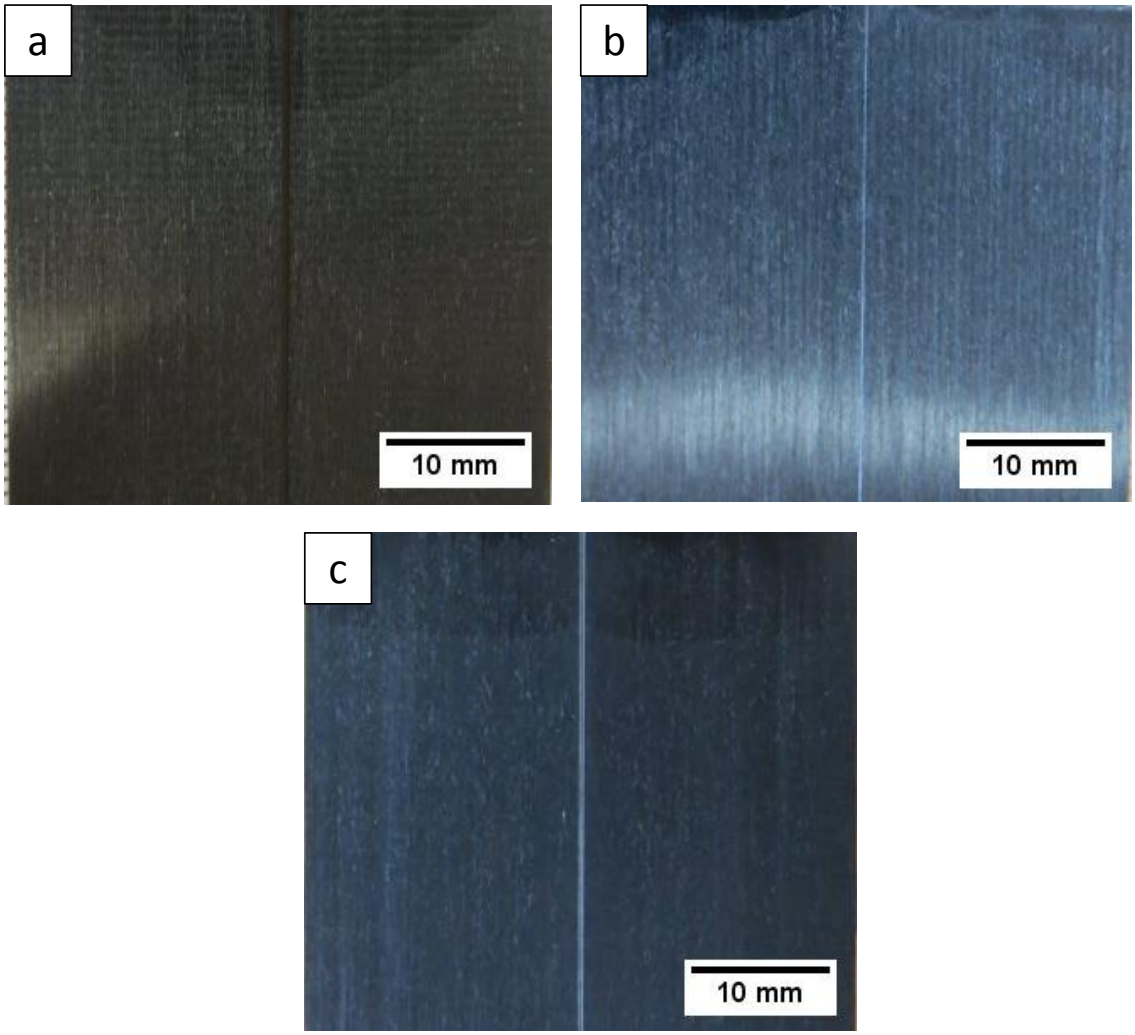

Figure 4.16 DCB tested fracture surfaces with PMMA deposits and without printing. (a) horizontal lines (*dx/dy* = 0.1/0.8 mm); (b) vertical lines (*dx/dy* = 0.8/0.1 mm); (c) NP .

SEM was used to analyse the fracture surfaces of polymer printed CFRP samples after DCB tests. As can be seen in Figure 4.17(a) and (b), non-printed samples showed relatively smooth and flat fracture surfaces, reflected a brittle fracture. However, upon applying PEG as the toughening material, "hackles" appeared on the fractured surfaces (Figure 4.17(c) and (d)), which indicated that PEG toughened interfaces require more energy to delaminate, resulting in a more ductile failure. Unfortunately, no printed pattern can be identified on the fracture surfaces.

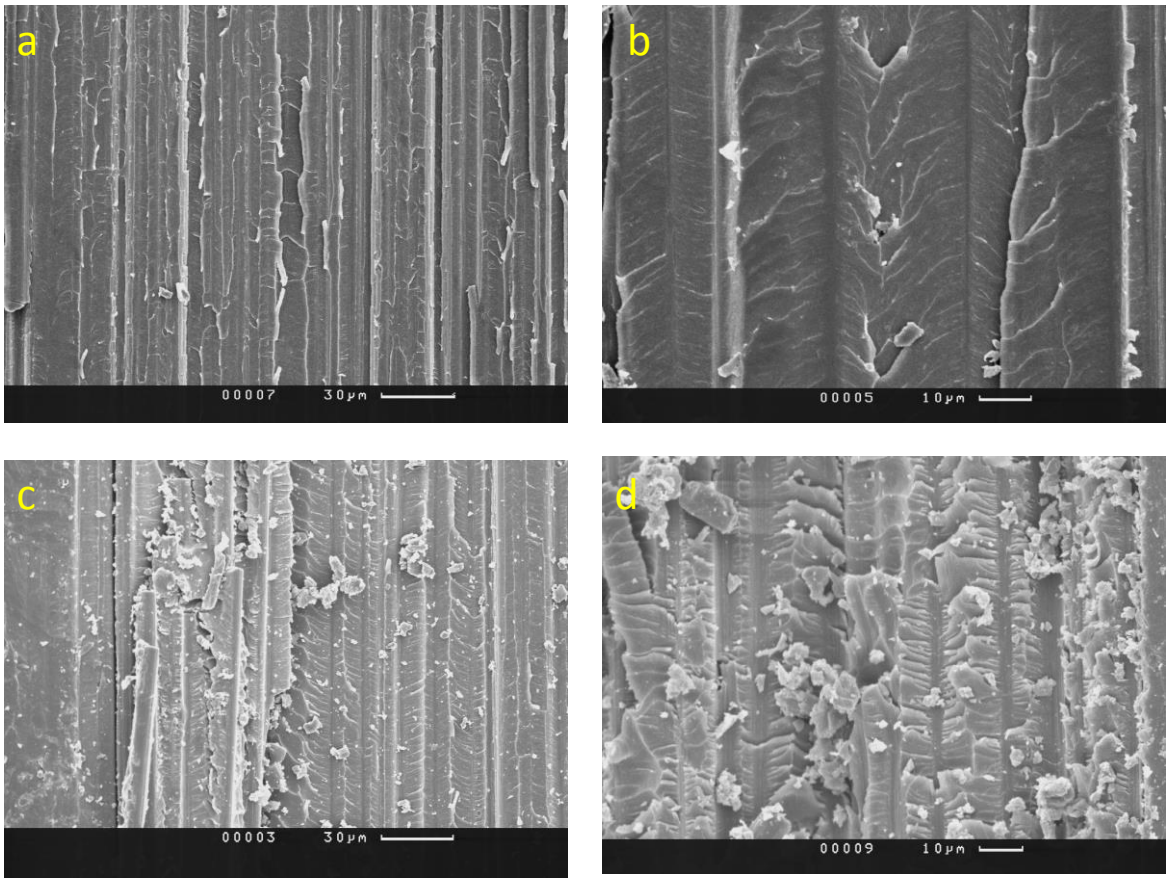

Figure 4.17 SEM images of fracture surfaces of DCB tested samples without and with PEG deposits. (a) and (b) NP; (c) and (d) hexagon, *dx/dy* = 0.4/0.2 mm.

However, when PMMA droplets were printed between laminate plies, as observed in Section 3.6.1, spherical PMMA particles formed as second phases as shown in Figures 4.18 and 4.19. As mentioned before, due to the complex texture of CFRP laminate, and the severe damage done to the test surface, the discrete dot patterns cannot be identified, but scattered particles can be spotted as shown in Figures 4.18(b), (d) and (f). Although the printed lines can be clearly observed in Figure 4.16, SEM images cannot show these lines very well (4.18(c) and (e)). However, particles located at reasonable positions can be found as shown in Figure 4.18(d) and (f). The fracture surfaces of samples with printed PMMA thin film highly agreed with the observation of epoxy coated glass substrate with printed PMMA thin film. The printed film broke down into randomly dispersed PMMA particles with a wide range of

diameters as shown in Figure 4.19. And the fracture surfaces are much rougher than that of the other groups, indicating more energy was involved in the failure.

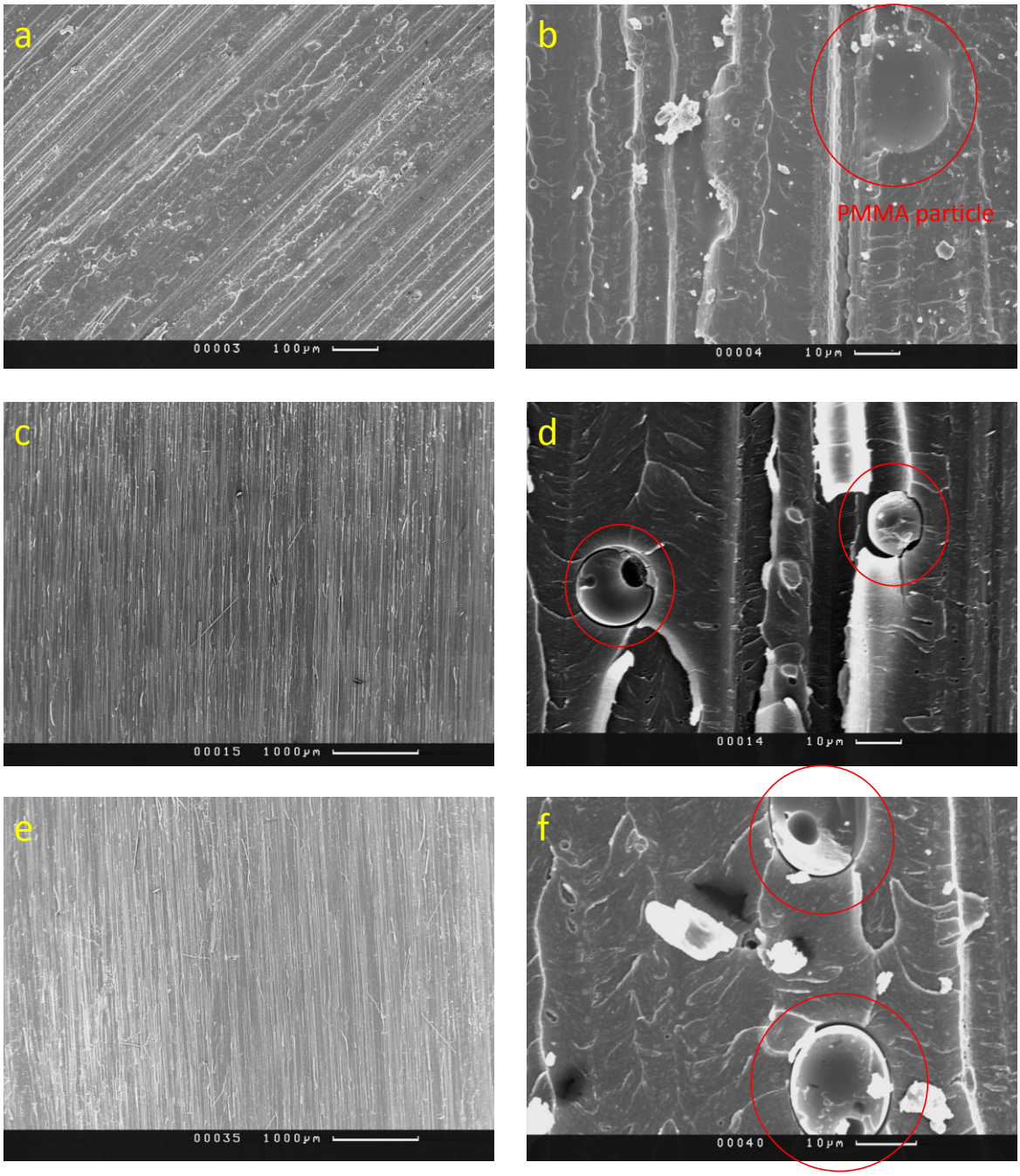

Figure 4.18 SEM images of fracture surfaces of DCB tested samples with PMMA depositions. (a) and (b): hexagon, *dx/dy* = 0.4/0.2 mm; (c) and (d) horizontal lines, *dx/dy* = 0.1/0.8 mm; (e) and (f) vertical lines, *dx/dy* = 0.8/0.1 mm.

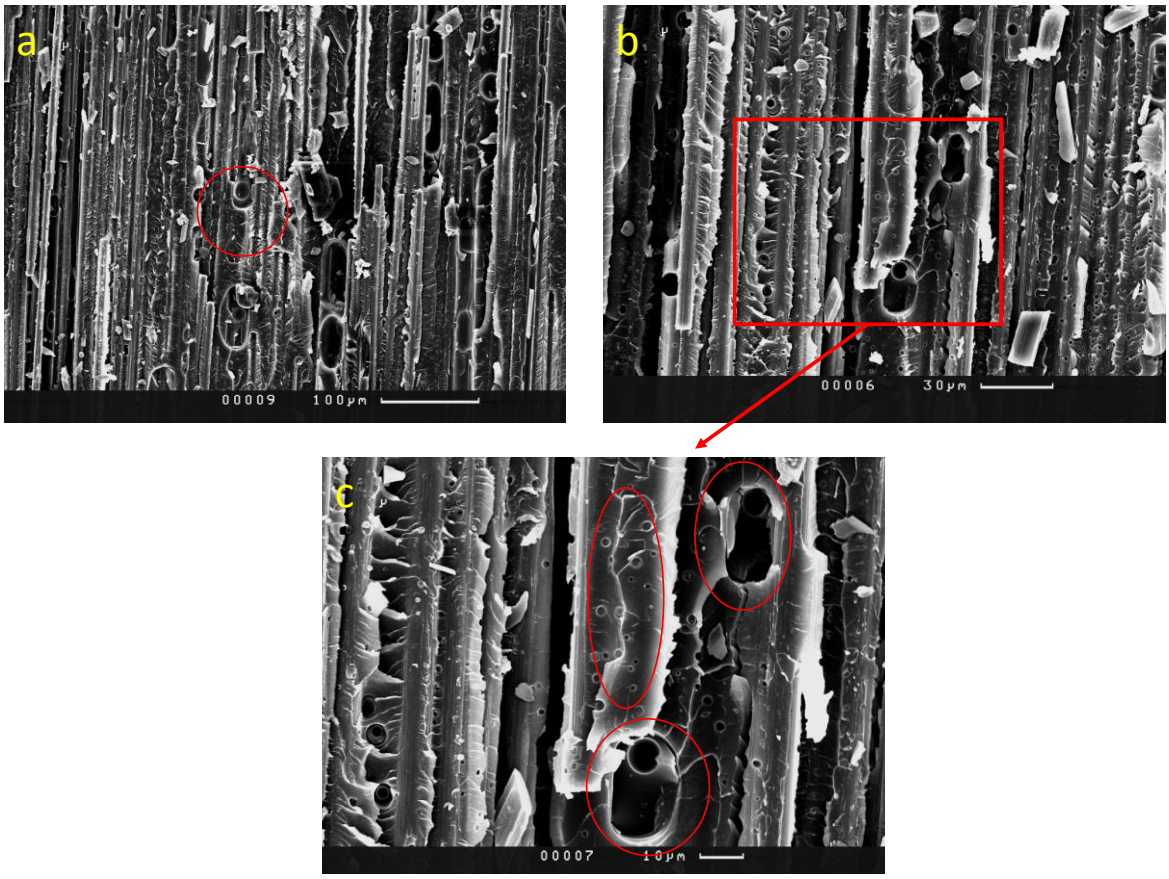

Figure 4.19 SEM images of fracture surfaces of DCB tested samples with printed PMMA thin film.

4.4.2 Possible mechanisms for improved G_{Ic}

System with printed PEG deposits

In the PEG system, the increase in G_{Ic} could be attributed to the evenly dispersed PEG dissolved regions in the epoxy matrix. It has been demonstrated that PEG is miscible with the epoxy resin, the subsequent formation of PEG second phase in epoxy resin is important to the mechanical performance of the matrix [19], because these PEG secondary phases could act as crack pinners or blunter.

Zavareh and Samandari reported that by adding a small amount (<10 wt.%) of a low molecular weight (M_n ~ 600) PEG into epoxy resin, the impact strength and fracture

resistance were improved by 5.7 and 5.4 times greater than that of unmodified epoxy resin respectively [3]. Figure 4.20 shows the SEM of epoxy/PEG after etching. PEG particles (second phases) which had an average diameter of 85 nm are clearly can be seen. They also conducted Fourier transform infrared spectrometry and differential thermal analysis of the blend, and found out that there was a strong interaction between epoxy and PEG phases at their interfacial area. The dispersion of PEG particles and the strong interaction were believed the reason for the increase in fracture properties in their system. Although the toughening mechanisms were not certainly identified, crack pinning, particle bridging and crack path deflecting were proposed.

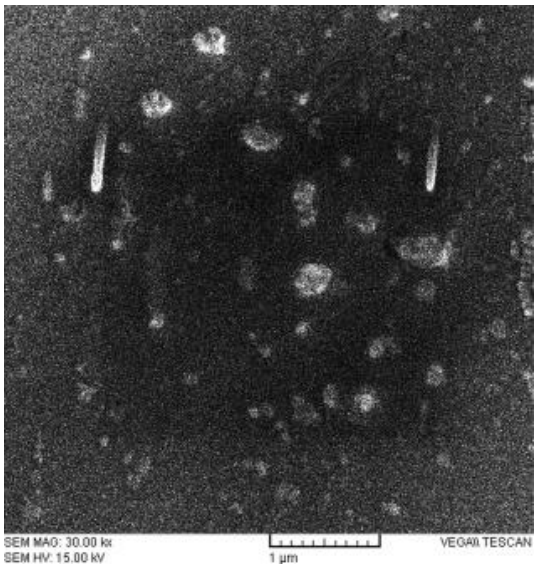

Figure 4.20 SEM image of epoxy/PEG after etching [3].

It was assumed that during the curing process, PEG has shallowly penetrated into the epoxy resin of the adjacent plies of the composite laminates and formed second phases after co-curing with the composite. These PEG secondary phases are believed to help increasing interlaminar fracture resistance by crack pinning or blunting, Figure 4.21 schematically shows the crack pinning mechanism (‘a’ and ‘2b’ are parameters used to predict the relationship between increased fracture energy, particle size and distance between particles. Since these parameters are not determined in this work, details about the calculation are not disused further). As the amount of PEG printed in laminates was sufficient small, and the

PEG is relatively weak compared to PMMA, it is not supervised that the toughening effectiveness was not significant.

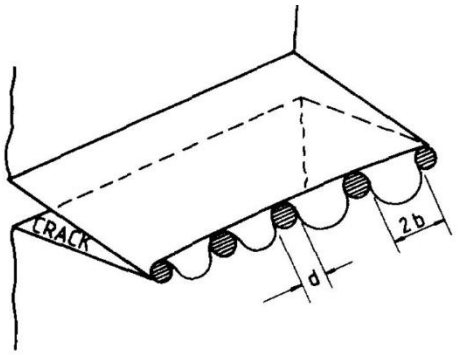

Figure 4.21 Crack pinning mechanism [16].

System with printed PMMA deposits

Epoxy toughened by thermoplastic modifiers have been reported as an effective method to overcome the drawbacks of using brittle epoxy as composite matrix. A variety of toughening mechanisms [20-26] have been proposed to explain the improved toughness as shown in Figure 4.22.

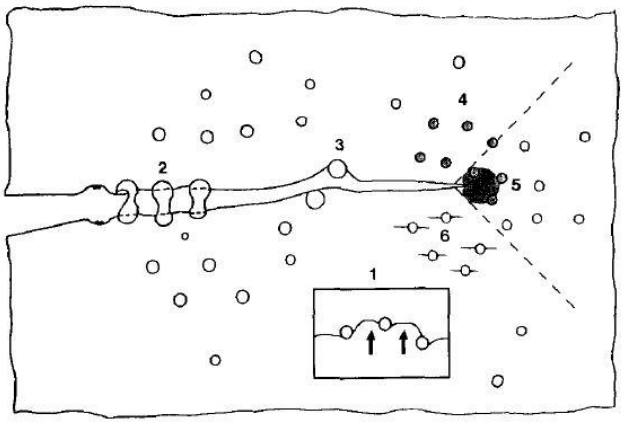

Figure 4.22 Schematic showing the toughening mechanisms proposed for epoxies toughened by thermoplastic modifiers. 1) crack pinning; 2) particle bridging; 3) crack path deflection; 4) particle yielding; 5) particle yielding induced shear banding and 6) microcracking [23].

The DCB results showed that G_{Ic} of CFRP laminates with printed PMMA deposits were increased up to 58% compared to non-printed samples. Based on the microscopy results in Sections 3.6.1 and 4.4.1, the following two mechanisms were assumed as the main reasons to explain the improvement in G_{Ic} of the PMMA printed systems: (1) PMMA particles acted as crack stoppers which can absorb energy by plastic deformation. Given the viscoelastic nature of PMMA, the well dispersed PMMA particles provided an energy absorption path by plastic deformation, which can decelerate crack growth as the crack tips were shielded by the thermoplastic regions; (2) debonding between PMMA particles and their surrounded epoxy resin matrix due to limited compatibility of PMMA with the epoxy resin. As can be seen from Figure 4.18 (d), (f) and 4.19, those PMMA particles tended to debond from the surrounded epoxy matrix, this process increased the fracture surfaces area due to the deflected crack path, which can absorb a great amount of energy.

Considering the effects of polymer concentrations in solutions, printed layers and pattern densities on the G_{Ic} of engineered laminates, it is reasonably understood that with the increased plastic zones either by increasing the number of plastic zones or the size of plastic zones or both, crack growth needs more energy to propagate. However, the increase in G_{Ic} was not linear with the increase in the number of PMMA particles. This observation could be attributed to the following reasons/assumptions: 1) the diameter of PMMA particles formed from deposits of 10 wt.% and 20 wt.% PMMA solutions was close (8% in variation), while the diameter of PMMA particles formed from deposits of 5 wt.% PMMA solution was 28% smaller than that of 10 wt.% group. This difference in particle diameter resulted in doubled difference in fracture surfaces area. Obviously, large fracture surfaces suggesting more energy involved; 2) the presence of reinforcing fibres constrained the plastic deformation of PMMA particles after the toughness was increased to an optimum extend. Therefore, there was no significant difference between 10 wt.% and 20 wt.% PMMA printed systems as shown in Figure 4.5. However, when applying excessive plastic zones (PMMA particles) such as printing a thin film between laminate plies, the G_{Ic} was likely to be noticeably increased due to crack bridging by deformed PMMA particles. The relatively large PMMA particles spanned the two crack surfaces and arrested the crack propagation, this process significantly reduced the stress generated around the crack tip. Considering the energy absorption, the opening of the crack cause the debonding or fracturing of PMMA

particles at the interface between plies, therefore, more energy was required to for crack propagation.

With regard to the effect of pattern shape on the G_{Ic} of PMMA printed laminate, Figure 4.8 shows that samples with printed hexagon pattern had the highest G_{Ic} compared to the other groups. It is assumed that the crack path was more diverted by using hexagon pattern. Figure 4.23 schematically shows the crack propagations by using different pattern shapes. As can be seen, the well lined patterns such as square and line patterns, cracks can propagate without too much interruptions, they can grow more easily than system with printed hexagon pattern. As a result, more diverted crack paths need more energy to propagate, which contributes to the improved fracture toughness.

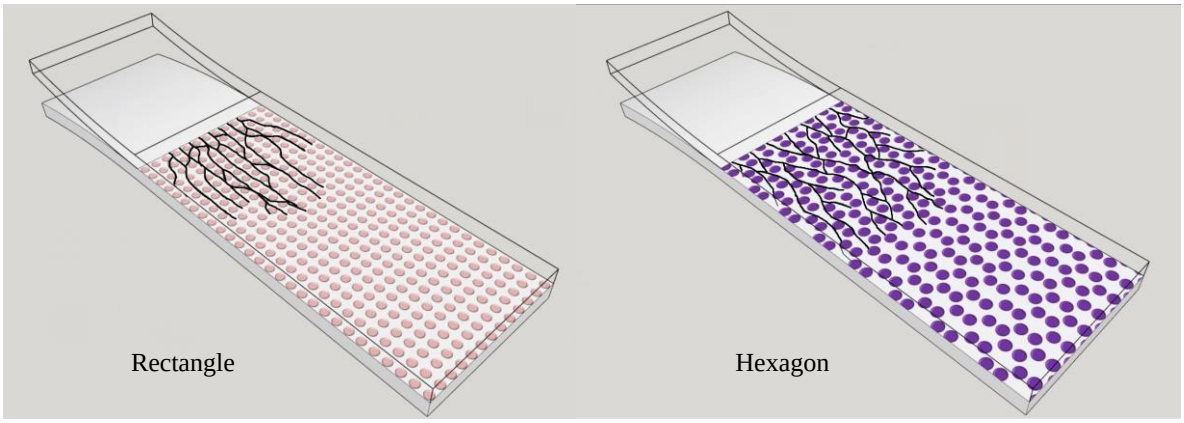

Figure 4.23 Schematically show the crack paths under different printed pattern shapes.

4.5 Conclusions

Using inkjet printing to deposit toughening materials as a solution between laminate plies has been shown to noticeably improve the G_{Ic}, which exhibited a strong correlation with the interlaminar fracture toughness. The increase in amount of toughening material usage led to a proportional increase in G_{Ic}, however, this increase was not further influenced by the amount of added polymer if keeping the same printing pattern. Patterns with higher surface coverage (high density) resulted in a higher G_{Ic} as the cracks encountered more toughening regions, hence needed more energy to propagate. Although laminates printed with a thin film possessed a higher interlaminar fracture resistance than that of laminates with printed discrete

dot and line patterns, the crack propagation was observed unstable which is not ideal for applications in industry. In addition to that, the toughening efficiency of using a discrete dot pattern is higher than using a thin film in terms of material usage.

Microscopy of DCB tested fracture surfaces agreed with the observation shown in Chapter 3. The printed PMMA deposits formed spherical particles after co-curing with the composites. However, the printed patterns could not be clearly identified on the fracture surfaces due to the severer failure nature of the DCB test. Fracture surfaces with printed polymer deposits are much rougher than that of non-printed samples, indicating more energy involved during failure.

Plastic deformation of polymers, crack pinning or blunting by polymer particles and debonding between particles and epoxy matrix were assumed the main reasons to explain the improved G_{Ic}. The geometrical distribution of PMMA particles also contributes to the toughening effectiveness.

References

[1] L. Carlsson, "Fracture of laminated composites with interleaves," *Key Engineering Materials*, vol. 120, pp. 489-520, 1996.

[2] Standsrd, "Fibre-reinforced plastic composites. Determination of mode I interlaminar fracture toughness," ed: BS ISO 15024:2001.

[3] S. Zavareh and G. Samandari, "Polyethylene glycol as an epoxy modifier with extremely high toughening effect: Formation of nanoblend morphology," *Polymer Engineering & Science*, vol. 54, pp. 1833-1838, 2014.

[4] Y. Fang, H. Kang, W. Wang, H. Liu, and X. Gao, "Study on polyethylene glycol/epoxy resin composite as a form-stable phase change material," *Energy Conversion and Management*, vol. 51, pp. 2757-2761, 2010.

[5] E. Schauer, L. Berglund, G. Pena, C. Marieta, and I. Mondragon, "Morphological variations in PMMA-modified epoxy mixtures by PEO addition," *Polymer*, vol. 43, pp. 1241-1248, 2002.

[6] M. Shokrieh, M. Salamat-Talab, and M. Heidari-Rarani, "Effect of initial crack length on the measured bridging law of unidirectional E-glass/epoxy double cantilever beam specimens," *Materials & Design*, vol. 55, pp. 605-611, 2014.

[7] S. Spearing and A. G. Evans, "The role of fiber bridging in the delamination resistance of fiber-reinforced composites," *Acta metallurgica et materialia*, vol. 40, pp. 2191-2199, 1992.

[8] B. F. Sørensen and T. K. Jacobsen, "Large-scale bridging in composites: R-curves and bridging laws," *Composites Part A: Applied Science and Manufacturing*, vol. 29, pp. 1443-1451, 1998.

[9] A. B. de Morais, "A new fibre bridging based analysis of the Double Cantilever Beam (DCB) test," *Composites Part A: Applied Science and Manufacturing*, vol. 42, pp. 1361-1368, 2011.

[10] M. Kuwata and P. J. Hogg, "Interlaminar toughness of interleaved CFRP using non-woven veils: Part 1. Mode-I testing," *Composites Part A: Applied Science and Manufacturing*, vol. 42, pp. 1551-1559, 2011.

[11] M. Arai, Y. Noro, K. I. Sugimoto, and M. Endo, "Mode I and mode II interlaminar fracture toughness of CFRP laminates toughened by carbon nanofiber interlayer," *Composites Science and Technology,* vol. 68, pp. 516-525, 2008.

[12] M. Hojo, T. Ando, M. Tanaka, T. Adachi, S. Ochiai, and Y. Endo, "Modes I and II interlaminar fracture toughness and fatigue delamination of CF/epoxy laminates with self-same epoxy interleaf," *International Journal of Fatigue,* vol. 28, pp. 1154-1165, 2006.

[13] S. Hamer, H. Leibovich, A. Green, R. Intrater, R. Avrahami, E. Zussman, *et al.*, "Mode I interlaminar fracture toughness of Nylon 66 nanofibrilmat interleaved carbon/epoxy laminates," *Polymer Composites,* vol. 32, pp. 1781-1789, 2011.

[14] M. Kuwata and P. Hogg, "Interlaminar toughness of interleaved CFRP using non-woven veils: Part 2. Mode-II testing," *Composites Part A: Applied Science and Manufacturing,* vol. 42, pp. 1560-1570, 2011.

[15] K. L. White and H. J. Sue, "Delamination toughness of fiber-reinforced composites containing a carbon nanotube/polyamide-12 epoxy thin film interlayer," *Polymer,* vol. 53, pp. 37-42, 2012.

[16] A. C. Garg and Y. W. Mai, "Failure mechanisms in toughened epoxy resins—A review," *Composites Science and Technology,* vol. 31, pp. 179-223, 1988.

[17] T. Hsieh, A. Kinloch, K. Masania, A. Taylor, and S. Sprenger, "The mechanisms and mechanics of the toughening of epoxy polymers modified with silica nanoparticles," *Polymer,* vol. 51, pp. 6284-6294, 2010.

[18] N. Sela and O. Ishai, "Interlaminar fracture toughness and toughening of laminated composite materials: a review," *Composites,* vol. 20, pp. 423-435, 1989.

[19] Y. P. Huang and E. M. Woo, "Effects of entrapment on spherulite morphology and growth kinetics in poly (ethylene oxide)/epoxy networks," *Polymer,* vol. 42, pp. 6493-6502, 2001.

[20] R. A. Pearson and A. F. Yee, "Influence of particle size and particle size distribution on toughening mechanisms in rubber-modified epoxies," *Journal of Materials Science,* vol. 26, pp. 3828-3844, 1991.

[21] C. K. Riew and A. J. Kinloch, "Toughened plastics I: science and engineering," American Chemical Society, Washington, 1993.

[22] C. B. Bucknall and A. H. Gilbert, "Toughening tetrafunctional epoxy resins using polyetherimide," *Polymer,* vol. 30, pp. 213-217, 1989.

[23] R. A. Pearson and A. F. Yee, "Toughening mechanisms in thermoplastic-modified epoxies: 1. Modification using poly(phenylene oxide)," *Polymer,* vol. 34, pp. 3658-3670, 1993.

[24] J. Spanoudakis and R. J. Young, "Crack propagation in a glass particle-filled epoxy resin," *Journal of Materials Science,* vol. 19, pp. 473-486, 1984.

[25] E. Girard‐Reydet, V. Vicard, J. Pascault, and H. Sautereau, "Polyetherimide‐modified epoxy networks: Influence of cure conditions on morphology and mechanical properties," *Journal of Applied Polymer Science,* vol. 65, pp. 2433-2445, 1997.

[26] D. Maxwell, R. J. Young, and A. J. Kinloch, "Hybrid particulate-filled epoxy-polymers," *Journal of Materials Science Letters,* vol. 3, pp. 9-12, 1984.

Chapter 5

Preserved interlaminar shear strength and improved damage tolerance

This chapter firstly introduces basic information about the short beam shear (SBS) test which is used to determine the apparent interlaminar shear strength (ILSS) of fibre reinforced plastic composites. Test results and discussion are then provided. The purpose of this first part of experimentation was to analyse the interlaminar properties of polymer added laminates subjected to shear loads. Impact resistance investigation was secondly investigated. The results show that the CFRP laminates with addition of polymer deposits have better impact resistance while preserving interlaminar shear strength. Finally, dynamic mechanical properties are explored by using dynamic mechanical analysis which shows the addition of polymer deposits did not degrade the mechanical integrity of printed CFRP laminates before 140^{o}C, indicating the toughened material can be used under relatively high temperature.

5.1 Introduction

As introduced in Chapter 1, fibre reinforced laminates have enhanced mechanical properties along fibre directions. Because no through laminate thickness reinforcement is available, the interlaminar properties entirely depend on the matrix resin. However, epoxy is commonly brittle due to its high cross-link density, thus, the relatively poor interlaminar strength of laminates usually leads to through thickness failure. This is a critical problem associated with their use, and this drawback has restricted wider utilisation of composite laminates in aerospace and other structural applications, as a consequence, industry is struggling to further reduce the bodyweight of their products.

Interlaminar strength is sensitive to defects such as microcracks, poor interlaminar bonding, defects and impurities [1-5]. In this research, polymer deposits have been inkjet printed onto interfaces between adjacent plies of composite laminates, which could potentially affect the

interlaminar strength or/and the interface adhesion between fibre and matrix of modified laminates. Therefore, it is necessary to find out the potential effect of polymer additions on these critical properties. The short beam shear (SBS) test has been widely used to characterise the interlaminar shear properties of the fibre reinforced composites. The horizontal shear failure generated in three point bending where the maximum shear stress arises at the middle-plane can be induced by using a suitable sample dimension [6]. The test samples are easy to prepare and the data processing is very simple, which make this test a useful screening tool.

5.1.1 Principle

A sample of rectangular cross-section is loaded as a simple beam in flexure so that interlaminar shear failure occurs. The sample rests on two supports with a preferable distance (span) and load is applied by means of a loading member midway between the supports as shown in Figure 5.1. This test is similar in nature to the three-point bending test which is used to measure the flexure properties of material. However, a smaller test span to sample thickness ratio is employed to increase the level of shear stress in the test sample to encourage interlaminar shear failure.

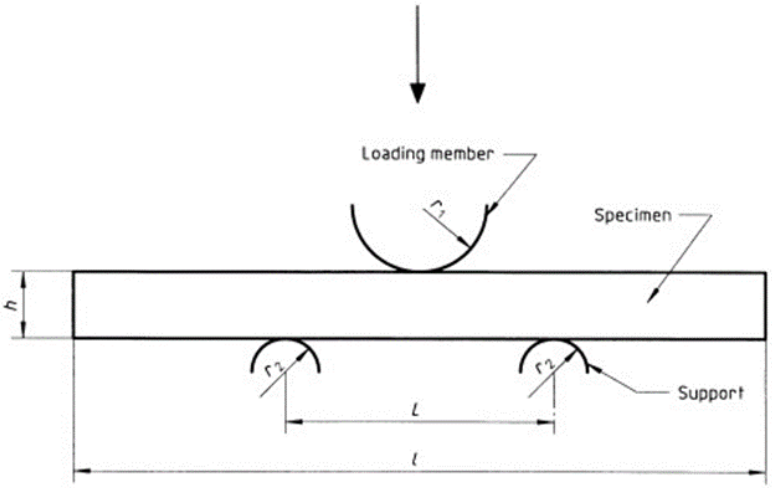

Figure 5.1 Schematically show the SBS loading configuration [7].

5.1.2 Definitions of interpreted points

Apparent interlaminar shear stress, τ – the interlaminar shear stress acting on the neutral plane of the test sample, it is calculated from Equation 5.1.

$$\tau = \frac{3F}{4bh} \tag{5.1}$$

Where F is the load, b is the width of the test sample, h is the thickness of the test sample.

Apparent interlaminar shear strength (ILSS), τ_M – the value of the apparent interlaminar shear stress at failure or when the load reaches a maximum value, it is calculated from Equation 5.2.

$$\tau_M = \frac{3F_M}{4bh} \tag{5.2}$$

Where F_M is the maximum load, b is the width of the test specimen, h is the thickness of the test specimen.

Note, these two equations presents the linear elasticity of test materials, but in practice the test material shows limited linearity, so the results calculated are not absolute values. But it is satisfactory on a comparative basis.

5.2 Test results and discussion

As the shear failure tested by using the SBS method is likely to happen between interlaminar interfaces of a laminate, the polymer deposits printed between laminate plies is more likely to affect the interlaminar shear properties. Previous research has shown that toughening was gained at the expense of other critical properties such as modulus, ILSS and stiffness [8-10]. Therefore, it is worth investigating the effect of inkjet printed polymer depositions between laminate plies on these properties.

5.2.1 Variation of polymer in printing solutions

Polyethylene glycol (PEG) and poly(methyl methacrylate) (PMMA) containing solutions were used to print a control pattern (hexagon, *dx/dy* = 0.4/0.2 mm) between every ply of laminates for making SBS test samples. It can be seen from Figure 5.2 that samples with inkjet printed polymer deposits did not show decreases in ILSS compared to that of non-printed (NP) group. Error bar represents the standard deviation over the five samples of each group according to the test standard. This is an encouraging result as improvement in mode I interlaminar fracture toughness (G_{Ic}) can be achieved by inkjet printing thermoplastic polymer deposits between laminate plies without sacrificing laminate ILSS. Although the grade level of improvement in G_{Ic} is not very high at this stage, the ILSS of polymer printed CFRP laminates are preserved. This has not been widely achieved by other toughening methods such as interleaving and matrix toughening, which suggests a promising benefit to using inkjet printing as a toughening method.

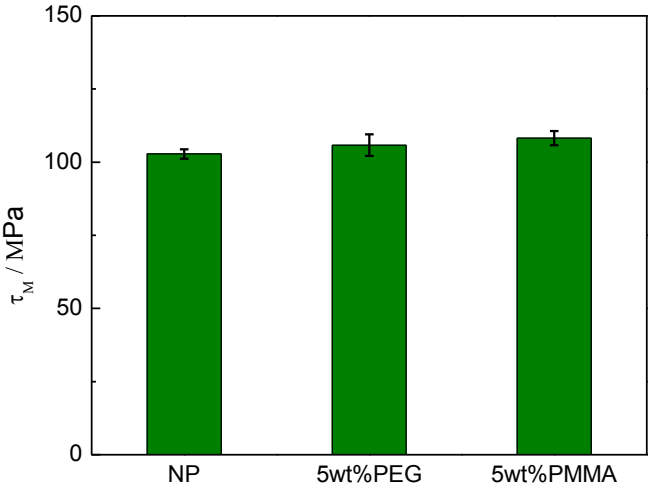

Figure 5.2 ILSS comparisons of samples with different polymer deposits (Pattern: hexagon, *dx/dy* = 0.4/0.2 mm, n = 5).

Wang et al. [11] reported the G_{Ic} of their toughened CFRP laminates by adding copolymer films (Figure 5.3) had up to 106% increase compared to the un-modified samples. However, the ILSS decreased about 33% compared to the un-modified ones. They claimed the reduction on ILSS was attributed to the low shear strength of their interleaves. The reduction

in ILSS due to the insert of interleaves was also observed in another work [12]. Although the G_{Ic} of toughened CFRP laminates was improved nearly three times, the flexure strength and modulus were decreased by 15% and 7.3% respectively compared to their baseline. These results revealed the drawback of using continuous thin film as a toughening method: the continuous toughening phase is the Achilles' heel embedded in composite laminates, because those toughening materials normally have inferior shear strength and modulus compared to rigid composite matrices, thus, the ILSS or/and modulus of interleave toughened laminates are normally decreased.

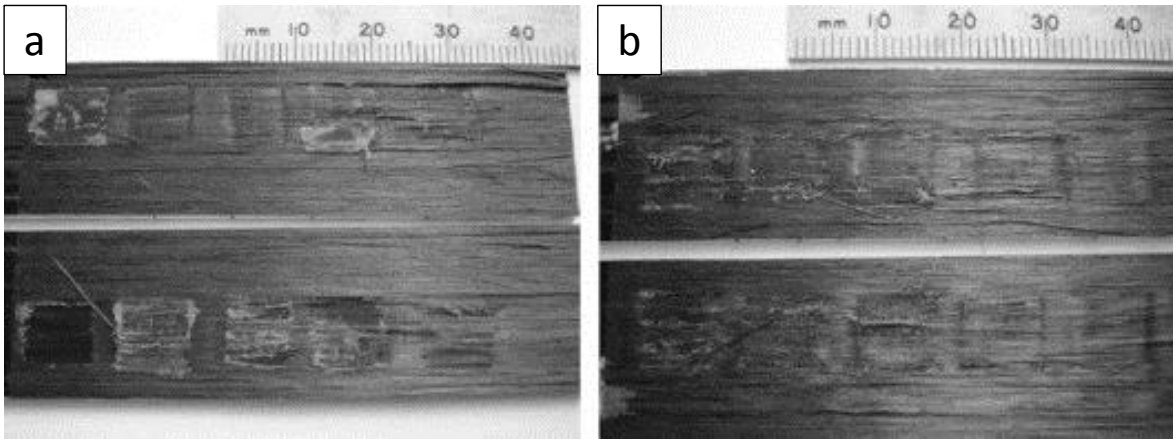

Figure 5.3 DCB tested fracture surfaces of samples with inserted films [11].

A matrix toughening method was employed by Miyagawa et al. [8] to increase the fracture toughness of matrix toughened CFRP laminates. A 67% improvement in G_{Ic} was observed compared to un-toughened samples. However, the ILSS of matrix toughened laminates decreased up to 21% compared to the un-toughened samples. There was another downside which was the added weight penalty. About 5 wt.% of toughening material was used to toughen the matrix.

Using inkjet printing to deposit discrete toughening regions instead of films resolves the problem raised in interleaving method. The large amount of toughening material added between laminate plies can be avoid. Inkjet printing can highly control the distribution and volume of toughening materials, thus minimising the interference of added toughening material in matrix curing. Another point needs to be emphasised is the material usage of

toughening material by employing inkjet printing. As discussed in Chapters 1 and 3, the volume of droplet generated by inkjet printing is in the pico-litre scale, and the toughening materials are only deposited where needed. Therefore, the volume fraction and weight percentage of toughening material added in discrete dot pattern was about 0.1 vol.% and 0.08 wt.% respectively (the uppermost example, based on the cases investigated in this PhD), which is considerably lower than that of the work done by Wang et.al (~ 2 vol.%) and the one done by Li et.al [12] (~ 1.5 vol.%). Although the toughening efficiency achieved in this project was not as high compared to the above mentioned works, the ILSS of inkjet printed laminates is preserved. This is important to material/structure design in industry, as a good mechanical integrity of an engineered material that is preferred rather than a material has improved mechanical properties at the expenses of others.

5.2.2 Variation of PEG concentration and solvent in printing solutions

As mentioned in Chapter 3, PEG can be dissolved in both organic and inorganic solvents. Although the solvent should not affect mechanical properties of the composites since any solvent ideally should fully evaporate before lay-up, it is worth investigating the potential effect of different solvents on the mechanical performance of polymer printed laminates. This is to ensure the above assumption is correct. In order to minimise the potential effect of evaporation rate of solvents on the possible amount of residue trapped in PEG deposits, solvents with similar boiling point (Deionised water, Dw, 100 ℃; 1-Propanol, Pp, 97 ℃) were adopted.

As expected, changing the solvent used for the PEG contained solutions does not have much influence on ILSS of printed samples compared to non-printed group (NP) as shown in Figure 5.4. This result indicates that solvent in deposits printed on substrate evaporates before lay-up, because the volume of a droplet is sufficient small.

It is also can be seen from Figure 5.4 that varying PEG concentration in the solutions (and using a control discrete dot pattern) does not show much difference in ILSS of printed samples. In other words, the amount of PEG deposits (in the range of investigated systems) between laminate plies hardly affect in terms of ILSS. This could be attributed to the even

distribution of PEG regions between laminate plies, and the tiny amount of added PEG minimised the interference in epoxy cure between adjacent plies. However, it is worth noting that the ILSS of PEG printed CFRP laminates was retained.

Although the longitudinal strength of unidirectional CFRP is dependent on the carbon fibre properties, the small span to sample thickness ratio (5) in this SBS test increases the interlaminar fracture failure which depends on the matrix domain properties. Previous research [13] reported that there is a strong interaction between PEG and epoxy, which means the adhesion between PEG and epoxy is good, these results agree with the preserved ILSS of PEG added CFRP laminates. As the PEG was deposited evenly onto the printing area, and the adhesion between PEG and epoxy is strong, therefore, the increase in amount of PEG deposited hardly affects the curing of epoxy, resulting in no decrease in ILSS of tested samples.

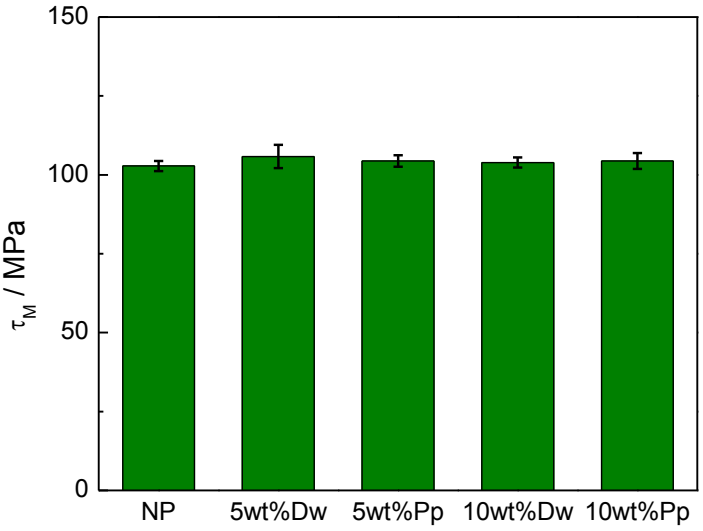

Figure 5.4 ILSS comparisons of samples printed using different PEG concentrations and solvents in solutions (Dw: Deionised water; Pp: 1-Propanol. Pattern: hexagon, *dx/dy* = 0.4/0.2 mm, n = 5).

5.2.3 Variation of PMMA concentration in printing solutions and printing patterns

Samples printed with solutions containing different PMMA concentrations were tested to investigate the potential effects of PMMA amount between laminate plies on the ILSS. Figure 5.5 shows that varying PMMA concentration in solutions (and using a control discrete dot pattern, hexagon *dx/dy* = 0.4/0.2 mm) does not make much difference in ILSS. In order to investigate the effects of discrete dot pattern and continuous thin film on ILSS of PMMA printed CFRP laminate samples, discrete pattern (hexagon, *dx/dy* = 0.4/0.2 mm) and continuous thin film (thickness ~ 3 μm) were printed between every ply of laminate respectively. It can be seen from Figure 5.5 that samples with printed thin film had 5.6% decreases in ILSS compared to that of NP group. This observation indicates that excessive PMMA deposits between laminate plies acted as flaws/defects which noticeably jeopardise the curability of epoxy of adjacent plies, resulting in a lower ILSS.

Furthermore, the standard deviation of the thin film printed group is considerably larger than that of the other groups. This increase in standard deviation is explained as being due to the poor controllability of PMMA deposits' size and distribution by printing a thin film between laminate plies. As observed in Chapter 3, the printed PMMA thin film broke into particles with a wide range of sizes embedded in resin matrix after curing. Therefore, unstable crack propagations were observed within every DCB test sample which was printed with a continuous thin film. As a consequence of the poor controllability of PMMA particles' size and distribution, the SBS test samples (cut from the initial parent plate) have completely different PMMA distributions between every ply, thus, the mechanical performances varied over a large range.

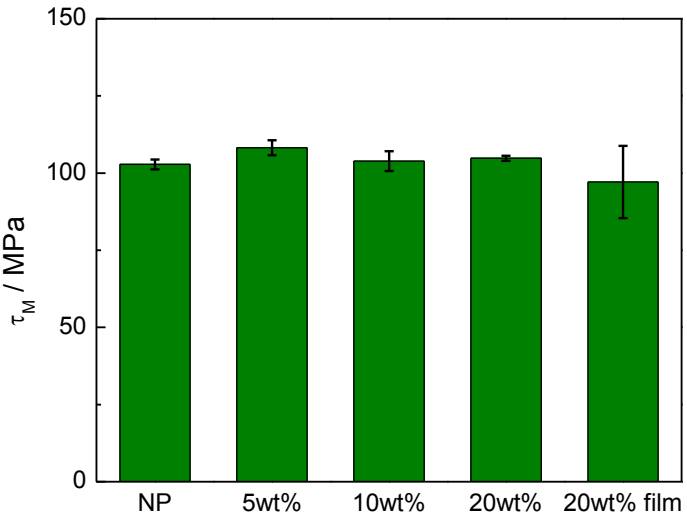

Figure 5.5 ILSS comparisons of samples printed by using different PMMA concentrations in inks and patterns.

The increased variation has been similarly observed in Hillermeier and Seferis's work [14]. They used two different methods to apply toughening material (polyamide 6 particles) onto interfaces between laminate plies. One of them used a sifter to manually apply toughening material onto target interfaces. Another one used a gun to spray modified toughening material onto interfaces. As shown in Figure 5.6, the toughening material was more evenly distributed on the sprayed interfaces than on the manually applied interfaces. The mechanical tests showed that the difference in material distribution has an effect on the mechanical performances of final toughened composites. It can be seen from Figure 5.7 that the test samples with more evenly distributed toughening material, i.e. sprayed, had 30% and 2.8% improvements in mode II interlaminar fracture toughness and ILSS respectively compared to their base line. This work proved the importance of an even distribution of toughening material, which supports the necessity of using inkjet printing to deposit a more evenly distributed toughening material on the micron scale.

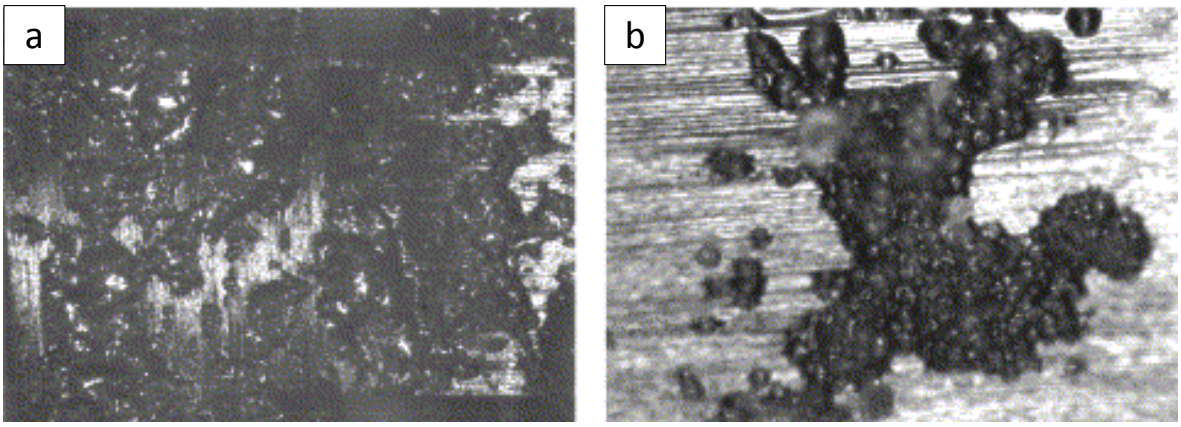

Figure 5.6 The different distribution of toughening material by using two different methods. (a) Spray tackifier (sprayed); (b) Powder tackifier (manually applied using a sifter) [14].

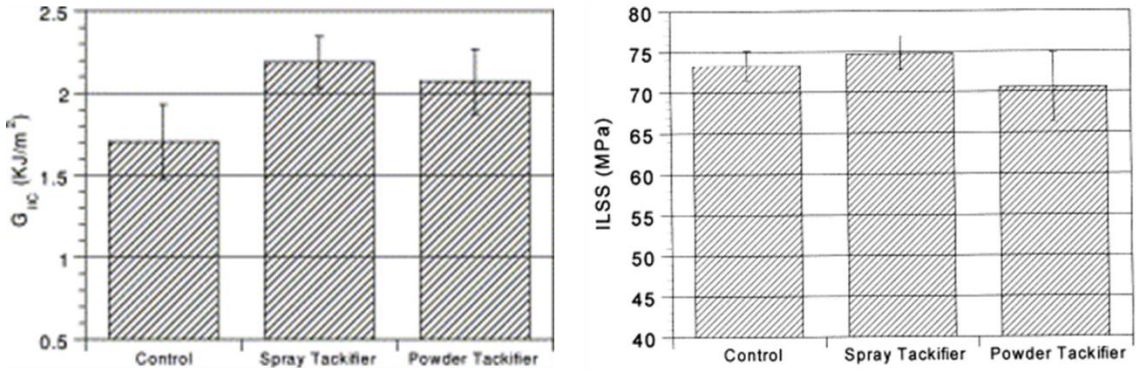

Figure 5.7 Comparisons of G_{IIc} and ILSS of samples prepared by two different methods [14].

5.2.4 Variation of printing pattern density

As discussed in Chapter 4, changing PMMA concentration in the printing solutions (and using a control pattern) varies the PMMA content on printed surfaces and leaves different sized PMMA particles embedded in epoxy after curing. It is understandable that increasing the toughening area (surface area of toughening material) should benefit the increase in toughness of engineered material within a certain range, because cracks need more energy to propagate through an area with more toughening regions. In this case, toughening area is the surface area of PMMA particles embedded in resin matrix. There are two ways to increase

the surface area of PMMA particles, one is to increase the size of PMMA particles, the other way is to increase the number of PMMA particles embedded in matrix. The first method can only increase the surface area of PMMA particles to a small extent, because the diameter of PMMA particles only increases a few micrometers by double the PMMA concentration in printing solution. However, the alternative way of increasing the surface area of PMMA particles in composite is by varying the printing pattern density, thus, the PMMA deposits can be close or loose patterned, and the surface area of PMMA can be changed noticeably. Table 5.1 compares the surface area of PMMA particles normalised by pattern unit area of several examples by using different PMMA solutions and pattern densities. It can be seen that increasing pattern density is more efficient in increasing the surface area of the deposited polymer than by increasing polymer concentration in the solutions.

Table 5.1 Comparisons of surface area of PMMA (normalised by pattern unit area) using different PMMA concentration solutions and pattern densities after curing (assuming the printed pattern does not shift).

PMMA wt.%	Pattern dimension (hexagon, *dx/dy* mm)	Diameter of PMMA beads (μm)	Surface coverage (%)
5 wt.%	0.7/0.35	26.3	0.9
5 wt.%	0.4/0.2	26.3	2.7
10 wt.%	0.7/0.35	33.7	1.5
10 wt.%	0.4/0.2	33.7	4.4
20 wt.%	0.7/0.35	36.4	1.7
20 wt.%	0.4/0.2	36.4	5.2

Section 5.2.3 identified the importance and influence of evenly distributed toughening material on the final mechanical performances of toughened composites. Therefore, it is worth investigating the effect of toughening material deposited in a high surface area coverage (and evenly distributed) alongside the delamination favoured interfaces on the mechanical performances of the printed CFRP laminates.

Figure 5.8 shows that the condensed printing pattern (*dx/dy* = 0.4/0.2 mm) hardly affect the ILSS of samples with printed PMMA deposits, even a noticeable increase in mode I interlaminar fracture toughness has been observed by increasing printing pattern density (see Section 4.2.4). Again, this result suggests that interlaminar fracture toughness of polymer printed CFRP laminate can be optimised by more condensed printing pattern (increasing surface coverage of printed polymer depositions) without losing the ILSS.

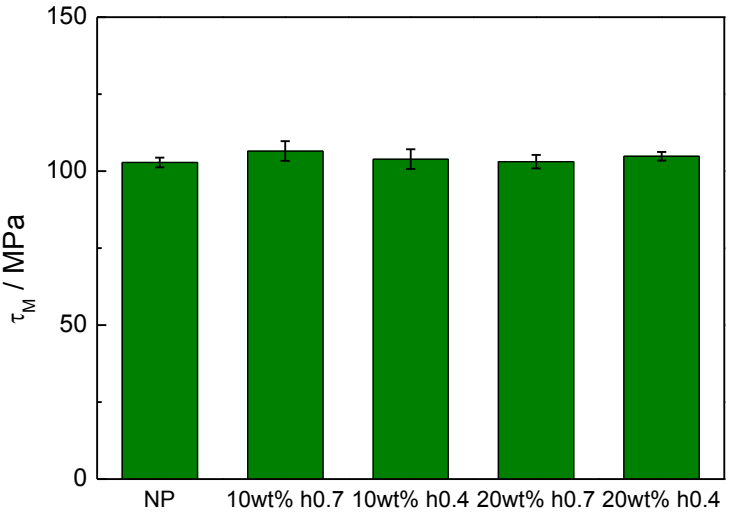

Figure 5.8 ILSS comparisons of samples printed by using different PMMA concentrations in solutions and pattern densities.

5.2.5 Effect of water aging

Moisture is a critical factor which has a negative effect on the mechanical properties of composite materials, which cannot be avoided during service [15-17]. Rege and Lakkad [16] reported that the ILSS of unidirectional CFRP laminates which were soaked in distilled water at 40˚C for 5 days decreased about 12.3% compared to their baseline, and the weight gain was about 0.26%. They also found that samples soaked at a high temperature had a more sever degradation in mechanical integrity than in distilled water. Therefore, whether the added PMMA would affect the performance under moisture of modified CFRP laminate needs to be investigated.

It can be seen from Figure 5.9 that samples with PMMA deposits did not have an increase in water absorption compared to non-printed (NP) samples. The weight gain of NP, 10 wt.% and 20 wt.% PMMA printed samples after soaking in distilled water for 31 days were 0.29%, 0.25 and 0.30% respectively. This suggests that the addition of PMMA deposits does not significantly affect the moisture absorption rate of CFRP laminate, if at all.

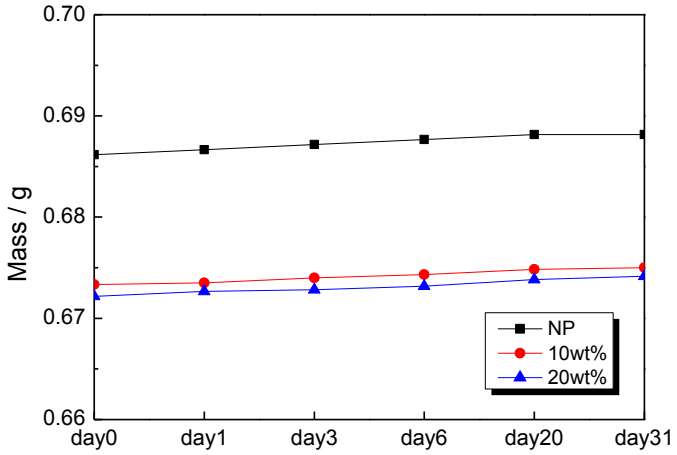

Figure 5.9 Mass changes of NP and polymer printed samples.

All samples (NP and PMMA printed) were tested by means of SBS method after soaking in distilled water for 31 days. Figure 5.10 shows that the ILSS of soaked samples (NP, 10 wt.% and 20 wt.% PMMA printed) dropped by approximately 1.3%, 5.5% and 2.1% respectively compared to their respect non-soaked samples. Although all soaked samples have a small amount of deceases in ILSS compared to the non-soaked samples, the addition of PMMA did not significantly affect the ILSS compared to the NP samples. These results illustrate that the addition of PMMA deposits between laminate plies barely harm the moisture resistance of CFRP laminate. Therefore, the CFRP composites toughened by inkjet printing of PMMA between laminate plies can be applied to areas where humid environment is unavoidable.

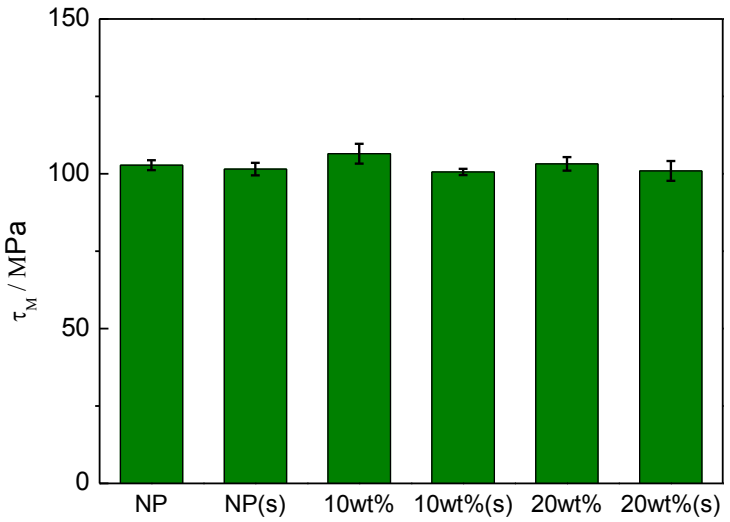

Figure 5.10 ILSS comparisons of samples with and without soaking (Pattern: hexagon, *dx/dy* = 0.4/0.2 mm).

5.3 Improved impact resistance

5.3.1 Introduction

As introduced in Chapter 1, although CFRP composites have many desirable mechanical properties and have been widely used in industries, they have serious limitations. Poor impact resistance, which can result in subsequent interlaminar or/and intralaminar microcracks and ultimately in delamination, is the main obstacle of using this material in more challenging structures (e.g. primary structure for aircraft). Unfortunately, the potential impact dangers are widespread, such as a dropped tool, a bird strike, and runway debris. Therefore, in order to further promote the utilisation of laminated composites, attention needs to be centred on optimising their response to impact loading, and ultimately on improving impact resistance.

The drop-weight impact test lets a weight fall from a pre-determined height striking the horizontally placed test plate. In general, the impact strike does not cause dramatically apparent damage to the test plate. In this work, the test is designed to generate barely visible impact damage in the test plate. Clearly, obvious damages are easily detectable by optical observation and results in a replacement being made. However, barely visible impact damage

is the initial form of failures, and it is very difficult to detect that level of damage at its early stage. As the DCB test results showed that inkjet printed PMMA deposits between CFRP laminate plies imparted a good toughening efficiency in CFRP laminates, it seemed reasonable to determine whether the resistance to impact damage of laminated composites has also been improved.

5.3.2 Results and discussion

X-ray tomography was used to investigate the damage tolerance of PMMA printed laminates after impact test. Figure 5.11 shows the non-printed (NP) laminates having visible microcracks after impact with only 1 J impact energy, however, laminates with 20 wt.% PMMA addition between every interface of laminates (pattern: hexagon, *dx/dy* = 0.4/0.2 mm) did not show any visible microcracks after the same impact test.

A similar method to improve the impact resistance of composites has been patented in the US [18]. The author reported that by placing thermoplastic particles between laminate plies, the laminated composites have improved toughness and impact resistance. This patent clarified an important detail which is the size of thermoplastic particles. It is stated that the thermoplastic particles should be large enough to prevent migration of particles from interfaces between plies into the intra-ply region during lamination. And the preferable size of particles ranges from 2 – 100 μm. As can be seen in Chapter 3, the size of the PMMA particles formed after curing of composite is in the right scale. The observed improvement in the impact resistance in this work is believed to be attributed to the evenly distributed PMMA particles in the epoxy resins. The impact energy could be absorbed by means of plastic deformation of PMMA particles.

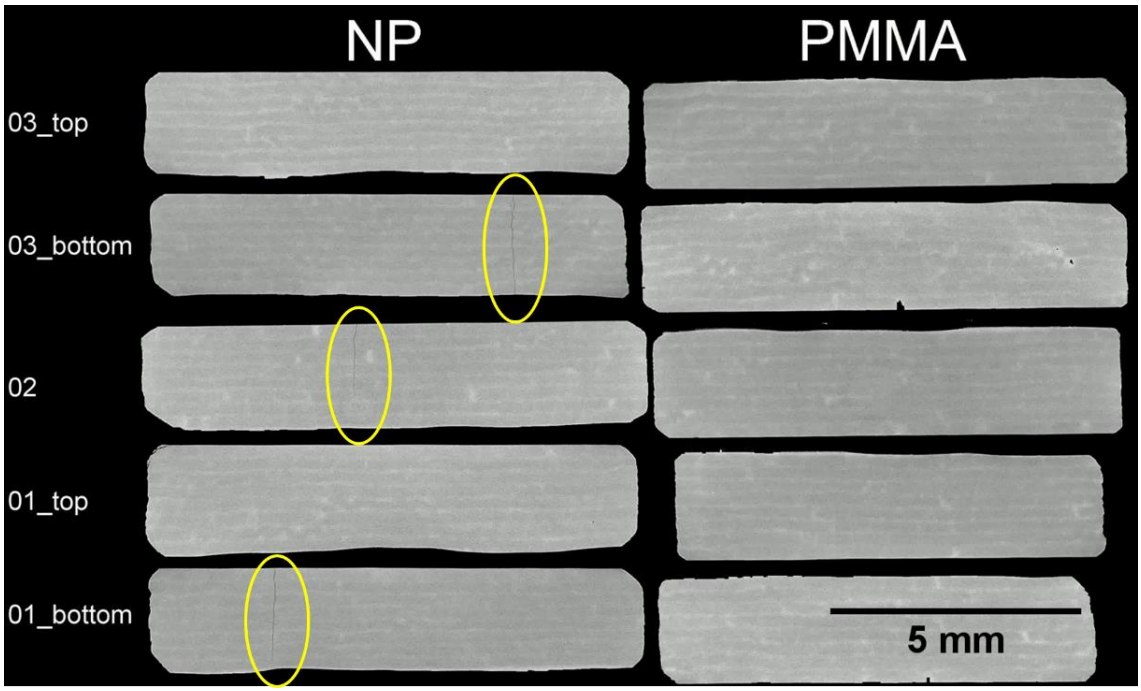

Figure 5.11 X-ray tomography of impacted laminates.

5.4 Dynamic mechanical analysis (DMA)

Dynamic mechanical properties of non-printed (NP) and 20 wt.% PMMA printed (hexagon, *dx/dy* = 0.4/0.2 mm) CFRP laminate samples are compared in Figure 5.12, in which each data curve represents the mean of three samples. It can be seen that samples with added PMMA deposits did not show a decrease in storage modulus before the temperature increased to 140˚C, where the matrix resin approaches its own glass transition temperature. However, the PMMA did not show its own glass transition, which is about 100˚C. The data shown in Figure 5.12 suggests that the storage modulus of PMMA printed laminates does not vary significantly over a wide range of temperatures during service.

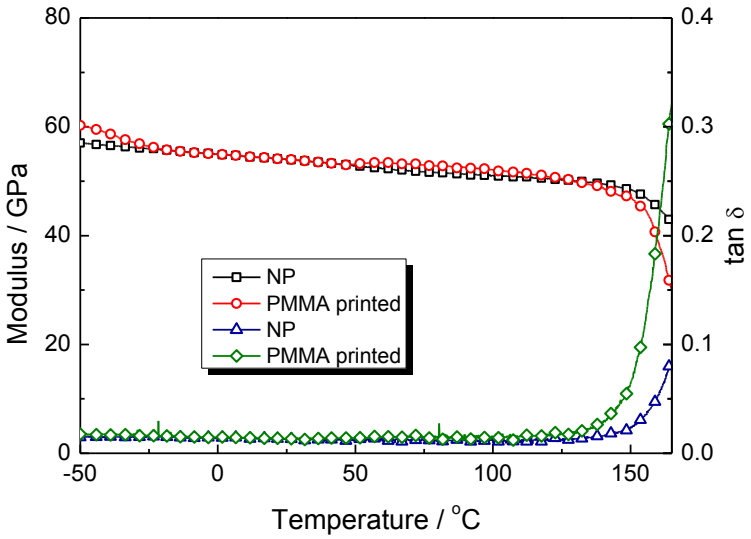

Figure 5.12 Dynamic mechanical data for NP and 20 wt.% PMMA printed (hexagon, *dx/dy* = 0.4/0.2 mm) CFRP laminates.

5.5 Improvement in damage tolerance

In terms of the industrial scale manufacturing of CFRP, it needs to be machined to meet various dimensional requirement of products. Drilling is one of the most common machining steps where joining is needed, however, this essential step unavoidably generates microcracks around the drilling area which introduces potential mechanical failure points in the final structures. Therefore, improving the damage tolerance during machining is of importance to the success of final products, because the material life time and the repair cost can be significantly reduced.

In order to investigate the effect of printing polymer deposits between composite plies on the drilling area, SEM was used to image the edges and surfaces of drilling holes of polymer added CFRP samples. Figure 5.13 schematically shows the SEM scanning areas of the drilling samples, two different drilling areas were scanned.

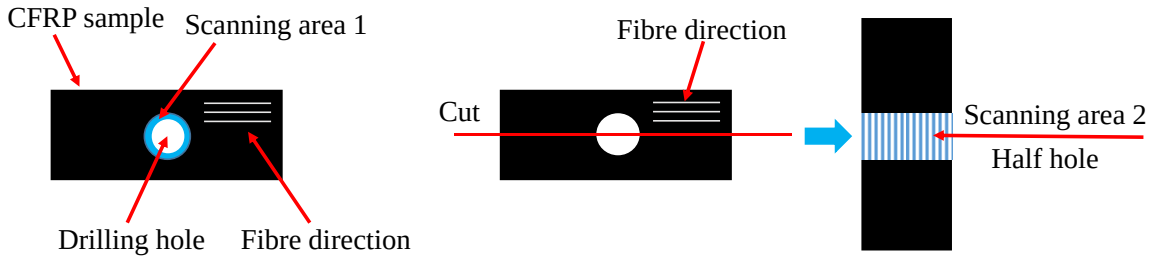

Figure 5.13 Two SEM scanning areas of drilled CFRP samples.

Figure 5.14 shows the SEM images of scanning area 1 of drilled CFRP samples. Three different groups were investigated which were non-printed (NP), 10 wt.% and 20 wt.% PMMA printed groups (pattern: hexagon, *dx/dy* = 0.4/0.2 mm). Polymer deposits were printed between every layer of samples. It can be seen that the edges of the drilling holes of the three groups did not show significant difference. However, the edges of polymer printed groups have been found smoother areas as shown in Figure 5.14(d) and (f), if at all. Figure 5.15 shows the SEM images of scanning area 2 (surface of hole) of drilled CFRP samples. It can be seen that the surface of drilling hole of the control CFRP sample (NP) was rougher than that of PMMA printed ones, although there was no obvious difference between those two PMMA printed groups. As discussed in Section 5.4, heat was generated during drilling, it is assumed that the PMMA deposits were softened and absorbed energy by deformation during drilling, which reduced the damage generation. As a result, the hole surfaces of PMMA printed samples were smoother than that of the NP group. This could be helpful as it would reduce the damage/microcracks generated during machining around machining areas, therefore, the lifetime of structures would be lengthened and the cost of manufacturing can be decreased as less repair is needed during service.

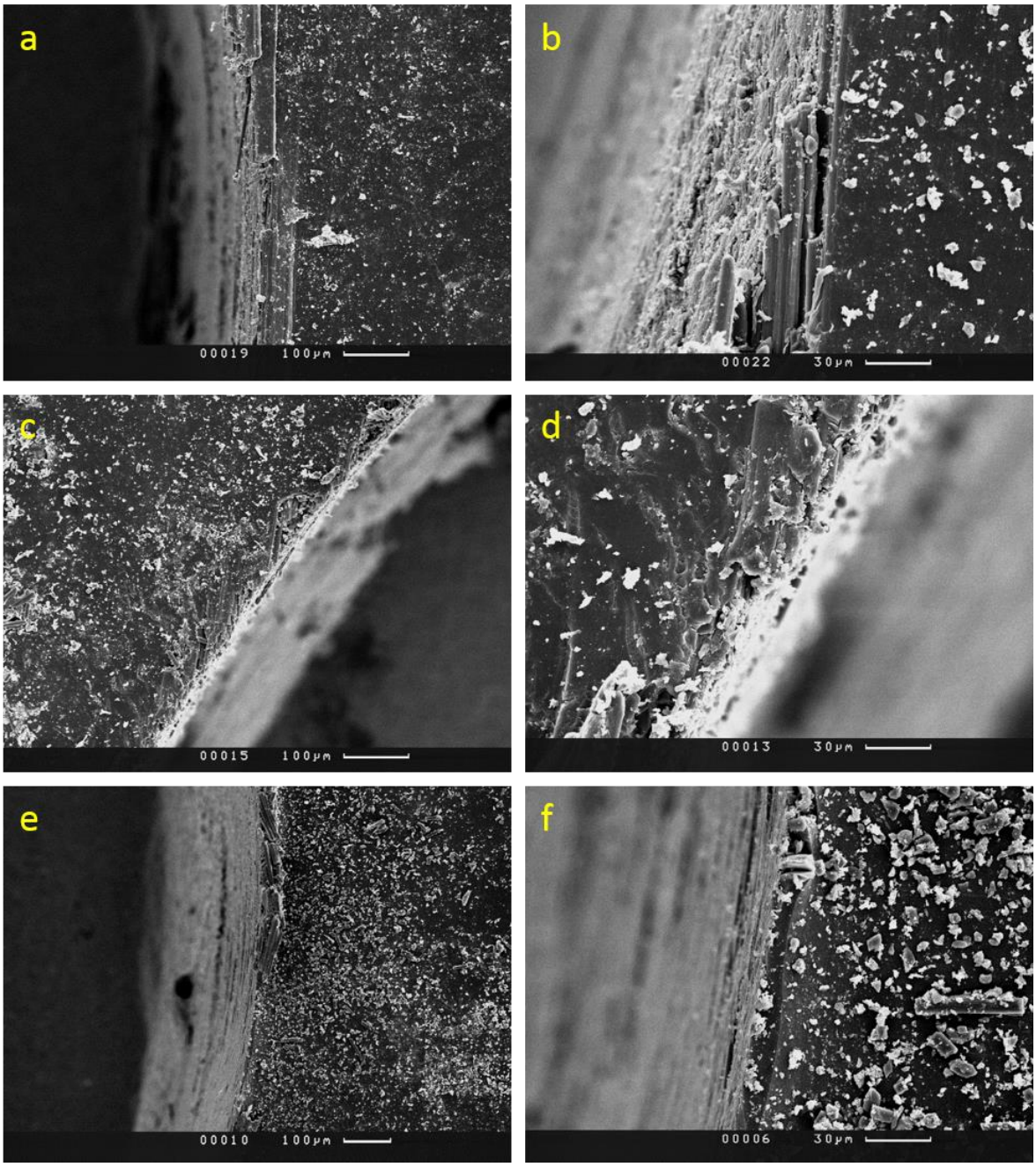

Figure 5.14 SEM images of edges of drilling holes. a) and b). NP group; c) and d). 10 wt.% PMMA printed group; e) and f). 20 wt.% PMMA printed group.

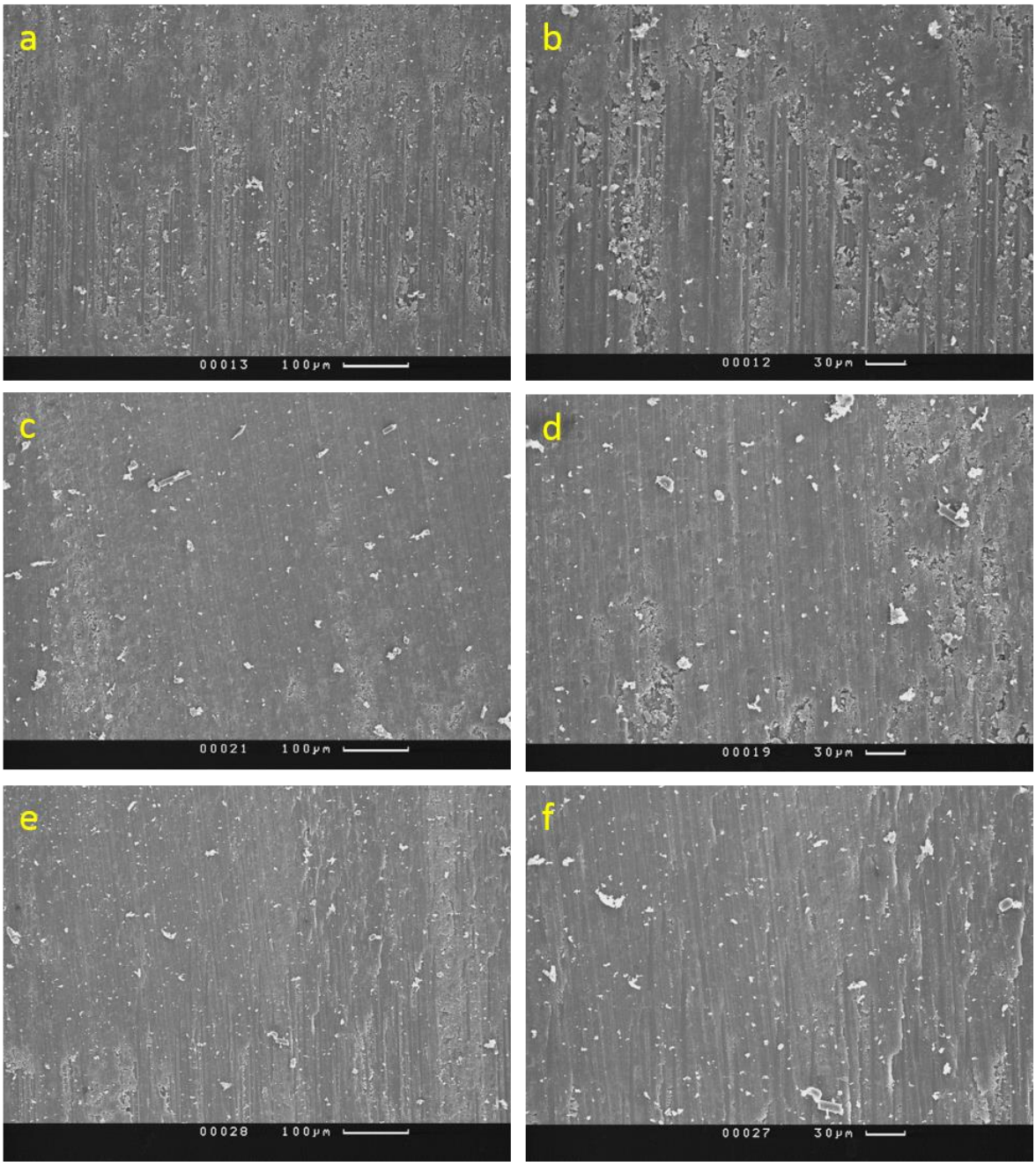

Figure 5.15 SEM images of surfaces of drilling holes. a) and b). NP group; c) and d). 10 wt.% PMMA printed group; e) and f). 20 wt.% PMMA printed group.

5.6 Conclusions

The addition of polymer deposits (PEG and PMMA) patterned in discrete dot pattern by inkjet printing between CFRP composite laminate did not decrease the ILSS of finished CFRP laminates compared to that of non-printed (NP) samples. Results also show that the different solvents which were used to dissolve PEG did not have an effect on the mechanical performances of inkjet printed laminates, which indicates the solvent has evaporated completely before lay-up or the amount of solvent residue is too small.

The effect of different amounts of polymer content on mechanical performances of inkjet printed laminates were investigated. The increase in polymer content on interfaces between laminate plies (keeping the discrete dot pattern) did not affect the ILSS of printed laminates. However, samples printed with continuous thin films between laminate plies had deceased ILSS compared to both NP and samples printed with discrete dot pattern. The explanation is that the excessive polymer acts as flaws/defects which affects the curability of epoxy from adjacent plies. The PMMA thin film broke up into a random distribution of widely sized PMMA beads, which resulted in large standard deviation in test samples. These results proved the advantage of patterning discrete and evenly distributed toughening material between laminates plies instead of using a conventional interleaf to toughen CFRP composites.

X-ray tomography shows that the laminate with printed PMMA deposits has better impact resistance compared to that of non-printed impacted sample. This result could mainly be attributed to the plastic deformation of PMMA particles embedded in the matrix, which absorbed the impact energy.

Dynamic mechanical analysis showed that the addition of PMMA between laminate plies did not decrease the storage modulus of printed laminate before 140˚C. The slightly decreased T_g might be a benefit in terms of machining since the early deformation of matrix system would decrease the generation of microcracks which occur during machining.

References

[1] W. J. Cantwell and J. Morton, "The impact resistance of composite materials — a review," *Composites*, vol. 22, pp. 347-362, 1991.

[2] M. R. Wisnom, T. Reynolds, and N. Gwilliam, "Reduction in interlaminar shear strength by discrete and distributed voids," *Composites Science and Technology*, vol. 56, pp. 93-101, 1996.

[3] N. L. Hancox and H. Wells, "The effects of fibre surface coatings on the mechanical properties of CFRP," *Fibre Science and Technology*, vol. 10, pp. 9-22, 1977.

[4] S. U. Khan and J. K. Kim, "Improved interlaminar shear properties of multiscale carbon fiber composites with bucky paper interleaves made from carbon nanofibers," *Carbon*, vol. 50, pp. 5265-5277, 2012.

[5] J. Jang and H. Yang, "The effect of surface treatment on the performance improvement of carbon fiber/polybenzoxazine composites," *Journal of materials science*, vol. 35, pp. 2297-2303, 2000.

[6] D. Adams. "The short beam shear test," acessed on 10/10/2013. Available: http://www.compositesworld.com/articles/the-short-beam-shear-test

[7] Standard: "Fibre-reinforced plastic composites. Determination of apparent interlaminar shear strength by short-beam method," ed: BS EN ISO 14130:1998.

[8] H. Miyagawa, R. J. Jurek, A. K. Mohanty, M. Misra, and L. T. Drzal, "Biobased epoxy/clay nanocomposites as a new matrix for CFRP," *Composites Part A: Applied Science and Manufacturing*, vol. 37, pp. 54-62, 2006.

[9] C. B. Bucknall and A. H. Gilbert, "Toughening tetrafunctional epoxy resins using polyetherimide," *Polymer*, vol. 30, pp. 213-217, 1989.

[10] M. Labronici and H. Ishida, "Toughening composites by fiber coating: a review," *Composite Interfaces*, vol. 2, pp. 199-234, 1994.

[11] C. H. Wang, K. Sidhu, T. Yang, J. Zhang, and R. Shanks, "Interlayer self-healing and toughening of carbon fibre/epoxy composites using copolymer films," *Composites Part A: Applied Science and Manufacturing*, vol. 43, pp. 512-518, 2012.

[12] G. Li, P. Li, C. Zhang, Y. Yu, H. Liu, S. Zhang, *et al.*, "Inhomogeneous toughening of carbon fiber/epoxy composite using electrospun polysulfone nanofibrous

membranes by in situ phase separation," *Composites Science and Technology,* vol. 68, pp. 987-994, 2008.

[13] S. Zavareh and G. Samandari, "Polyethylene glycol as an epoxy modifier with extremely high toughening effect: Formation of nanoblend morphology," *Polymer Engineering & Science,* vol. 54, pp. 1833-1838, 2014.

[14] R. Hillermeier and J. Seferis, "Interlayer toughening of resin transfer molding composites," *Composites Part A: Applied Science and Manufacturing,* vol. 32, pp. 721-729, 2001.

[15] C. Y. Lundemo and S. E. Thor, "Influence of environmental cycling on the mechanical properties of composite materials," *Journal of Composite Materials,* vol. 11, pp. 276-284, 1977.

[16] S. K. Rege and S. C. Lakkad, "Effect of salt water on mechanical properties of fibre reinforced plastics," *Fibre Science and Technology,* vol. 19, pp. 317-324, 1983.

[17] O. K. Joshi, "The effect of moisture on the shear properties of carbon fibre composites," *Composites,* vol. 14, pp. 196-200, 1983.

[18] A. Maranci, S. L. Peake, and S. S. Kaminski, "Advance composites with thermoplastic particles at the interface between layers," ed: Google Patents, 1990.

Chapter 6

Conclusions and Future work

This thesis addresses experimental aspects of using inkjet printing to deposit polymer deposits between CFRP composite laminates before curing. The research focused on the mechanical properties of laminates with two different polymer deposits patterned in a range of different patterns and pattern densities. The selection of toughening material plays a critical role in the mechanical performance of final composites. The amount of polymer deposited and pattern design are the most important factors which determine the success of toughening the laminates. Toughening mechanisms were preliminarily investigated based on microscopy of morphology of polymer deposits embedded in the resin system. The highly controllable distribution and size of the discrete deposits are believed to be the main contributions to the observed improvement in mode I interlaminar fracture toughness and preservation of interlaminar strength.

6.1 Conclusions

Poly(ethylene) glycol (PEG) and poly(methyl methacrylate) (PMMA) were dissolved in suitable solvents to make inkjet printable solutions. In order to investigate the pattern repeatability by using inkjet printing, different patterns and substrates were used to confirm the feasibility of using inkjet printing to deposit designed patterns onto target substrates with controllable pattern dimensions. Optical microscopy showed that the designed patterns can be repeatedly deposited onto both glass slide and prepreg. Although the printing speed or production speed is a limitation of using the specific research inkjet printer employed in this research, this problem can be resolved by using a larger industry scale printer. The pattern dimensions can be optimised/modified according to the diameters of different polymer deposits on substrates. The discrete polymer deposits can be close and loose packed or even overlapped to form continuous phases such as line and film. This flexibility allows the effect

of different patterns printed between laminate plies on the mechanical performance of final laminates to be investigated.

Using inkjet printing to deposit polymers between CFRP composite laminate plies prior to the curing cycle to achieve toughening is a creative idea. The main unique aspect of this method was that the toughening materials were not diffused in the bulk matrix neither did they cover the whole interface between laminate plies, but remained strategically dispersed along predicted crack pathways patterned in dimension controllable patterns. In order to examine the interlaminar fracture toughness of polymer added CFRP laminates, double cantilever beam (DCB) test was adopted to determine mode I interlaminar fracture toughness (G_{Ic}) of test samples. The key finds are as follows:

- CFRP laminates with printed polymer deposits had an up to 40% improvement in G_{Ic} corresponding to crack propagation.
- Increasing PMMA concentration in printing solutions yielded an increase in GIc, however, this increase did not follow a linear trend. At the present stage, 10 wt.% PMMA solution has the best toughening efficiency.
- CFRP laminate with printed PMMA thin film had the highest GIc compared to the other printing groups, however, the crack propagation is unstable.
- High pattern density contributed to a higher improvement in GIc, while discrete hexagon dot pattern possessed the highest increase in GIc among the groups with printed discontinuous patterns.
- Selective printing was achieved, indicating this technique can be further used to selectively toughen critical places of composite laminates where high mechanical performance is required.

Short beam shear test (SBS) was adopted to measure the apparent interlaminar shear strength (ILSS) of the polymer printed CFRP laminates. Key finds are as follows:

- No deteriorations in ILSS were observed of the polymer printed CFRP laminates with printed discrete dot patterns. However, laminates with a printed PMMA thin film had a 5.4% decrease in ILSS compared to the non-printed group. Also the standard deviation

was larger than the other groups, indicating that the crack propagation was hardly controlled by the introduced polymer deposits, indicating the necessity of dispersing evenly distributed toughening material by using inkjet printing.

- Water aging experiments illustrated that the printed PMMA deposits did not significantly affect the water absorption of the non-modified CFRP laminates. ILSS of all water aged samples were decreased though.

PMMA and PEG deposits were printed on neat resin coated glass slides to investigate their formations before and after heating when surrounded by epoxy resin. These observations were helpful for understanding the toughening mechanism.

- The printed PMMA deposits tended to form particles after heating while PEG seemed to have a good miscibility with the epoxy resin.
- The size of the PMMA particles can be controlled by the amount of material deposited, and the distribution can be highly controlled by the discrete dot pattern dimensions.
- The size and distribution of PMMA particles of printed film after curing cannot be controlled by either pattern dimensions or polymer concentrations in solutions. Although the printed PMMA lines broke into random sizes of PMMA particles, these particles were still patterned in lines.

The possible toughening mechanisms were proposed based on the microscopy of DCB tested fracture surfaces and the morphology of polymer deposits embedded in the epoxy resin. Particle deformation, particle debonding from surrounding matrix and matrix plasticization were believed to be the main contributions to the enhanced G_{Ic} and preserved interlaminar strength.

With the aid of inkjet printing, the amount of toughening materials used was considerably smaller than other toughening methods such as matrix toughening and interleaving. An observed increase in G_{Ic} up to 40% was achieved by using about 0.05 vol.% of PMMA. This amount of toughening material equates to a film with a thickness of about 140nm, which would be difficult for handling. The thickness of interleaves is important to the toughening efficiency of laminates, using inkjet printing eliminates the problems associated with manually applying toughening material and the thickness of toughening materials.

6.2 Future work

The work conducted in this thesis has identified that inkjet printing can be used to print toughening materials onto prepreg with pre-designed patterns, and these patterned discrete polymer deposits toughened the CFRP laminates up to 40% compared to the baseline. The key mechanism has been identified as the debonding between PMMA and the epoxy resin. However, the relative importance of other toughening mechanisms requires further work. Consideration needs to be focused on the parameters associated with the printing and the formation (morphology) of printed polymer surrounded by matrix resin and fibres after curing e.g. the surface coverage of polymer deposits printed on prepreg, the amount of polymer deposited, the particle size if the printed polymer deposits tend to form particles etc. it is suggested that an approach involving microscale testing and observation would be helpful to understanding the toughening mechanisms.

In this work, the results have shown that the rigid thermoplastic polymer PMMA toughened the CFRP laminates up to 40% in terms of G_{Ic} with less than 1 vol.% of usage. Whether this efficient toughening effectiveness can be achieved by using other toughening materials such as polyimide, polyetherimide and polycarbonate is worth exploring. In addition to that, self-healing materials are attractive to researchers as this smart function would allow structures to be used in more challenging areas such as aerospace and the deep ocean where manual repair is not possible at the present time. Also, as the inkjet printing is capable of printing more than one materials in a single printing session, different materials with respect functions could be printed into composites to achieve a multifunctional composite.

A variety of mechanical properties could be further measured according to the application purposes. For instance, in this work, mode I interlaminar fracture toughness (G_{Ic}) was measured to quantify the resistance to delamination of polymer printed laminates under opening. Mode II and mixture of mode I/II would be worth investigating to find out the mechanical behaviour of toughened laminates under shearing and combination of opening and shearing.

Based on the results found in this work, it is necessary to establish modelling to simulate the toughening processes. These models would help to understand the toughening mechanisms and the influence of pattern dimensions on the mechanical performance of toughened

composites, ultimately, helping to select more effective materials and design more effective patterns for toughening.

Appendix

A. Adjusting inkjet printer

As mentioned in Chapter 1, the formation of a droplet ejected from the nozzle is of great importance to the high resolution of the finished features. Ideally, a single and stable droplet observed on the stroboscopic image is preferred for printing as the stable droplet can be deposited at desired positions. However, if the droplets formed as shown in Figure A.1(b), the printed feature will be messy due to a lack of stability of droplet formation.

In order to obtain an ideal droplet formation, firstly, the viscosity and surface tension of printing solutions are preferred in a suitable range. Derby *et al*. proposed that the systems with a *Z* number ranged from 1 to 10 should be printable by using DOD printing [1]. However, in practice, systems with a larger *Z* number were reported printable. The *Z* number in this work ranged from 7.39 to 35.36, and all systems were printable and stable. Schubert *et al*. stated that the solutions' vapour pressure is likely to be the main factor which determine the printability of solutions. They defined that solutions with vapour pressure higher than 100 mmHg would not be able to form stable droplets for printing [2].

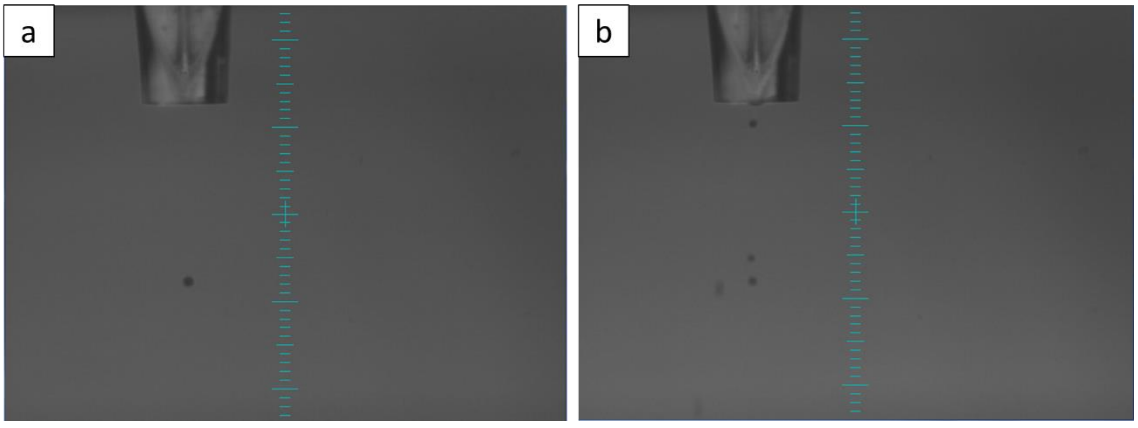

Figure A.1 Droplet formation ejected from the nozzle of printhead. a) acceptable droplet formation for printing; b) unacceptable droplet formation for printing.

Secondly, the parameters including rise time, fall time, voltage and frequency work as a combination to control the formation of a droplet. The volume of droplet has been proven to

be linear with the driving voltage (Figure A.2). In this work, the driving voltage was one of the main parameters used to adjust the formation and size of droplet. Also, a high printing frequency tends to negatively affect the droplet formation. The frequency used in this work ranged from 44 to 350 Hz, varied accordingly to the droplet spacing (*dx* and *dy*) and printing speed used.

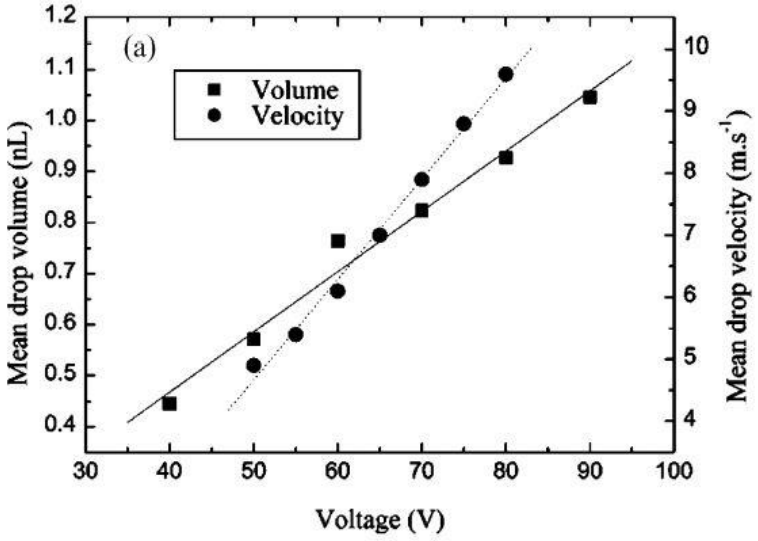

Figure A.2 The influence of driving voltage on volume and velocity of droplet [2].

B. Manufacturing CFRP laminates

A customised autoclave (Figure B.1) was used to consolidate all CFRP laminates used in this work. The quality of cured laminates depends on various factors such as material handling, lay-up, vacuum bagging and curing process. Prepreg needs to be defrosted completely in a sealed bag before using, this step prevents water from condensing on the surface of prepreg. It is important to eliminate the air between plies during lay-up, because the air trapped between plies forms voids after laminate consolidating, which decreases the mechanical integrity of laminates. Vacuum bagging is one of the most critical steps in composite fabrication. Any leak during the temperature elevating stage will decrease the mechanical properties of laminates. Although it has been reported that losing vacuum after the highest temperature during curing does not affect the mechanical performance of the final laminates, vacuum was provided during the whole curing process in this work. Figure B.2 shows a prepared vacuum bag ready for autoclaving.

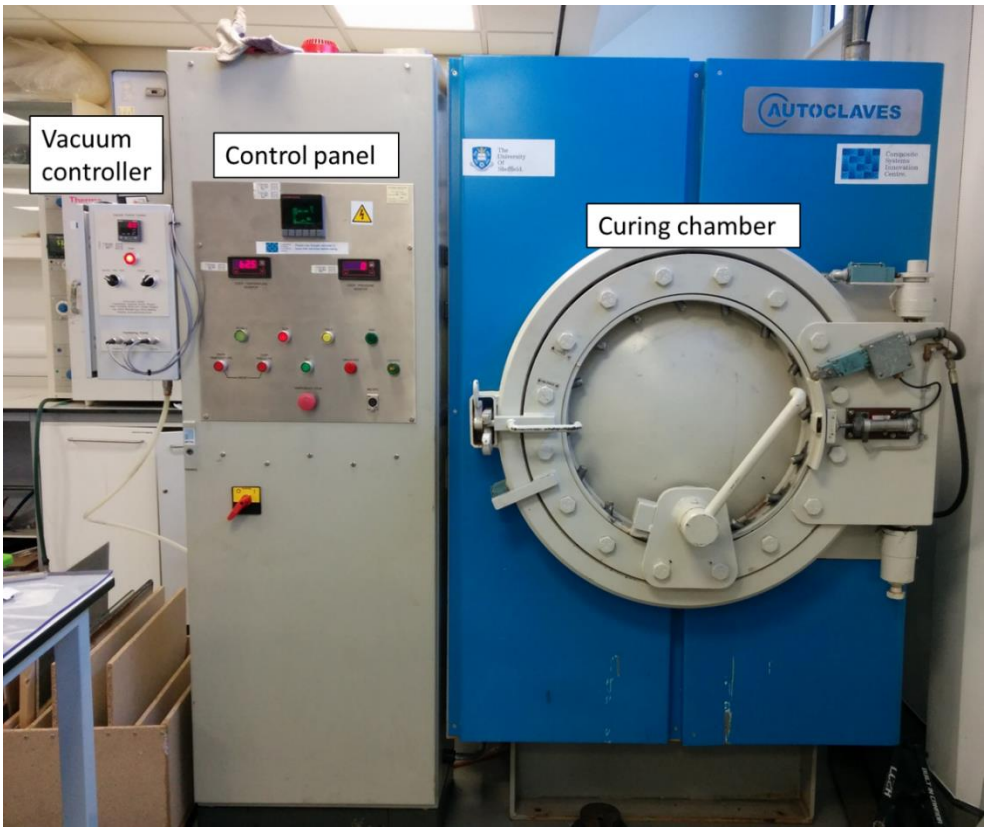

Figure B.1 Autoclave used in this work.

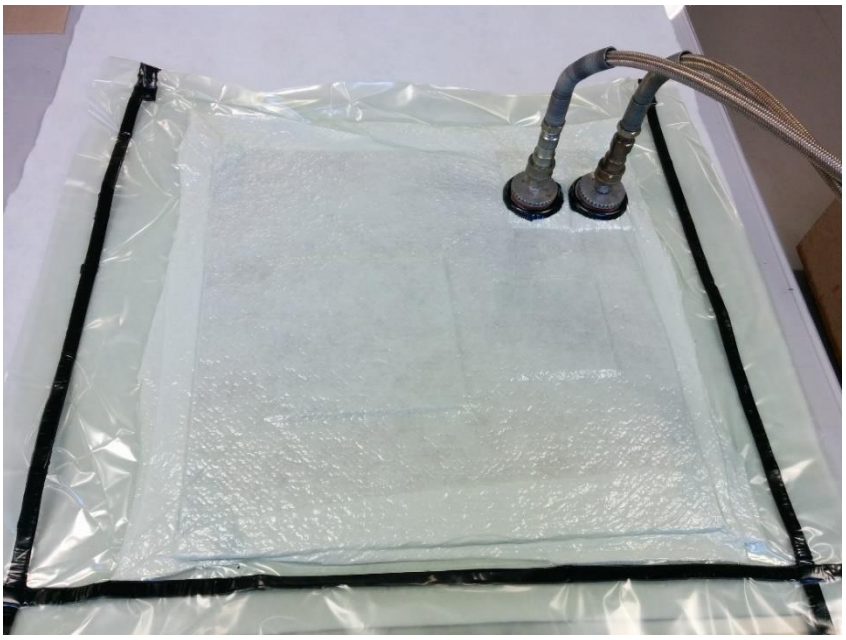

Figure B.2 A prepared vacuum bag ready for autoclaving.

C. Reactive inkjet printing

Reactive inkjet printing uses two or more solutions (inks) to deposit different droplets at the same position to form a new substance chemically. This utilisation of inkjet printing is useful for printing substances which are not dissolvable or their solutions are not possible for inkjet printing. *In situ* polymerisation of polyurethane (PU) was conducted to investigate the feasibility of the reactive inkjet printing.

C.1 Inks for synthesis of polyurethane

Isophorone diisocyanate (IPDI, Sigma Aldrich, UK) and poly(ethylene glycol) (PEG-400, M_n ~ 400, Sigma Aldrich, UK) were used to formulate separate solutions for polymerising polyurethane [3] between CFRP laminate plies. PU was chosen to be polymerised due to its excellent elasticity and impact strength. Research [4, 5] showed that the fracture properties and impact resistance of PU modified epoxy was improved. As the monomers for polymerising PU can be dissolved or diluted to form solutions with suitable viscosities and surface tensions for inkjet printing, *in situ* polymerisation of PU was adopted.

N,N-Dimethylformamide (DMF, ≥99.8%, Sigma Aldrich, UK) was used as solvent to dissolve IPDI and PEG-400 respectively. The addition of DMF aims to improve the printability of IPDI and PEG-400. Bismuth neodecanoate (BiNeo, Sigma Aldrich, UK) was added into IPDI solution as catalyst to form printing solution A. The PEG-400/DMF solution was used as printing solution B. All materials were used without further purification. The composition of solution A and B are detailed in Table C.1.

In this work, IPDI and PEG-400 containing droplets were precisely printed together to form PU within several minutes. The parameters of the printer used to print solutions A and B are listed in Table C.2. The chemistry of this polymerisation involves forming urethane bonds by the presence of diol groups and diisocyanate groups. A low molecular weight PEG-400 was selected because low viscosity solution is preferred in term of printing. High molecular weight PEG tends to form high viscosity solution compared to low molecular weight PEG with the same PEG concentration in solution. Catalyst was used to promote the reaction.

Table C.1 Solution compositions of solutions A and B.

Solution		Solution compositions		
		Solute	vol.%	Solvent
Synthesis PU	A	IPDI/BiNeo	74/0.5	DMF
	B	PEG-400	50	DMF

Table C.2 Parameters used for printing solutions A and B.

Solution	Rise time 1 (μs)	Dwell time (μs)	Fall time (μs)	Echo time (μs)	Rise time 2 (μs)	Idle Voltage (V)	Dwell Voltage (V)	Echo Voltage (V)
A	4.0	7.0	10.0	6.0	3.0	0.0	42.0	-4.0
B	4.0	12.0	14.0	6.0	3.0	0.0	48.5	-4.0

C.2 Microscopy of *in situ* polymerised PU

PU was firstly *in situ* polymerised on a glass slide to confirm the repeatability and accuracy

of the inkjet printed pattern. Figure C.1 shows a good accuracy of using the DOD printer to deposit different droplets at the same position. The repeatability of printed pattern was also confirmed, suggesting it is feasible to using this method to conduct the reactive inkjet printing with a good precision. Secondly, solutions A and B was overlapped in a hexagon pattern on the carbon fibre reinforced prepreg to investigate the *in situ* polymerisation of PU in the presence of the epoxy resin system. SEM was used to scan the printed prepreg after printing and heating respectively. It is can be seen from Figure C.2(a) that the hexagon pattern can be repeatly printed on the prepreg. The overlapped deposits tended to extend along the fibre directions. Figure C.2(b) shows the printed prepreg after heating (177˚C for 30 min), the *in situ* polymerised PU dots patterned in hexagon can be clearly identified. Note, the printed prepreg was heated with an open surface (not covered), therefore, the hexagon pattern and polymerised PU dots can be retained without too much interference.

Since it is difficult to control the polymerisation process of PU *in situ* in terms of the molecular weight and structure, the mechanical and physical properties cannot be precisely predicted or monitored.

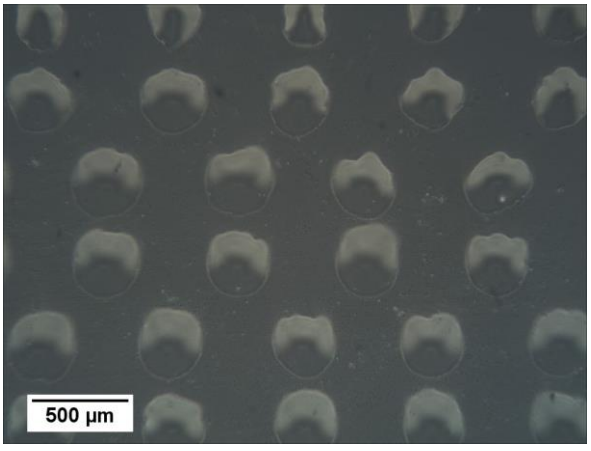

Figure C.1 *In situ* polymerised PU deposits printed glass slide (hexagon, *dx/dy* = 0.7/0.35 mm).

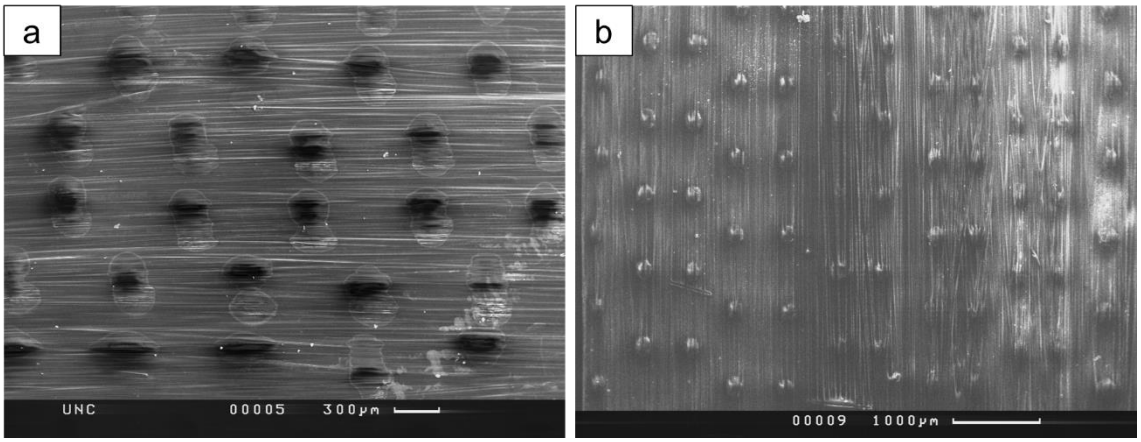

Figure C.2 *In situ* polymerised PU deposits on prepreg patterned in hexagon, *dx/dy* = 0.7/0.35 mm.

D. Publications resulting from this thesis

Published

1. Yi Zhang, Christopher Tse, Davood Rouholamin, and Patrick J. Smith, "Scaffolds for tissue engineering produced by inkjet printing," Central European Journal of Engineering, vol. 2, pp. 325-335, 2012
2. Yi Zhang, Jonathan Stringer, Richard Grainger, Patrick J. Smith, and Alma Hodzic, "Improvements in carbon fibre reinforced composites by inkjet printing of thermoplastic polymer patterns," Physica status solidi (RRL) – Rapid Research Letters, vol. 8, pp. 56-60, 2014
3. Yi Zhang, Jonathan Stringer, Richard Grainger, Patrick J. Smith, and Alma Hodzic, "Fabrication of patterned thermoplastic microphases between composite plies by inkjet printing," Journal of Composite Materials, vol. 0(0), pp. 1-7, 2014
4. Yi Zhang, Jonathan Stringer, Patrick J. Smith, Alma Hodzic, and Richard Grainger, "Toughening composites with self-ameliorating capability using inkjet printing technique," 16th European Conference on Composite Materials (ECCM16), Seville, Spain, 22-26 June, 2014

In progress

1. Yi Zhang, Jonathan Stringer, Alma Hodzic and Patrick J Smith, "Elaborating printing parameters in using inkjet printing to toughen carbon fibre reinforced plastic composites," 20th International Conference on Composite Materials (ICCM20), Copenhagen, Denmark, 19-24 July, 2015

Other papers

1. Elliot J. Fleet, Yi Zhang, Simon A. Hayes, and Patrick J. Smith, "Inkjet printing of self-healing polymers for enhanced composite interlaminar properties," Journal of Materials Chemistry A, vol. 3, pp. 2283-2293, 2015
2. Patrick Rider, Christopher Tse, Yu Zhang, Yi Zhang, Jonathan Stringer, Xiubo Zhao and Patrick J. Smith, "Reactive inkjet preparation of dental membranes patterned with silk fibroin structures". (In progress)

References

[1] N. Reis, C. Ainsley, and B. Derby, "Ink-jet delivery of particle suspensions by piezoelectric droplet ejectors," *Journal of Applied Physics,* vol. 97, pp. 094903, 2005.

[2] E. Tekin, P. J. Smith, and U. S. Schubert, "Inkjet printing as a deposition and patterning tool for polymers and inorganic particles," *Soft Matter,* vol. 4, pp. 703-713, 2008.

[3] P. Krober, J. T. Delaney, J. Perelaer, and U. S. Schubert, "Reactive inkjet printing of polyurethanes," *Journal of Materials Chemistry,* vol. 19, pp. 5234-5238, 2009.

[4] M. Bakar, R. Duk, M. Przybylek, and M. Kostrzewa, "Mechanical and thermal properties of epoxy resin modified with polyurethane," *Journal of Reinforced Plastics and Composites*, 2008.

[5] S. Lu, J. Ban, C. Yu, and W. Deng, "Properties of epoxy resins modified with liquid crystalline polyurethane," *Iran Polym J,* vol. 19, pp. 669-678, 2010.